

AD 733756

REPORT NO. DOT-TSC-FAA-71-8

D JS

LINEARIZED MATHEMATICAL MODELS FOR DE HAVILLAND CANADA "BUFFALO & TWIN OTTER" STOL TRANSPORTS

R.A. MACDONALD, MEL GARELICK, J. O'GRADY
TRANSPORTATION SYSTEMS CENTER
55 BROADWAY
CAMBRIDGE, MA. 02142



JUNE 1971
TECHNICAL NOTE

AVAILABILITY IS UNLIMITED. DOCUMENT MAY BE RELEASED
TO THE NATIONAL TECHNICAL INFORMATION SERVICE,
SPRINGFIELD, VIRGINIA 22151, FOR SALE TO THE PUBLIC.

D D C
RECEIVED
DEC 16 1971
NATIONAL TECHNICAL
INFORMATION SERVICE
A

Reproduced by
NATIONAL TECHNICAL
INFORMATION SERVICE
Springfield, Va. 22151

Prepared for

FEDERAL AVIATION ADMINISTRATION
WASHINGTON, D.C. 20590

A

112

1. Report No.	2. Government Accession No.	3. Recipient's Catalog No.	
4. Title and Subtitle Linearized Mathematical Models for DeHavilland Canada "Buffalo & Twin Otter" STOL Transports		5. Report Date	
		6. Performing Organization Code PGS	
7. Author(s) R. A. MacDonald*, Mel Garelick*, and J. O'Grady		8. Performing Organization Report No. DOT-TSC-FAA-71-8	
9. Performing Organization Name and Address Transportation Systems Center 55 Broadway Cambridge, Mass. 02142		10. Work Unit No. FA-18	
		11. Contract or Grant No.	
12. Sponsoring Agency Name and Address Department of Transportation		13. Type of Report and Period Covered Technical Note	
		14. Sponsoring Agency Code	
15. Supplementary Notes *Service Technology Corporation Cambridge, Ma. 02142			
16. Abstract Linearized six degree of freedom rigid body aircraft equations of motion are presented in a stability axes system. Values of stability derivatives are estimated for two representative STOL aircraft - the DeHavilland of Canada "Buffalo" and "Twin Otter." These estimates are based on analytical expressions included in the report. The combination of the equations of motion and the estimated stability derivatives provides an aircraft model which is useful for Navigation, Guidance and ATC Studies. Resulting transient responses to control inputs are presented.			
17. Key Words •Aircraft Math Models •STOL Aircraft Stability & Control		18. Distribution Statement Unlimited	
19. Security Classif. (of this report) Unclassified	20. Security Classif. (of this page) Unclassified	21. No. of Pages	22. Price

ABSTRACT

Linearized six degree of freedom rigid body aircraft equations of motion are presented in a stability axes system.

Values of stability derivatives are estimated for two representative STOL aircraft - the DeHavilland of Canada "Buffalo" and "Twin Otter". These estimates are based on analytical expressions included in the report. The combination of the equations of motion and the estimated stability derivatives provides an aircraft model which is useful for Navigation, Guidance and ATC Studies.

Resulting transient responses to control inputs are presented.

TABLE OF CONTENTS

	<u>Page</u>
Symbols	iii
1.0 Introduction	1
2.0 Applicability of Mathematical Model	3
3.0 Definition of Reference Coordinate Frames	5
4.0 Derivation of Generalized Kinematic Equations of Motion	8
5.0 Derivation of Linearized Equations of Motion	14
6.0 Summary of Analytical Expressions for Stability Derivatives	22
7.0 Tabulation of Analytically-Determined Stability Derivative Values for DeHavilland "Buffalo" and "Twin Otter"	27
Figures	32
References	36
Appendix A: Derivation of Analytical Expressions for Selected Stability Derivatives	A1
Appendix B: Estimate of Moments and Products of Inertia	B1
Appendix C: Calculation of Stability Derivatives	C1
Appendix D: Transient Responses to Control Inputs	D1

SYMBOLS

a	Airplane lift curve slope	rad^{-1}
$a_{()}$	lift curve slope of surface () (of wing when no subscript)	rad^{-1}
$AR_{()}$	aspect ratio of surface () = $b_{()}^2/S_{()}$ (of wing when no subscript)	-
$b_{()}$	span of surface () (of wing when no subscript)	ft
$c_{()}$	mean chord of surface () (of wing when no subscript)	ft
$C_{()}$	nondimensional stability derivative (defined in Section VI)	-
C_{D_f}	parasite drag coefficient of aircraft	-
C_{L_α}	lift curve slope of wing	rad^{-1}
D_f	aircraft parasite drag	lbs
e	wing efficiency factor	-
$F_{()}$	force component along the () axis	lbs
g	gravitational constant = 32.2	ft/sec^2
h	altitude	ft
h	height of fuselage at wing root	ft
h	CG position, fraction of c	-
h_n	neutral point of aircraft, fraction of c	-
$H_{()}$	component of angular momentum along the () axis	$\text{slug-ft}^2/\text{sec}$
$\bar{i}_{()} \bar{j}_{()} \bar{k}_{()}$	unit vectors along the X, Y, and Z axes of the () coordinate frame, respectively	-
I_x, I_y, I_z	aircraft rolling, pitching, and yawing moment of inertia, respectively (further defined in equations 13-15)	slug-ft^2

J_{xy}	product of inertia = $\int xy dm$	slug-ft ²
J_{yz}	product of inertia = $\int yz dm$	slug-ft ²
$J_{zx} = J_{xz}$	product of inertia = $\int xz dm$	slug-ft ²
L, M, N,	scalar components of the applied external moment along the X_A , Y_A , and Z_A axes, respectively	ft-lbs
l ()	distance, quarter chord of aircraft mac to quarter chord of surface ()	ft
m	mass of aircraft	slugs
P, Q, R	scalar components of the angular rotation vector of the aircraft along the X_A , Y_A , and Z_A axes, respectively	rad/sec
$\Delta P, \Delta Q, \Delta R$	perturbed portion of P, Q, R, e.g. $\Delta P = P - P_0$	rad/sec
q	dynamic pressure = $\frac{1}{2} \rho V_R^2$	lbs/ft ²
s	laplace transform variable = $\frac{d}{dt}$	sec ⁻¹
S ()	area of surface () (of wing when no subscript)	ft ²
t	time	sec
ΔT	change in thrust due to pilot throttle input	lbs
U, V, W	scalar components of velocity of the aircraft along the X_A , Y_A and Z_A axes, respectively	ft/sec
$\Delta U, \Delta V, \Delta W$	perturbed portion of U, V, W, e.g. $\Delta U = U - U_0$	ft/sec
U_0	equilibrium or reference value of U	ft/sec
V_R	resultant velocity vector of aircraft = $\sqrt{U^2 + V^2 + W^2}$	ft/sec
w	width of fuselage at wing root	ft
W	weight of aircraft = mg	lbs
X, Y, Z	scalar components of the applied non-gravitational external forces along the X_A , Y_A , and Z_A axes, respectively	lbs

$X_{()}, Y_{()}, Z_{()}$	axes defining the $()$ coordinate frame	-
$\Delta X, \Delta Y, \Delta Z$	perturbation portion of X, Y, Z , e.g., $\Delta X = X - X_0$	lbs
$x, y, z,$	distances along the X_A, Y_A, Z_A axes, clarified by subscript	ft
Y_1	distance, aircraft centerline to inboard end of aileron	ft
Y_2	distance, aircraft centerline to outboard end of aileron	ft
α	angle of attack = $\tan^{-1} W/U$	rad
β	angle of sideslip = $\tan^{-1} V/U$	rad
$\delta_{()}$	deflection of control surface $()$ (positive deflection produces positive moment)	rad
$\Delta \delta_{()}$	perturbation portion of $\delta_{()}$, e.g., $\Delta \delta_{()} = \delta_{()} - \delta_{()_0}$	rad
γ	flight path angle of aircraft $= \theta - \alpha$	rad
Γ	dihedral angle	deg, rad
ϵ	downwash angle	rad
$\eta_{()}$	efficiency of tail surface $()$	-
θ, ϕ, ψ	Euler angles, defined in Figure 2	rad
$\Delta \theta, \Delta \phi, \Delta \psi$	perturbed portion of θ, ϕ, ψ , e.g., $\Delta \theta = \theta - \theta_0$	rad
ρ	atmospheric air density	slug/ft ³
σ	sidewash angle	rad
τ	aileron effectiveness	

Subscripts

A	aircraft body coordinate frame
C	Earth-aircraft control coordinate frame
E	Earth-centered coordinate frame
I	inertial coordinate frame
L	Earth local-vertical coordinate frame

f	flaps
F	fin
g	due to gravity
n	stick-fixed neutral point
T	horizontal tail
o	equilibrium or reference condition
w	wing

1.0 Introduction

There is no such thing as an exact mathematical model of any physical phenomenon. All mathematical models are, therefore, approximations to reality; approximations based on an assumption set which should be clearly recognized by both the writer and the user of the equations comprising the model.

The basic set of assumptions must always be derived from the desired application of the model. To develop and utilize a more exact model than that required for the job at hand is to pay an unnecessarily high price in man-hours and computer time both in the use of the model and in the gathering and formatting of the data required by the model.

The model presented herein is a linear perturbation model. It was developed for use in exercising sets of 4-D guidance equations which are being developed for application in STOL terminal area guidance. The aircraft which are modeled (the C-8 and the Twin Otter) were selected as representative of two classes of aircraft, i.e. light and medium STOL propeller aircraft, and are of interest only as representations of the classes from a guidance and ATC viewpoint.

This report is submitted as partial documentation of work carried out in support of PPA 18-0, dated December 1, 1970. In particular, it documents the work performed under Task 2 of this PPA for the "Buffalo" and "Twin Otter" aircraft. (Similar data are required under this task for a third STOL at a later date.)

The applicability of the present model is discussed in detail in the next section, Section 2.0.

The next 3 sections are devoted to the derivation of the required linearized equations: In Section 3.0, required coordinate frames are defined. Section 4.0 derives the generalized kinematic equations of motion, utilizing very few approximations. Finally, in Section 5.0, the desired linearized equations are developed from the generalized ones.

Section 6.0 presents analytical expressions for the required stability derivatives. These expressions are used to generate numerical values, given in Section 7.0, for two representative STOL aircraft.

Supporting material is included in the Appendices. In Appendix A, analytical expressions for selected stability derivatives are developed. Appendix B contains estimates of moments and products of inertia for the two aircraft under consideration. Appendix C contains a step-by-step calculation of the stability derivatives summarized in Section VII. Appendix D presents typical transient responses to control inputs, calculated using the equations and derivatives developed in this report.

2.0 Applicability of Mathematical Model

As stated in the Introduction, a linearized representation of aircraft motions is required.

The model is intended for use as a tool in the preliminary design and analysis of STOL aircraft control, guidance, and navigation systems. In this phase of analysis and design, the unstabilized response of the vehicle is adequately established by means of a linearized analysis. The linearized model lends itself to the use of such techniques as root locus analysis and frequency domain analysis.

Many approximations are required to develop a linearized set of equations from the generalized kinematic equations of motion. All assumptions used in the derivations are explicitly stated in Sections 4.0 and 5.0. They are introduced as they are needed and are consecutively numbered so that the reader can easily establish the degree of simplification at any point.

The major simplification is the introduction of small disturbance (or "perturbation") assumptions. Under these assumptions, aircraft motions are restricted to small excursions - perturbations - from an equilibrium flight condition. The major virtue of this assumption is that it vastly simplifies the equations.

Its use, of course, limits the applicability of the equations to a certain extent. The reader is cautioned, therefore, to determine the effect of this assumption (and of the others) before applying the equations.

A reservation must also be stated concerning the stability derivatives presented in Sections 6.0 and 7.0. These derivatives are *not* based on wind tunnel or flight tests, because data from these sources were not available. They have been developed by analytical methods, and have been augmented in some cases by generally-applicable empirical data.

The intended purpose of the estimated derivatives is to establish in representative fashion the dynamics of small and medium types of STOL aircraft. They should not be used as the basis for an evaluation of the flying qualities of the "Buffalo" or "Twin Otter" or of the suitability of these aircraft for any specific mission.

3.0 Definition of Reference Coordinate Frames

The equations of motion of an aircraft are based on Newton's second law. This law relates the forces applied to the aircraft to the acceleration (or change of momentum) of the aircraft with respect to inertial space. It is usually convenient to define applied forces and moments with respect to a frame fixed in the aircraft. Further, aerodynamic forces depend on the motion of the aircraft with respect to the air mass. Finally, the motion of the aircraft with respect to the Earth is frequently of interest. Thus it can be readily seen that several reference coordinate frames are required to completely describe the applied forces and the resulting motions of the aircraft.

Reference coordinate frames to be used in this analysis are defined in this section. Insofar as possible, axis systems have been defined so that senses of rotation and translation are similar for small rotations. Positive force, moment, and motion vector components are defined to be in the positive sense of the axis. To the largest extent possible, the symbols and conventions used are consistent with those in common usage in the guidance and control fields and with those used by NASA for aircraft stability and control work.

The *Inertial Coordinate Frame (I)* will be defined first. This frame is nonrotating with respect to inertial space. The origin is the center of the Earth, with the Z_I axis coincident with the Earth's axis of rotation. The X_I and Y_I axes then lie in the equatorial plane. It is assumed that the linear and angular accelerations of the Earth with respect to inertial space as it moves in its solar orbit are not of interest. This

coordinate frame (as well as the E and L frames following) is shown in the sketch of Figure 1.

The *Earth-Centered Coordinate Frame (E)* is fixed with respect to the Earth. Its origin is at the Earth's center with the Z_E axis coincident with the Z_I axis. The X_E and Y_E axes lie in the equatorial plane, intersecting the Earth's surface at convenient points. The E-frame can be chosen to coincide with the I-frame at a particular instant of time.

The *Earth Local-Vertical Frame (L)* is a local geographic frame. Its origin is the center of mass of the aircraft with Z_L along the vertical defined by the local gravity vector (positive downward), X_L parallel to geographic North (positive to the North), and Y_L parallel to geographic East (positive to the East).

The *Aircraft Body Coordinate Frame (A)* is fixed to the aircraft and rotates and translates with the aircraft. Its origin is the center of mass of the aircraft. The X_A axis is chosen in a convenient forward direction in the plane of symmetry. (The exact X_A axis location is specified in Section V.) The Y_A axis is normal to the aircraft's plane of symmetry (positive to the right), and the Z_A axis is in the plane of symmetry (positive downward) and orthogonal to the X_A and Y_A axes. The A-frame is related to the L-frame (and to the next-defined C-frame) in Figure 2.

The *Earth-Aircraft Control Coordinate Frame (C)* is also centered at the center of mass of the aircraft. The Z_C axis is aligned with the local gravity vector (positive downward) and

is therefore coincident with the Z_L axis. The X_C axis is the intersection of the horizontal X_L - Y_L plane with the vertical plane containing the X_A axis. The Y_C axis completes the orthogonal right-hand system. The C-frame is an intermediate frame needed to define the Euler angles describing the relationship between the Earth local-vertical (L) frame and the Aircraft body (A) frame. In their order of rotation (which must be preserved) the Euler angles are defined as:

1. Heading (ψ): angle of rotation about Z_L from X_L to X_C ;
2. Pitch (θ): angle of rotation about Y_C from X_C to X_A ;
3. Roll (ϕ): angle of rotation about X_A from Y_C to Y_A .

These Euler angle rotations are shown in Figure 2.

4.0 Derivation of Generalized Kinematic Equations of Motion

The generalized equations of motion are obtained (as, for example, in References 1 and 2) by equating forces and moments acting on the aircraft to the rates of change of linear and angular momentum of the aircraft with respect to inertial space:

$$\bar{F} = \frac{d}{dt} (\bar{mV}) \Big|_I \quad (1)$$

$$\bar{M} = \frac{d}{dt} (\bar{H}) \Big|_I \quad (2)$$

In these equations, \bar{F} is the force vector and \bar{M} is the moment vector acting on the aircraft. Linear and angular momentum vectors are represented by \bar{mV} and \bar{H} respectively. The subscript I indicates that the time rate of change of the momentum vectors is with respect to inertial space.

It is of more interest, however, to express these momentum changes in terms of an axis system that is fixed in the aircraft and that is therefore translating and rotating with respect to inertial space. This axis system is the A-frame defined in Section 3.0. Equations 1 and 2 can be expressed in A-frame coordinates as

$$\bar{F} = \frac{d}{dt} (\bar{mV}) \Big|_A + \bar{\omega} \times \bar{mV} \quad (3)$$

$$\bar{M} = \frac{d}{dt} (\bar{H}) \Big|_A + \bar{\omega} \times \bar{H} \quad (4)$$

In these equations, the subscript A indicates momentum changes with respect to the rotating A-frame. The cross product terms account for the fact that the A-frame is rotating at a rate $\bar{\omega}$ with respect to inertial space.

Equations 3 and 4 are completely rigorous. At this point, however, it is convenient to make several assumptions to facilitate further development of the equations:

Assumption 1: The mass of the aircraft does not change significantly in the interval of interest, that is

$$\frac{d}{dt} (m\bar{V}) = m \frac{d}{dt} (\bar{V})$$

Assumption 2: The rotating earth can be considered an inertial frame for the purposes of this analysis. Therefore the E-frame is assumed to be an inertial frame.

Assumption 3: The aircraft is a rigid body. The contribution to \bar{H} of spinning propellers can be neglected. Control surface dynamics need not be considered.

Assumption 4: The Y_A axis is a principal axis so that the products of inertia J_{xy} and J_{yz} are zero.

By virtue of assumption 2, the vectors \bar{V} and $\bar{\omega}$ of equations 3 and 4 are the motions of the aircraft with respect to the Earth. These vectors are further defined in terms of their A-frame components.

$$\bar{V} = U \bar{i}_A + V \bar{j}_A + W \bar{k}_A \quad (5)$$

$$\bar{\omega} = P \bar{i}_A + Q \bar{j}_A + R \bar{k}_A \quad (6)$$

where \bar{i}_A , \bar{j}_A , and \bar{k}_A are unit vectors along the X_A , Y_A , and Z_A axes, respectively. Similarly, \bar{F} , \bar{M} , and \bar{H} of equations 3 and 4 can be expressed in their A-frame components:

$$\bar{F} = F_x \bar{i}_A + F_y \bar{j}_A + F_z \bar{k}_A \quad (7)$$

$$\bar{M} = L \bar{i}_A + M \bar{j}_A + N \bar{k}_A \quad (8)$$

$$\bar{H} = H_x \bar{i}_A + H_y \bar{j}_A + H_z \bar{k}_A \quad (9)$$

Development of expressions for the scalar components of H is rather lengthy and will be omitted here. Following the derivations in Chapter 1 of Reference 1 or Chapter 4 of Reference 2, for example, produces these expressions for the components of \bar{H} :

$$H_x = PI_x - QJ_{xy} - RJ_{xz} \quad (10)$$

$$H_y = QI_y - RJ_{yz} - PJ_{xy} \quad (11)$$

$$H_z = RI_z - PJ_{xz} - QJ_{yz} \quad (12)$$

where the moments and products of inertia are:

$$I_x = \int (y^2 + z^2) dm \quad (13)$$

$$I_y = \int (z^2 + x^2) dm \quad (14)$$

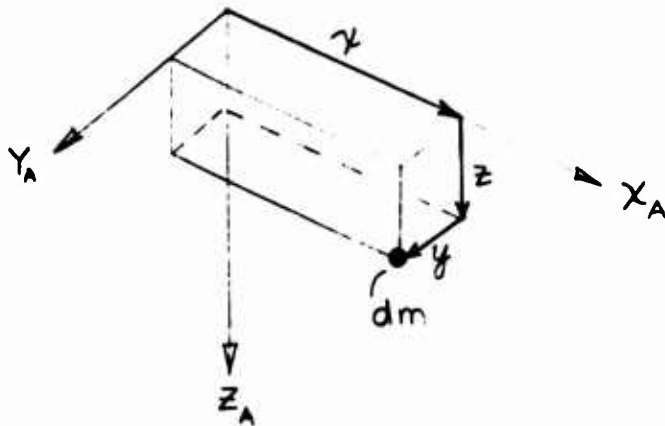
$$I_z = \int (x^2 + y^2) dm \quad (15)$$

$$J_{xy} = \int xy dm \quad (16)$$

$$J_{yz} = \int yz dm \quad (17)$$

$$J_{xz} = \int xz dm \quad (18)$$

and x , y , z , and the mass element dm are defined in the sketch:



By virtue of Assumption 4, equations 10, 11, and 12 reduce to

$$H_x = PI_x - RJ_{xz} \quad (19)$$

$$H_y = QI_y \quad (20)$$

$$H_z = RI_z - PJ_{xz} \quad (21)$$

Now, by using equations 5 through 9 and equations 19 through 21, equations 3 and 4 can be expanded to give A-frame components of aircraft accelerations with respect to the Earth:

Force Equations

$$F_x = m [\dot{U} + QW - RV] \quad (22)$$

$$F_y = m [\dot{V} + RU - PW] \quad (23)$$

$$F_z = m [\dot{W} + PV - QU] \quad (24)$$

Moment Equations

$$L = I_x \dot{P} + (I_z - I_y) QR - J_{xz} (\dot{R} + PQ) \quad (25)$$

$$M = I_y \dot{Q} + (I_x - I_z) RP - J_{xz} (R^2 - P^2) \quad (26)$$

$$N = I_z \dot{R} + (I_y - I_x) PQ - J_{xz} (\dot{P} - QR) \quad (27)$$

The A-frame forces (F_x, F_y, F_z) and moments (L,M,N) in equations 22 through 27 represent all of the external forces and moments acting upon the aircraft. These forces and moments are due to aerodynamic loads, control and propulsion systems, and gravity.

Gravitation Forces - The gravity force is a vector quantity of magnitude mg acting along the positive Z_L axis. The resolution of this force into A-frame components can be accomplished by referring to Figure 2 where Euler angles (Ψ, θ, ϕ) are used to relate the L-frame and A-frame coordinate frames:

$$X_g = - mg \sin \theta \quad (28)$$

$$Y_g = mg \cos \theta \sin \phi \quad (29)$$

$$Z_g = mg \cos \theta \cos \phi \quad (30)$$

No moments are produced by gravity because the A-frame origin is located at the aircraft's center of gravity. Therefore $L_g, M_g,$ and N_g are zero.

Non-Gravitational Forces and Moments - The remaining forces and moments are due primarily to aerodynamic, propulsive and control effects. They are denoted simply X, Y, Z, L, M, and N. Thus, for example, $F_x = X_g + X$. These forces and moments are developed in Section V.

The A-frame force and moment equations (22 through 27) can be restated on the basis of the above discussion. Also stated are the relationships between A-frame angular rates (P,Q,R) and Euler angle rates. These relationships have been obtained from Figure 2 by projecting the Euler rates (Ψ, θ, ϕ) onto the A-frame

axes:

$$m [\dot{U} + QW - RV + g \sin \theta] = X \quad (31)$$

$$m [\dot{V} + RU - PW - g \cos \theta \sin \phi] = Y \quad (32)$$

$$m [\dot{W} + PV - QU - g \cos \theta \cos \phi] = Z \quad (33)$$

$$I_x \dot{P} + (I_z - I_y) QR - J_{zx} (\dot{R} + PQ) = L \quad (34)$$

$$I_y \dot{Q} + (I_x - I_z) RP - J_{xz} (R^2 - P^2) = M \quad (35)$$

$$I_z \dot{R} + (I_y - I_x) PQ - J_{xz} (\dot{P} - QR) = N \quad (36)$$

$$P = \dot{\phi} - \dot{\psi} \sin \theta \quad (37)$$

$$Q = \dot{\theta} \cos \phi + \dot{\psi} \cos \theta \sin \phi \quad (38)$$

$$R = \dot{\psi} \cos \theta \cos \phi - \dot{\theta} \sin \phi \quad (39)$$

These nine equations are an almost exact description of the motions of an aircraft operating near the Earth's surface. The derivation to this point has used only four simplifying assumptions, repeated here:

1. Aircraft mass is constant
2. The Earth can be considered an inertial frame
3. The aircraft is a rigid body
4. The aircraft is symmetrical about its x - z plane.

The equations can be further developed along any one of several paths. In this case they will be manipulated (in Section V) into the form generally used for linearized aircraft stability and control studies.

5.0 Derivation of Linearized Equations of Motion

A number of simplifying assumptions are required to develop linearized equations of motion from the general equations discussed in Section 4.0. These approximations are (continuing the numbering sequence begun in Section 4.0):

Assumption 5: The aircraft is assumed initially to be in equilibrium flight with no linear or angular accelerations, no angular rates, and no initial roll angle or lateral velocity.

Assumption 6: The X_A axis is fixed in the aircraft and is parallel to the projection on the $X_A - Z_A$ plane of the relative wind vector during equilibrium flight. In other words, stability axes will be used.

Assumption 7: Small disturbance (perturbation) theory will be used. Motions and forces will be referred to the equilibrium flight condition of Assumption 1. Variables at this flight condition will be identified by the subscript o. Change from this condition will be indicated by the prefix Δ . Thus:

$$U = U_o + \Delta U$$

$$V = V_o + \Delta V$$

$$W = W_o + \Delta W$$

$$P = P_o + \Delta P$$

$$Q = Q_o + \Delta Q$$

$$R = R_o + \Delta R$$

$$\Psi = \Psi_o + \Delta \Psi$$

$$\Theta = \Theta_o + \Delta \Theta$$

$$\Phi = \Phi_o + \Delta \Phi$$

(40)

Assumption 8: Small angle approximations will be made. For example,
 $\sin \Delta\theta \approx \Delta\theta$
 $\cos \Delta\theta \approx 1$

Assumption 9: Higher order terms will be neglected.
For example, $(U_0 + \Delta U)(\Delta Q) \approx U_0 \Delta Q$

By virtue of Assumption 5, P_0 , Q_0 , R_0 , ϕ_0 , and V_0 are zero.

By virtue of Assumption 6, W_0 is zero. ψ_0 is a special case.

Since it is the angle between the X_L and X_C axes, it can vary

from 0 to 2π . In this analysis, we will specify that heading

angle be referred to the initial X_C axis. Thus ψ_0 can be

treated as if it were zero. The perturbation relations of

equation 40 can therefore be revised:

$$U = U_0 + \Delta U$$

$$V = \Delta V$$

$$W = \Delta W$$

$$P = \Delta P$$

$$Q = \Delta Q$$

(41)

$$R = \Delta R$$

$$\psi = \Delta\psi$$

$$\theta = \theta_0 + \Delta\theta$$

$$\phi = \Delta\phi$$

The derivative with respect to time of each of these variables can be easily determined, e.g.,

$$\dot{U} = \frac{d}{dt} (U_0 + \Delta U) = \dot{\Delta U}$$

Equations 41, Assumptions 8 and 9, and the trigonometric identities

$$\begin{aligned}\sin(A + B) &= \sin A \cos B + \cos A \sin B \\ \cos(A + B) &= \cos A \cos B - \sin A \sin B\end{aligned}\tag{42}$$

can be applied to equations 31 through 39 to produce

$$\begin{aligned}m [\dot{\Delta U} + g \sin \theta_0 + g \cos \theta_0 \Delta \theta] &= X \\ m [\dot{\Delta V} + U_0 \Delta R - g \cos \theta_0 \Delta \phi] &= Y \\ m [\dot{\Delta W} - U_0 \Delta Q - g \cos \theta_0 + g \sin \theta_0 \Delta \theta] &= Z \\ I_x \dot{\Delta P} - J_{zx} \dot{\Delta R} &= L \\ I_y \dot{\Delta Q} &= M \\ I_z \dot{\Delta R} - J_{zx} \dot{\Delta P} &= N\end{aligned}\tag{43}$$

and

$$\begin{aligned}P = \Delta P &= \dot{\Delta \phi} - \dot{\Delta \psi} \sin \theta_0 \\ Q = \Delta Q &= \dot{\Delta \theta} \\ R = \Delta R &= \dot{\Delta \psi} \cos \theta_0\end{aligned}\tag{44}$$

Equations 43 can be evaluated at the equilibrium flight condition where Δ quantities are zero:

$$\begin{aligned}mg \sin \theta_0 &= X_0 \\ 0 &= Y_0 \\ -mg \cos \theta_0 &= Z_0 \\ 0 &= L_0 \\ 0 &= M_0 \\ 0 &= N_0\end{aligned}$$

Subtracting these equations from equations 43 produces the following perturbation equations:

$$\begin{aligned}
m [\dot{\Delta U} + g \cos \theta_0 \Delta \theta] &= \Delta X \\
m [\dot{\Delta V} + U_0 \Delta R - g \cos \theta_0 \Delta \phi] &= \Delta Y \\
m [\dot{\Delta W} - U_0 \Delta Q + g \sin \theta_0 \Delta \theta] &= \Delta Z \\
I_x \dot{\Delta P} - J_{zx} \dot{\Delta R} &= L \\
I_y \dot{\Delta Q} &= M \\
I_z \dot{\Delta R} - J_{zx} \dot{\Delta P} &= N
\end{aligned}
\tag{45}$$

where $\Delta X = X - X_0$, etc.

Next to be developed are the right-hand sides of equations 45. The conventional practice of expressing these terms as a Taylor series expansion is utilized. The development presented in Chapter 4 of Reference 2 is closely followed.

The Taylor series is of the form (neglecting higher order terms):

$$\Delta X = X_A \Delta A + X_B \Delta B + X_C \Delta C + \dots
\tag{46}$$

where $\Delta A, \Delta B, \Delta C \dots$ are the variables which describe the motions of the aircraft or which otherwise contribute to ΔX and where

$$X_A = \frac{\partial X}{\partial A}$$

evaluated at the equilibrium flight condition.

Several additional approximations and assumptions are desirable at this point:

Assumption 10: Higher-order terms in the Taylor series expansions can be neglected.

Assumption 11: The air mass is fixed with respect to the Earth; that is, there is no wind. This simplifying assumption allows use of components of ground speed V_R ($\Delta U, \Delta V, \Delta W$) as variables in the Taylor series instead of components of airspeed.

Assumption 12: Series terms involving the derivatives with respect to these variables will be considered: ΔU , ΔV , ΔW , $\Delta \dot{W}$, ΔP , ΔQ , ΔR , $\Delta \delta_e$, $\Delta \delta_a$, and $\Delta \delta_r$. The last three variables are the perturbation deflections of the elevator, aileron, and rudder, respectively.

Assumption 13: Series terms involving derivatives of ΔX , ΔZ , and ΔM with respect to ΔV , ΔP , ΔR , $\Delta \delta_a$ and $\Delta \delta_r$ can be neglected. Terms involving derivatives of ΔY , ΔL , and ΔN with respect to ΔU , ΔW , $\Delta \dot{W}$, ΔQ , and $\Delta \delta_e$ can also be neglected.

Assumption 14: The derivatives $\partial X / \partial Q$, $\partial X / \partial \Delta W$, $\Delta X / \Delta \delta_e$, and $\Delta Y / \Delta \delta_a$ are negligibly small.

These assumptions are discussed and justified in Chapter 4 of Reference 2. Assumption 10 is necessary in order to retain linearity in equations 45. Assumption 13, while not essential, is made because experience has shown that it is a reasonable one (for most applications) and because it allows separation of the six equations (45) into two sets of three.

The definition of equation 46 and the above assumptions yield expressions for the non-gravity perturbation forces of equations 45:

$$\begin{aligned}
 \Delta X &= X_u \Delta U + X_w \Delta W + \Delta T \\
 \Delta Y &= Y_v \Delta V + Y_p \Delta P + Y_r \Delta R + Y_{\delta_r} \Delta \delta_r \\
 \Delta Z &= Z_u \Delta U + Z_w \Delta W + Z_{\dot{w}} \Delta \dot{W} + Z_q \Delta Q + Z_{\delta_e} \Delta \delta_e \\
 \Delta L &= L_v \Delta V + L_p \Delta P + L_r \Delta R + L_{\delta_a} \Delta \delta_a + L_{\delta_r} \Delta \delta_r \\
 \Delta M &= M_u \Delta U + M_w \Delta W + M_{\dot{w}} \Delta \dot{W} + M_q \Delta Q + M_{\delta_e} \Delta \delta_e \\
 \Delta N &= N_v \Delta V + N_p \Delta P + N_r \Delta R + N_{\delta_a} \Delta \delta_a + N_{\delta_r} \Delta \delta_r
 \end{aligned} \tag{47}$$

Before these expressions are substituted into equations 45, one question must be resolved: Equations 45 contain as variables A-frame rates ($\Delta P, \Delta Q, \Delta R$) as well as Euler angle displacements ($\Delta \Psi, \Delta \theta, \Delta \phi$). A decision must be made as to which set of variables will be carried henceforward.

For the X-Z-M set of equations 45, there is no difficulty. By virtue of equations 44, $\Delta Q = \Delta \dot{\theta}$, from which can be obtained $\Delta \dot{Q} = \Delta \ddot{\theta}$. Thus ΔQ and $\Delta \dot{Q}$ can be readily eliminated in favor of $\Delta \theta$ and its derivatives.

For the Y-L-N set, there is no difficulty either, except that some additional terms must be accepted for either set of variables. One can solve equations 44 for $\Delta \dot{\phi}$:

$$\Delta \dot{\phi} = \Delta P + \tan \theta_0 \Delta R,$$

but attempts to integrate this equation in order to obtain an expression for $\Delta \phi$ (needed in the Y equation) encounter the difficulty that $\int \Delta P$ and $\int \Delta R$ cannot be uniquely determined since they depend on the order that rotations are taken about the A-frame axes. To avoid this difficulty (and to retain uniformity since the Euler angle $\Delta \theta$ is used in the X-Z-M equations) the Euler angles $\Delta \phi$ and $\Delta \Psi$ are used as the variables in this analysis. Thus equations 44 are used to eliminate ΔP and ΔR in equations 45.

We will combine several steps in arriving at the final form of the aircraft equations of motion:

1. The six equations will be separated into the X-Z-M set and the Y-L-N set.
2. ΔQ will be eliminated in favor of $\Delta \dot{\theta}$, and ΔP and ΔR in favor of $\Delta \phi$ and $\Delta \dot{\psi}$ by using equations 44.
3. The Laplace notation $(\dot{}) = s()$ will be introduced.
4. Equations (47) will be substituted into equations (45).

The X-Z-M set - the longitudinal equations - are thus developed from equations 45 as:

$$[ms - X_u] \Delta U + [-X_w] \Delta W + [mg \cos \theta_0] \Delta \theta = \Delta T \quad (48)$$

$$[-Z_u] \Delta U + [(m - Z_w) s - Z_w] \Delta W + [-(mU_0 + Z_q) s + mg \sin \theta_0] \Delta \theta = [Z_{\delta_e}] \Delta \delta_e \quad (49)$$

$$[-M_u] \Delta U + [-M_w s - M_w] \Delta W + [I_y s^2 - M_q s] \Delta \theta = [M_{\delta_e}] \Delta \delta_e \quad (50)$$

The Y-L-N set - the lateral equations - become:

$$[ms - Y_v] \Delta V + [-Y_p s - mg \cos \theta_0] \Delta \phi + [(mU_0 - Y_r) \cos \theta_0 + Y_p \sin \theta_0] s \Delta \psi = [Y_{\delta_r}] \Delta \delta_r \quad (51)$$

$$[-L_v] \Delta V + [I_x s^2 - L_p s] \Delta \phi + [-(I_x \sin \theta_0 + J_{zx} \cos \theta_0) s^2 - (L_r \cos \theta_0 - L_p \sin \theta_0) s] \Delta \psi = [L_{\delta_a}] \Delta \delta_a + [L_{\delta_r}] \Delta \delta_r \quad (52)$$

$$\begin{aligned}
& [-N_v] \Delta V + [-J_{xz} s^2 - N_p s] \Delta \phi \\
& + [(I_z \cos \theta_0 + J_{xz} \sin \theta_0) s^2 - (N_r \cos \theta_0 - N_p \sin \theta_0) s] \Delta \psi \\
& = [N_{\delta_a}] \Delta \delta_a + [N_{\delta_r}] \Delta \delta_r \qquad (53)
\end{aligned}$$

Equations 48 through 53 are, to summarize, the six linearized rigid body equations of motion, written in aircraft stability axes. Dependent variables are the perturbed aircraft body (A-frame) velocities ($\Delta U, \Delta V, \Delta W$) and the perturbed Euler angles ($\Delta \theta, \Delta \phi, \Delta \psi$) and their derivatives. Longitudinal (X-Z-M) and lateral (Y-L-N) equations are not coupled.

Coefficients of the variables in these equations are constants whose values are determined by the aircraft's geometric and mass properties and its equilibrium speed, U_0 . These coefficients will be developed in literal form in Section 6.0.

6.0 Summary of Analytical Expressions for Stability Derivatives

The equations of motion developed in Section V have specified a set of aircraft stability derivatives (e.g. X_u) which are defined analytically in this section.

Each derivative represents the (partial) change in a force (or moment) due to an incremental change in a variable from the reference value. Thus the derivative X_u represents the change in force along the aircraft X_A axis due to a change in forward speed, or

$$X_u = \left. \frac{\partial X}{\partial U} \right|_0$$

where the subscript 0 indicates that $\partial X/\partial U$ is to be evaluated at the reference (equilibrium) flight condition.

Definition of these derivatives here will utilize extensively the material contained in Chapter 4 of Reference 2. Emphasis in this report will be placed on assembling the desired material into a compact and usable form rather than on repeating the derivations given in the reference.

Reference 2 develops the derivatives in their non-dimensional form. Table 4.1 of the reference defines the relation between these non-dimensional coefficients and the dimensional coefficients used here. For example,

$$X_u = \frac{qS}{U_0} C_{x_u} \quad \frac{\text{lbs}}{\text{fps}}$$

Analytical expressions for the non-dimensional coefficients are derived in References 1, 2, and 3 and are reproduced here. For example, on pp 148-150 of Reference 2 is developed an expression for C_{x_u} :

$$C_{x_u} = -3 C_{D_0} - C_{L_0} \tan \theta_0 \text{ (constant speed prop)}$$

Table I presents similar information for each of the required derivatives: Each derivative is defined in terms of the corresponding non-dimensional derivative. Then, the expression for the non-dimensional derivative is given together with the source of the expression.

In Section 7.0, these expressions are evaluated for the "Buffalo" and "Twin Otter" aircraft at several flight conditions

TABLE I
ANALYTICAL EXPRESSIONS FOR STABILITY DERIVATIVES

$X_u = \frac{qS}{U_0} C_{x_u} \frac{\text{lbs}}{\text{fps}}$	$C_{x_u} = -3 C_{D_0} - C_{L_0} \tan \theta_0$ (constant speed prop) (Ref. 2, pp 148-150)
$X_w = \frac{qS}{U_0} C_{x_\alpha} \frac{\text{lbs}}{\text{fps}}$	$C_{x_\alpha} = C_{L_0} \left(1 - \frac{2C_{L\alpha}}{\pi eAR} \right)$ (Ref. 2, p 147)
$Z_u = \frac{qS}{U_0} C_{z_u} \frac{\text{lbs}}{\text{fps}}$	$C_{z_u} = -2 C_{L_0}$ (Ref. 2, pp 129-130, p 150)
$Z_w = \frac{qS}{U_0} C_{z_\alpha} \frac{\text{lbs}}{\text{fps}}$	$C_{z_\alpha} = -(C_{L\alpha} + C_{D_0})$ (Ref. 2, p 147)
$Z_{\dot{w}} = \frac{c}{2U_0^2} qS C_{z_{\dot{\alpha}}} \frac{\text{lbs}}{\text{ft/sec}^2}$	$C_{z_{\dot{\alpha}}} = -2 a_T \eta_T \frac{l_t}{c} \frac{S_T}{S} \frac{d\varepsilon}{d\alpha}$ (tail contribution) (Ref. 2, p 165)
$Z_q = \frac{c}{2U_0} qS C_{z_q} \frac{\text{lbs}}{\text{rad/sec}}$	$C_{z_q} = -2 a_T \eta_T \frac{l_t}{c} \frac{S_T}{S}$ (tail contribution) (Ref. 2, p 154)
$Z_{\delta_e} = qS C_{z_{\delta_e}} \frac{\text{lbs}}{\text{rad}}$	$C_{z_{\delta_e}} = a_T \frac{d\alpha_T}{d\delta_e} \frac{S_T}{S} \eta_T$ (Ref. 3, p 250)
$M_u = \frac{qSc}{U_0} C_{m_u} \frac{\text{ft lbs}}{\text{fps}}$	$C_{m_u} = 0$ (Ref. 2, p 151)
$M_w = \frac{qSc}{U_0} C_{m_\alpha} \frac{\text{ft lbs}}{\text{fps}}$	$C_{m_\alpha} = C_{L_\alpha} (h-h_n)$ (Ref. 2, p147)
$M_{\dot{w}} = \frac{c}{2U_0^2} qSc C_{m_{\dot{\alpha}}} \frac{\text{ft lbs}}{\text{fps}^2}$	$C_{m_{\dot{\alpha}}} = C_{z_{\dot{\alpha}}} \frac{l_T}{c}$ (tail only) (Ref. 2, p 165)
$M_q = \frac{c}{2U_0} qSc C_{m_q} \frac{\text{ft lbs}}{\text{rad/sec}}$	$C_{m_q} = C_{z_q} \frac{l_T}{c}$ (tail only) (Ref. 2, p 155)
$M_{\delta_e} = qSc C_{m_{\delta_e}} \frac{\text{ft lbs}}{\text{rad}}$	$C_{m_{\delta_e}} = C_{z_{\delta_e}} \frac{l_T}{c}$ (Ref. 3, p 250)

TABLE I (continued)

$Y_v = \frac{qS}{U_o} C_{Y_\beta} \frac{\text{lbs}}{\text{fps}}$	$C_{Y_\beta} \approx -a_F \frac{S_F}{S} \left(1 - \frac{d\sigma}{d\beta}\right) \text{ (tail only)}$ <p>(Ref. 2, p 168)</p>
$Y_p = \frac{b}{2U_o} qS C_{Y_p} \frac{\text{lbs}}{\text{rad/sec}}$	$C_{Y_p} \approx C_{Y_{pF}} = -\frac{2}{3} a_F \frac{b_F S_F}{b S} \frac{1+2\lambda_F}{1+\lambda_F}$ <p>(App. A, this report)</p>
$Y_r = \frac{b}{2U_o} qS C_{Y_r} \frac{\text{lbs}}{\text{rad/sec}}$	$C_{Y_r} \approx C_{Y_{rF}} = 2 a_F \frac{l_F S_F}{b S}$ <p>(tail only) (Ref. 2, p 74)</p>
$Y_{\delta_r} = qS C_{Y_{\delta_r}} \frac{\text{lbs}}{\text{rad}}$	$C_{Y_{\delta_r}} = -a_F \frac{S_F}{S} \cdot \frac{d\alpha_F}{d\delta_r}$ <p>(Ref. 3, p 329)</p>
$L_v = \frac{qSb}{U_o} C_{l_\beta} \frac{\text{ft lbs}}{\text{fps}}$	$C_{l_\beta} = C_{l_{\beta_w}} + C_{l_{\beta_{\text{fuselage}}}} + C_{l_{\beta_F}}$ <p>$C_{l_{\beta_w}}$: See item 90, Table III</p> $C_{l_{\beta_{\text{fuse}}}} \approx 1.2 \sqrt{AR} \frac{Zw}{b} \cdot \frac{h+w}{b} \text{ (Ref. 2, p 486)}$ $C_{l_{\beta_F}} = C_{Y_\beta} \frac{ZF}{b} \text{ (Ref. 2, p 89)}$
$L_p = \frac{b}{2U_o} qSb C_{l_p} \frac{\text{ft lbs}}{\text{rad/sec}}$	C_{l_p} : See item 91, Table III
$L_r = \frac{b}{2U_o} qSb C_{l_r} \frac{\text{ft lbs}}{\text{rad/sec}}$	$C_{l_r} = C_{l_{r_w}} + C_{l_{r_F}}$ $C_{l_{r_w}} = C_{L_o} / 4 \text{ (Ref. 1, p 112)}$ $C_{l_{r_F}} = C_{Y_r} \frac{ZF}{b} \text{ (Ref. 2, p 175)}$
$L_{\delta_r} = qSb C_{l_{\delta_r}} \frac{\text{ft lbs}}{\text{rad}}$	$C_{l_{\delta_r}} = C_{Y_{\delta_r}} \cdot \frac{ZF}{b} \text{ (Ref. 3, p 329)}$

TABLE I (continued)

$L_{\delta a} = qSb C_{l_{\delta a}} \frac{\text{ft lbs}}{\text{rad}}$	$C_{l_{\delta a}} = \frac{2a\tau}{SB} \int_{y_1}^{y_2} cy dy \quad (\text{Ref. 3, p 354})$
$N_v = \frac{qSb}{U_o} C_{n_{\beta}} \frac{\text{ft lbs}}{\text{fps}}$	$C_{n_{\beta}} = C_{n_{\beta F}} + C_{n_{\beta}} \text{ fuselage}$ $C_{n_{\beta F}} = - C_{y_{\beta F}} \frac{l_F}{b} \quad (\text{Ref. 2, p 82})$ $C_{n_{\beta}} \text{ fuselage}$ $= - 1.3 \frac{\text{volume of fuseage}}{Sb} \cdot \frac{h}{w}$ <p style="text-align: right;">(Ref. 2, p 492)</p>
$N_p = \frac{b}{2U_o} qSb C_{n_p} \frac{\text{ft lbs}}{\text{rad/sec}}$	$C_{n_p} = C_{n_{pw}} + C_{n_{pF}}$ $C_{n_{pw}} = - \frac{C_{L_o}}{4} \left[1 - \frac{C_{L_{\alpha}}}{\pi AR} \right] \quad (\text{App A, this report})$ $C_{n_{pF}} = - C_{y_{pF}} \frac{l_F}{b} \quad (\text{Ref. 2, p 171})$
$N_r = \frac{b}{2U_o} qSb C_{n_r} \frac{\text{ft lbs}}{\text{rad/sec}}$	$C_{n_r} = C_{n_{rF}} + C_{n_{rw}}$ $C_{n_{rF}} = - \frac{l_r}{b} C_{y_{rF}} \quad (\text{Ref. 1, p 112})$ $C_{n_{rw}} = - C_{D_w} / 4 \quad (\text{Ref. 1, p 112})$
$N_{\delta r} = qSb C_{n_{\delta r}} \frac{\text{ft lbs}}{\text{rad}}$	$C_{n_{\delta r}} = - C_{y_{\delta r}} \frac{l_F}{b} \quad (\text{Ref. 3, p 329})$
$N_{\delta a} = qSb C_{n_{\delta a}} \frac{\text{ft lbs}}{\text{rad}}$	$C_{n_{\delta a}} : \text{no simple analytical expression available; assumed zero here.}$

7.0 Tabulation of Analytically-Determined Stability Derivative Values for DeHavilland "Buffalo" and "Twin Otter"

In this section, stability derivatives and other numerical data required to model these aircraft are presented. The derivatives are estimated using the analytical expressions summarized in Section 6.0.

Step-by-step calculation of each derivative is carried out in Appendix C. The geometric and mass data needed in Appendix C to calculate the derivatives have been obtained from Reference 4; this material is summarized in Figures 3 and 4 of this report.

For each aircraft, three flight conditions are investigated. These are: cruise, slow flight, and landing approach. Table II presents the parameters needed to define each of these flight conditions.

All stability derivative information is summarized in Tables III, IV, and V. In Table III, the non-dimensional derivatives calculated in Appendix C are collected and presented for both aircraft at all three flight conditions. In Table IV, the derivatives are presented in their "dimensional" form, utilizing the definitions of Table I.

For convenience, the derivatives are also presented in "normalized" form in Table V. The "normalized" derivatives are obtained by dividing each dimensional derivative by the appropriate mass or inertia parameter. Specifically, force derivatives are divided by m , aircraft mass. The roll, pitch, and yaw moment derivatives are divided by I_x , I_y , and I_z , respectively.

TABLE II

Definition of Flight Conditions

	Buffalo			Twin Otter		
	Cruise	Slow Flight	Landing Approach	Cruise	Slow Flight	Landing Approach
W, weight, lbs	40000	40000	40000	12000	12000	12000
U_0 , speed, fps	400	215	154	278	176	120
h, altitude, ft	10000	0	0	10000	0	0
γ_0 , flight path angle, degrees	0	0	-7.5	0	0	-7.5
δ_f , flap deflection, degrees	0	0	40	0	0	40

Note: 1 Normal C.G. used for all flight conditions.

2 Max T.O. weight for "Twin Otter" is listed as 11,579 lbs in Ref. 4. However, later editions of Ref. 4 show an increase to 12500 lbs. The weight to be used here has been arbitrarily chosen as 12000 lbs.

3 $\theta_0 = \gamma_0$ in this report because of use of stability axis system.

TABLE III Summary of Derivatives in Non-Dimensional Form

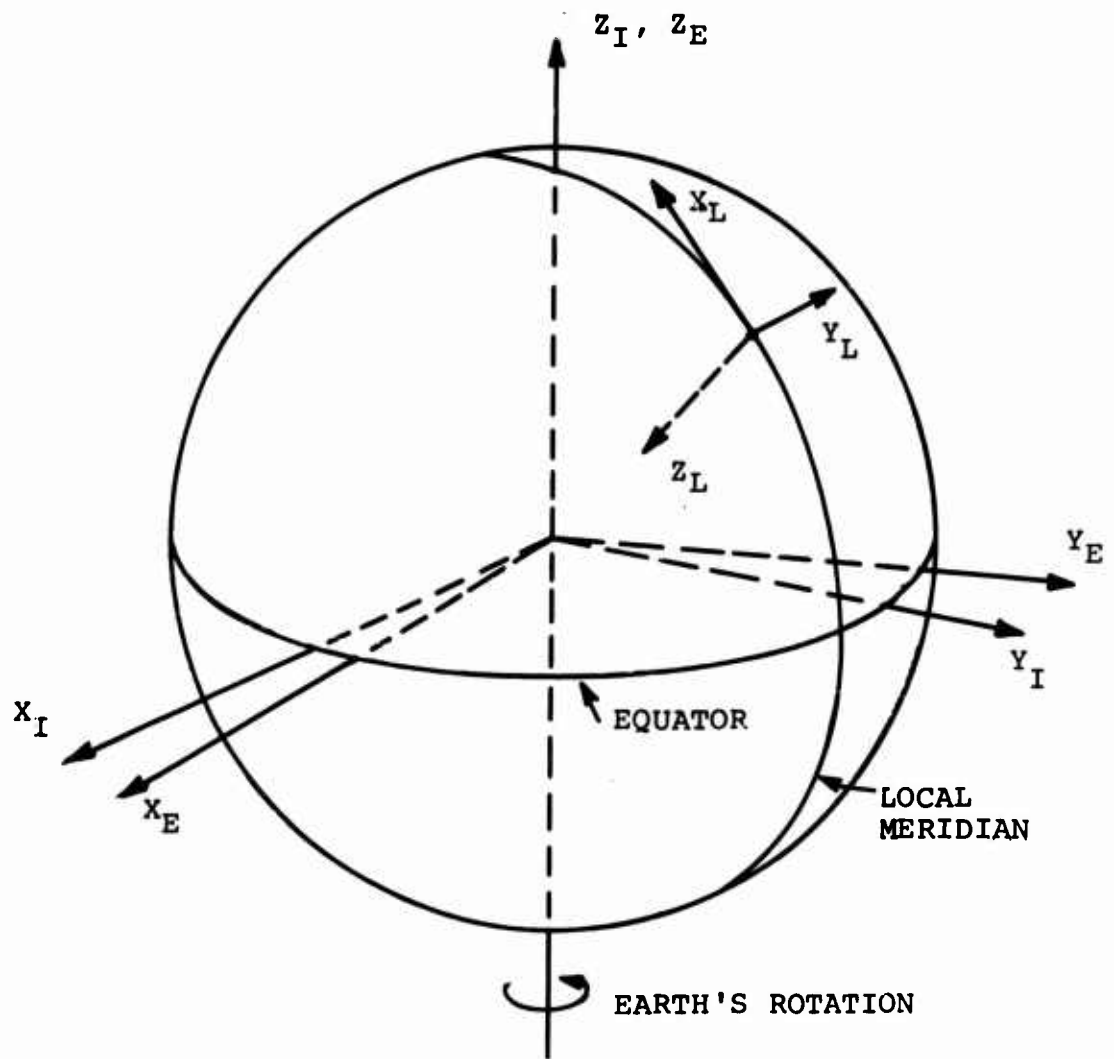
Non-Dimensional Derivative	Buffalo			Twin Otter		
	Cruise	Slow Flight	Landing Approach	Cruise	Slow Flight	Landing Approach
C_{x_u}	-.108	-.171	-.186	-.141	-.195	-.237
C_{x_α}	.164	.441	.815	.234	.435	.920
C_{z_u}	-.60	-1.54	-2.98	-.84	-1.56	-3.30
C_{z_α}	-5.24	-5.26	-5.33	-5.25	-5.27	-5.36
$C_{z_{\dot{\alpha}}}$	-1.33	-1.33	-1.33	-1.60	-1.60	-1.60
C_{z_q}	-7.83	-7.83	-7.83	-6.40	-6.40	-6.40
$C_{z_{\delta_e}}$.465	.465	.465	.450	.450	.450
C_{m_u}	0	0	0	0	0	0
C_{m_α}	-.78	-.78	-.78	-.78	-.78	-.78
$C_{m_{\dot{\alpha}}}$	-6.05	-6.05	-6.05	-6.15	-6.15	-6.15
C_{m_q}	-35.6	-35.6	-35.6	-24.6	-24.6	-24.6
$C_{m_{\delta_e}}$	2.12	2.12	2.12	1.73	1.73	1.73
C_{y_β}	-.362	-.362	-.362	-.492	-.492	-.492
C_{y_p}	-.055	-.055	-.055	-.085	-.085	-.085
C_{y_r}	.368	.368	.368	.429	.429	.429
$C_{y_{\delta_r}}$	-.233	-.233	-.233	-.317	-.317	-.317
C_{l_β}	-.125	-.125	-.125	-.103	-.103	-.103
C_{l_p}	-.53	-.53	-.53	-.60	-.60	-.60
C_{l_r}	.113	.231	.410	.138	.233	.451
$C_{l_{\delta_r}}$	-.024	-.024	-.024	-.024	-.024	-.024
$C_{l_{\delta_a}}$.20	.20	.20	.38	.38	.38
C_{n_β}	.101	.101	.101	.121	.121	.121
C_{n_p}	-.037	-.134	-.283	-.054	-.129	-.310
C_{n_r}	-.171	-.175	-.188	-.171	-.174	-.191
$C_{n_{\delta_r}}$.107	.107	.107	.124	.124	.124
$C_{n_{\delta_a}}$	0	0	0	0	0	0

TABLE IV Summary of Derivatives in Dimensional Form

Dimensional Derivative	Buffalo			Twin Otter		
	Cruise	Slow Flight	Landing Approach	Cruise	Slow Flight	Landing Approach
X_u lbs/fps	-35.7	-41.4	-32.4	-14.5	-17.2	-14.5
X_w lbs/fps	54.3	106.8	141.8	24.1	38.2	56.1
Z_u lbs/fps	-199	-372	-519	-86.5	-137	-201
Z_w lbs/fps	-1733	-1273	-927	-541	-464	-327
$Z_{\dot{w}}$ lbs/fps ²	-5.55	-7.56	-7.60	-1.93	-2.16	-2.19
Z_q $\frac{\text{lbs}}{\text{rad/sec}}$	-13,090	-9560	-6900	-2155	-1836	-1253
Z_{δ_e} $\frac{\text{lbs}}{\text{rad}}$	61600	24150	12500	12920	6975	3265
M_u $\frac{\text{ft-lbs}}{\text{fps}}$	0	0	0	0	0	0
M_w $\frac{\text{ft-lbs}}{\text{fps}}$	-2610	-1910	-1372	-520	-446	-306
$M_{\dot{w}}$ $\frac{\text{ft-lbs}}{\text{fps}^2}$	-255	-347	-347	-48	-65	-65
M_q $\frac{\text{ft-lbs}}{\text{rad/sec}}$	$-.600 \times 10^6$	$-.440 \times 10^6$	$-.317 \times 10^6$	$-.534 \times 10^5$	$-.459 \times 10^5$	$-.313 \times 10^5$
M_{δ_e} $\frac{\text{ft-lbs}}{\text{rad}}$	2.84×10^6	1.112×10^6	$.575 \times 10^6$	$.320 \times 10^6$	$.174 \times 10^6$	$.0615 \times 10^6$
Y_v lbs/fps	-120	-87.5	-63	-50.6	-43.1	-30.0
Y_p $\frac{\text{lbs}}{\text{rad/sec}}$	-880	-637	-460	-284	-243	-167
Y_r $\frac{\text{lbs}}{\text{rad/sec}}$	5850	4260	3070	1430	1228	840
Y_{δ_r} $\frac{\text{lbs}}{\text{rad}}$	-30,800	-12,100	-6,260	-9100	-4910	-2300
L_v $\frac{\text{ft-lbs}}{\text{fps}}$	-3980	-2900	-2085	-686	-589	-404
L_p $\frac{\text{ft-lbs}}{\text{rad/sec}}$	$-.80 \times 10^6$	$-.59 \times 10^6$	$-.426 \times 10^6$	-13000	-111800	-76400
L_r $\frac{\text{ft-lbs}}{\text{rad/sec}}$	$+1.73 \times 10^5$	$+2.58 \times 10^5$	$+3.30 \times 10^5$	+30000	+43500	+57400
L_{δ_r} $\frac{\text{ft-lbs}}{\text{rad}}$	-3.06×10^5	-1.20×10^5	$-.62 \times 10^5$	-44500	-24200	-11300
L_{δ_a} $\frac{\text{ft-lbs}}{\text{rad}}$	$+2.55 \times 10^6$	$+1.00 \times 10^6$	$+5.16 \times 10^6$	$+7.05 \times 10^5$	$+3.83 \times 10^5$	$+1.79 \times 10^5$
N_v $\frac{\text{ft-lbs}}{\text{fps}}$	3215	2340	1685	806	692	475
N_p $\frac{\text{ft-lbs}}{\text{rad/sec}}$	-56500	-149500	-22800	-11700	-24100	-39500
N_r $\frac{\text{ft-lbs}}{\text{rad/sec}}$	-2.62×10^5	-1.95×10^5	-1.51×10^5	-37100	-32400	-24300
N_{δ_r} $\frac{\text{ft-lbs}}{\text{rad}}$	1.365×10^6	$.535 \times 10^6$	$.276 \times 10^6$	2.30×10^5	1.25×10^5	$.585 \times 10^5$
N_{δ_a} $\frac{\text{ft-lbs}}{\text{rad}}$	0	0	0	0	0	0

TABLE V Summary of Derivatives in Normalized Form

Normalized Derivative	Buffalo			Twin Otter		
	Cruise	Slow Flight	Landing Approach	Cruise	Slow Flight	Landing Approach
X_U/m	-.0288	-.0334	-.0261	-.039	-.0462	-.039
X_W/m	.0437	.0860	.114	.065	.1027	.151
Z_U/m	-.160	-.300	-.418	-.232	-.368	-.540
Z_W/m	-1.397	-1.026	-0.747	-1.454	-1.247	-0.880
$Z_{\dot{W}}/m$	-.0045	-.0061	-.0061	-.0052	-.0058	-.0059
Z_Q/m	-10.53	-7.70	-5.55	-5.80	-4.93	-3.37
Z_{δ_e}/m	49.6	19.45	10.08	34.8	18.72	8.79
M_U/I_y	0	0	0	0	0	0
M_W/I_y	-.0121	-.0089	-.0064	-.0236	-.0202	-.0139
$M_{\dot{W}}/I_y$	-.0012	-.0016	-.0016	-.0022	-.0030	-.0030
M_Q/I_y	-2.79	-2.04	-1.47	-2.42	-2.08	-1.42
M_{δ_e}/I_y	13.2	5.17	2.675	14.52	7.9	3.7
Y_V/m	-.097	-.0705	-.0508	-.136	-.116	-.0806
Y_P/m	-.710	-.514	-.371	-.764	-.654	-.449
Y_R/m	4.71	3.44	2.48	3.84	3.30	2.26
Y_{δ_r}/m	-24.8	-9.76	-5.05	-24.4	-13.2	-6.19
L_V/I_x	-.0146	-.0106	-.0076	-.0282	-.0242	-.0166
L_P/I_x	-2.96	-2.16	-1.56	-5.35	-4.60	-3.14
L_R/I_x	.633	.945	1.208	1.233	1.790	2.360
L_{δ_r}/I_x	-1.12	-.44	-.227	-1.83	-.996	-.465
L_{δ_a}/I_x	9.34	3.66	1.89	29.0	15.77	7.36
N_V/I_z	.0072	.0052	.0038	.0197	.0169	.0116
N_P/I_z	-.126	-.334	-.510	-.286	-.588	-.965
N_R/I_z	-.586	-.436	-.338	-.905	-.790	-.593
N_{δ_r}/I_z	3.05	1.195	.617	5.61	3.05	1.43
N_{δ_a}/I_z	0	0	0	0	0	0



I: INERTIAL COORDINATE FRAME

E: EARTH-CENTERED COORDINATE FRAME

L: EARTH LOCAL-VERTICAL COORDINATE FRAME

FIGURE 1: REFERENCE COORDINATE FRAMES

- L: EARTH LOCAL VERTICAL COORDINATE FRAME
- C: EARTH-AIRCRAFT CONTROL COORDINATE FRAME
- A: AIRCRAFT BODY COORDINATE FRAME

EULER ANGLES

Ψ = ROTATION ABOUT Z_L AXIS

Θ = ROTATION ABOUT Y_C AXIS

Φ = ROTATION ABOUT X_A AXIS

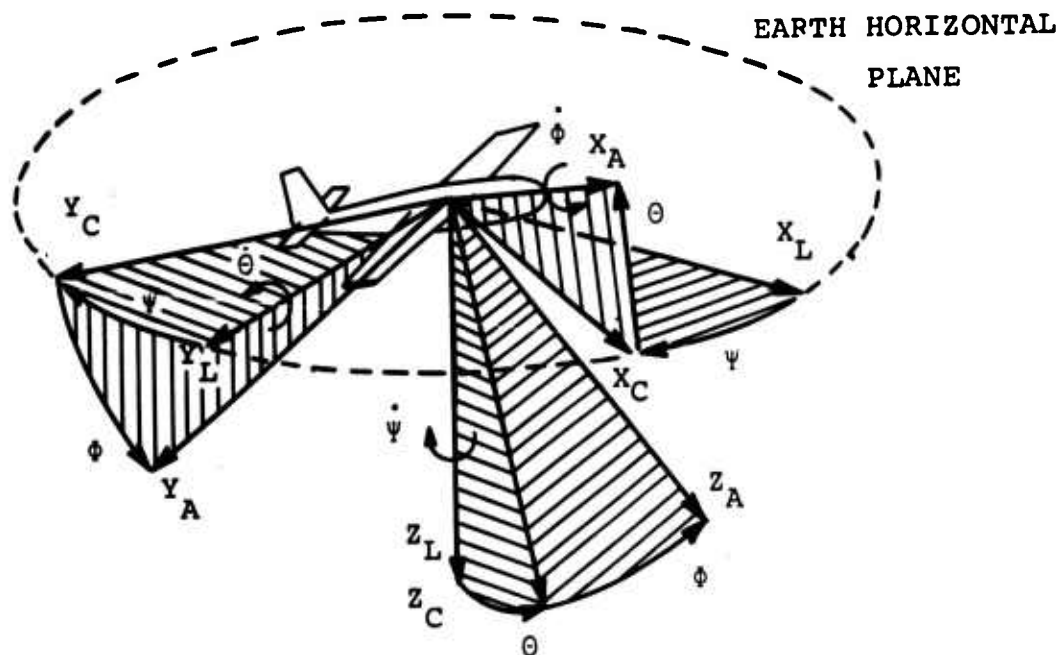
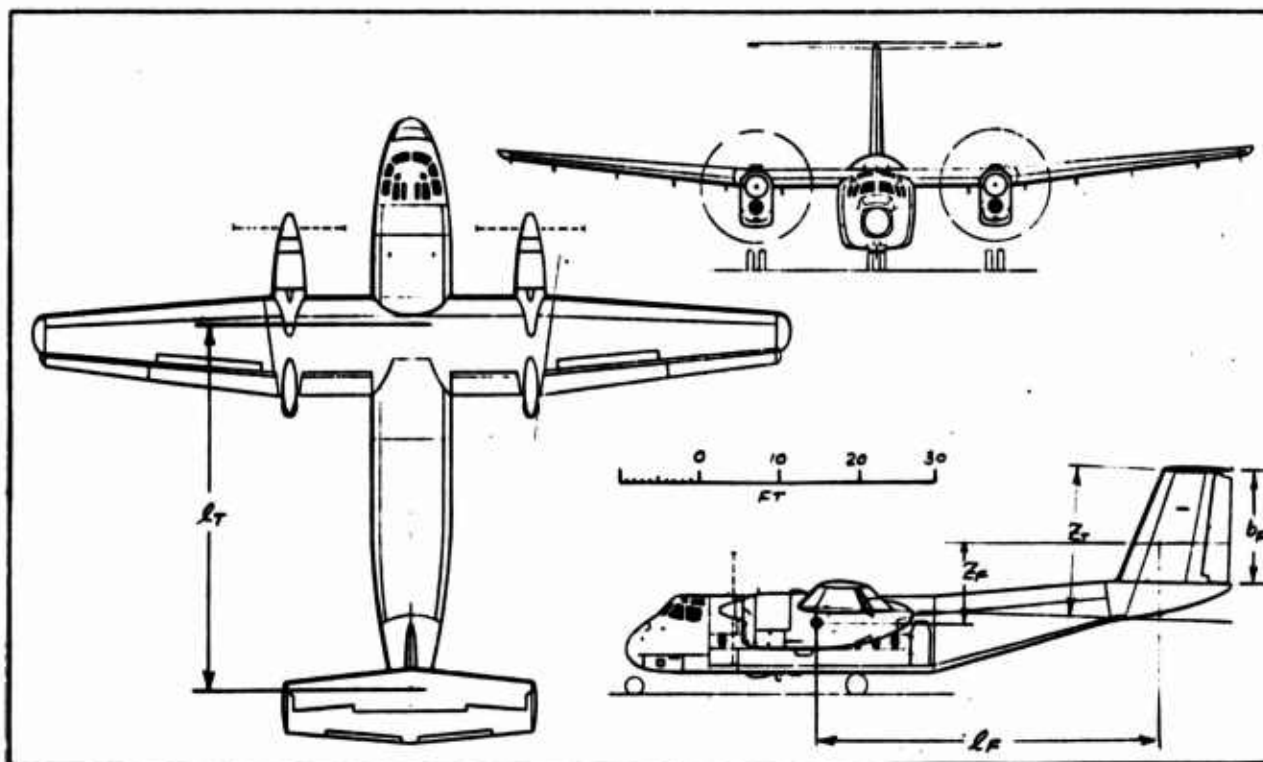


FIGURE 2: ADDITIONAL REFERENCE COORDINATE FRAMES



DHC-5 Buffalo twin-turboprop STOL utility transport

DHC-5 BUFFALO

Differences between the US and Canadian versions are as follows:

CV-7A. US model, with 2,850 cshp General Electric T64/GP-10 turboprops. Overall length 77 ft 4 in (23.57 m). Designation may be changed following transfer of responsibility for aircraft in this category from US Army to USAF.

CC-115. Canadian Defence Force model, with 3,055 cshp General Electric T64/P2 turboprops. Overall length 79 ft 0 in (24.08 m). Otherwise similar to CV-7A, with only small differences in performance.

WINGS: Cantilever high-wing monoplane. Wing section NACA 64A417.5 (mod) at root, NACA 63A615 (mod) at tip. Aspect ratio 9.75. Chord 11 ft 9 1/2 in (3.59 m) at root, 5 ft 11 in (1.80 m) at tip. Dihedral 0° inboard of nacelle, 5° outboard. Incidence 2° 30'. Sweepback at quarter-chord 1° 40'. Conventional fail-safe multi-spar structure of high-strength aluminium alloy. Full-span double-slotted aluminium alloy flaps, outboard sections functioning as ailerons. Aluminium alloy slot-lip spoilers, forward of inboard flaps, are actuated by Jarry Hydraulics unit. Spoilers coupled to manually-operated ailerons for lateral control, uncoupled for symmetrical ground operation. Electrically-actuated trim-tab in starboard aileron. Geared tab in each aileron. Rudder-aileron interconnect tab on port aileron. Outer wing leading-edges fitted with electrically-controlled flush pneumatic rubber de-icer boots.

FUSELAGE: Fail-safe structure of high-strength aluminium alloy. Cargo floor supported by longitudinal keel members.

TAIL UNIT: Cantilever structure of high-strength aluminium alloy, with fixed-incidence tailplane mounted at tip of fin. Elevator aerodynamically and mass-balanced. Fore and trailing serially-hinged rudders are powered by tandem systems manufactured by Jarry Hydraulics. Trim-tab on port elevator, spring-tab on starboard elevator. Electrically-controlled flush pneumatic rubber de-icer boot on tailplane leading-edge.

LANDING GEAR: Retractable tricycle type. Hydraulic retraction, nose unit aft, main units forward. Jarry Hydraulics oleo-pneumatic shock-absorbers. Goodrich main wheels and tyres, size 37-00 x 15-00-12, pressure 45 lb/sq in (3.16 kg/cm²). Goodrich nose wheels and tyres size 8-00 x 12-50, pressure 38 lb/sq in (2.67 kg/cm²). Goodrich multi-disc brakes.

POWER PLANT: Two General Electric T64 turboprop engines (details under entries for individual versions, above), each driving a Hamilton Standard 63E60-13 three-blade propeller, diameter 14 ft 6 in (4.42 m). Fuel in one integral tank in each inner wing, capacity 533 Imp gallons (2,423 litres) and rubber bag tanks in each outer wing, capacity 336 Imp gallons (1,527 litres). Total fuel capacity 1,739 Imp gallons (7,900 litres). Refuelling points above wings and in side of fuselage for pressure refuelling. Total oil capacity 10 Imp gallons (45.6 litres).

DIMENSIONS, EXTERNAL:

Wing span	96 ft 0 in (29.26 m)
Length overall:	
CV-7A	77 ft 4 in (23.57 m)
CC-115	79 ft 0 in (24.08 m)
Height overall	29 ft 8 in (9.13 m)
Tailplane span	32 ft 0 in (9.75 m)
Wheel track	30 ft 6 in (9.29 m)
Wheelbase	27 ft 11 in (8.50 m)
Cabin doors (each side):	
Height	5 ft 6 in (1.68 m)
Width	2 ft 9 in (0.84 m)
Height to sill	3 ft 10 in (1.17 m)
Emergency exits (each side, below wing leading-edge):	
Height	3 ft 4 in (1.02 m)
Width	2 ft 2 in (0.66 m)
Height to sill approx	5 ft 0 in (1.52 m)
Rear cargo loading door and ramp:	
Height	20 ft 0 in (6.33 m)
Width	7 ft 8 in (2.33 m)
Height to ramp hinge	3 ft 10 in (1.17 m)

DIMENSIONS, INTERNAL:

Cabin, excluding flight deck:	
Length, cargo floor	31 ft 5 in (9.58 m)
Max width	8 ft 9 in (2.67 m)
Max height	6 ft 10 in (2.08 m)
Floor area	243.5 sq ft (22.63 m ²)
Volume	1,715 cu ft (48.56 m ³)

AREAS:

Wings, gross	943 sq ft (87.8 m ²)
Ailerons (total)	30 sq ft (3.62 m ²)
Trailing-edge flaps (total, including ailerons)	280 sq ft (26.01 m ²)
Spoilers (total)	25.2 sq ft (2.34 m ²)
Fin	92 sq ft (8.55 m ²)
Rudder, including tab	60 sq ft (5.57 m ²)
Tailplane	151.5 sq ft (14.07 m ²)
Elevators, including tab	81.5 sq ft (7.57 m ²)

WEIGHTS AND LOADINGS:

Operating weight empty, including 3 crew at 200 lb (91 kg) each, plus trapped fuel and oil and full cargo handling equipment	23,157 lb (10,505 kg)
Max payload	13,843 lb (6,279 kg)
Max T-O weight	41,000 lb (18,598 kg)
Max zero-fuel weight	37,000 lb (16,783 kg)
Max landing weight	39,000 lb (17,690 kg)
Max wing loading	43.4 lb/sq ft (212 kg/m ²)
Max power loading	7.2 lb/cshp (3.27 kg/cshp)

PERFORMANCE (CV-7A, at max T-O weight):

Max level speed at 10,000 ft (3,050 m)	271 mph (435 kmh)
Max permissible diving speed	334 mph (537 kmh)
Max cruising speed at 10,000 ft (3,050 m)	271 mph (435 kmh)
Econ cruising speed at 10,000 ft (3,050 m)	208 mph (333 kmh)
Stalling speed, 40° flaps at 39,000 lb (17,690 kg) AEW	75 mph (120 kmh)
Stalling speed, flaps up at max AEW	105 mph (169 kmh)
Rate of climb at S/L	1,890 ft (575 m) min
Service ceiling	30,000 ft (9,150 m)
Service ceiling, one engine out	14,300 ft (4,360 m)
T-O run on firm dry sod	1,040 ft (317 m)
T-O to 50 ft (15 m) from firm dry sod	1,540 ft (470 m)
Landing from 50 ft (15 m) on firm dry sod	1,120 ft (342 m)
Landing run on firm dry sod	610 ft (186 m)

Source: Reference 4

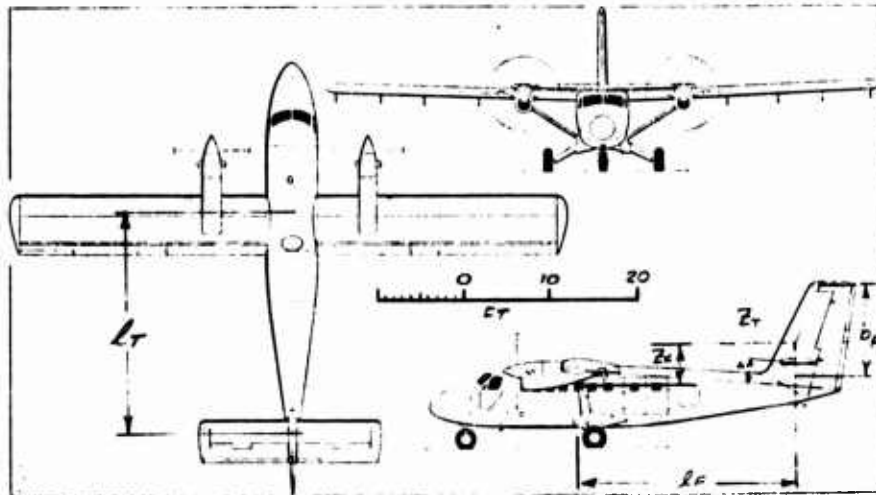
Figure 3

DHC-6 TWIN OTTER

Announced in August 1964, the Twin Otter is a STOL transport powered by two Pratt & Whitney (UAC) PT6A-20 turboprop engines. Design work began in January 1964. Construction of an initial batch of Twin Otters was started in November of the same year and the first of these flew on May 20, 1965.

At the beginning of 1967, a total of 32 Twin Otters had been delivered or were on order, with options on 11 more. They included eight for the Cuban Air Force, two for Trans-Australian Airlines, one for the Canadian Department of Lands and Forests, four for Aerapi of Italy, one for Northern Consolidated Airlines, and others for Pilgrim Airlines and Air Wisconsin, USA. Production was scheduled to be at the rate of six a month through 1967.

Under development for delivery in 1968 is a version of the Twin Otter with more powerful (610 cshp) Pratt & Whitney PT6A-27 turboprop engines, longer nose to provide more baggage space, and AEW of 12,500 lb (5,670 kg). The following data refer to the current production model.



de Havilland Canada DHC-6 Twin Otter twin-turboprop transport

TYPE: Twin-turboprop STOL transport.

WINGS: Braced high-wing monoplane, with a single streamline-section bracing strut on each side. Wing section NACA 8A series mean line; NACA 0018 (modified) thickness distribution. Aspect ratio 10. Constant chord of 6 ft 6 in (1.98 m). Dihedral 2°. Incidence 2° 30'. No sweepback. All-metal safe-life structure. All-metal ailerons which also droop for use as flaps. Double-slotted all-metal full-span trailing-edge flaps. No spoilers. Trim-tabs in ailerons. Pneumatic-boost de-icing equipment optional.

FUSELAGE: Conventional all-metal semi-monocoque safe-life structure.

TAIL UNIT: Cantilever all-metal structure of high-strength aluminium alloys. Fin integral with fuselage. Fixed-incidence tailplane. Trim-tabs in rudder and port elevator, latter interconnected with flaps. Pneumatic de-icing boots on tailplane leading-edge optional.

LANDING GEAR: Non-retractable tricycle type, with steerable nose-wheel. Rubber shock-absorption on main units. Oleo-pneumatic nose-wheel shock-absorber. Goodyear main wheel tyres size 11-00 x 12, pressure 32 lb/sq in (2.25 kg/cm²). Goodyear nose-wheel tyre size 8-00 x 12-50, pressure 31 lb/sq in (2.18 kg/cm²). Goodrich hydraulic brakes. Provision for alternative float and ski gear.

POWER PLANT: Two 579 cshp Pratt & Whitney (UAC) PT6A-20 turboprop engines, each driving a Hartzell three-blade reversible-pitch fully-feathering metal propeller, diameter 8 ft 0 in (2.44 m). Fuel in two tanks (8 cells) under cabin floor; total capacity 919 Imp gallons (4,178 litres). Two refuelling points on port side of fuselage. Oil capacity 2 Imp gallons (9 litres) per engine. Electric de-icing system for propellers and air-intakes optional.

Accommodation: Two seats side-by-side on flight deck. Seats for 13-18 passengers in main cabin. Cabin divided by bulkhead into main passenger or freight compartment and baggage or toilet compartment. Door on each side of main cabin, at rear. Baggage compartments in nose and aft of cabin, each with upward-hinged door on port side.

SYSTEMS: Hydraulic system, pressure 1,500 lb/sq in (105 kg/cm²), for flaps, brakes and nose-wheel steering. No pneumatic system. One 200A starter-generator on each engine.

ELECTRONICS AND EQUIPMENT: Radio and radar to customer's specification. Blind-flying instrumentation standard.

DIMENSIONS, EXTERNAL:

Wing span	65 ft 0 in (19.81 m)
Length overall	49 ft 6 in (15.09 m)
Height overall	18 ft 7 in (5.69 m)
Tailplane span	21 ft 0 in (6.40 m)
Wheel track	12 ft 5 in (3.78 m)
Wheelbase	14 ft 8 in (4.50 m)
Passenger door (port side):	
Height	4 ft 2 in (1.27 m)
Width	2 ft 6 in (0.76 m)
Height to sill	3 ft 10 in (1.17 m)
Passenger door (starboard side):	
Height	3 ft 9 in (1.15 m)

Width	2 ft 6 in (0.76 m)
Height to sill	3 ft 10 in (1.17 m)
Baggage compartment door (nose):	
Height to sill	3 ft 10 in (1.17 m)
Baggage compartment door (port, rear):	
Height	4 ft 2 in (1.27 m)
Width	4 ft 8 in (1.42 m)
Height to sill	3 ft 10 in (1.17 m)

DIMENSIONS, INTERNAL:

Cabin, excluding flight deck, galley and baggage or toilet compartment:	
Length	18 ft 6 in (5.64 m)
Max width	5 ft 3 in (1.60 m)
Max height	4 ft 11 in (1.50 m)
Floor area	80.2 sq ft (7.45 m ²)
Volume	381 cu ft (10.87 m ³)
Baggage compartment (nose) volume	22 cu ft (0.62 m ³)
Baggage compartment (rear) volume	52 cu ft (1.47 m ³)

AREAS:

Wings, gross	420 sq ft (39.02 m ²)
Ailerons (total)	33.2 sq ft (3.08 m ²)
Trailing-edge flaps (total)	112.2 sq ft (10.42 m ²)
Fin	48.0 sq ft (4.46 m ²)
Rudder, including tab	34.0 sq ft (3.16 m ²)

Tailplane	100 sq ft (9.29 m ²)
Elevators, including tab	35 sq ft (3.25 m ²)

WEIGHTS:

Basic operating weight, including pilot (170 lb = 77 kg), radio (100 lb = 45 kg) and full oil	6,170 lb (2,800 kg)
Max payload (for 100 miles = 160 km range)	4,430 lb (2,010 kg)
Max T.O weight	11,570 lb (5,252 kg)
Max landing weight	11,000 lb (4,990 kg)

PERFORMANCE (at max T.O weight):

Max cruising speed at 10,000 ft (3,050 m)	184 mph (297 km/h)
Econ cruising speed at 10,000 ft (3,050 m)	156 mph (251 km/h)
Landing speed	64.5 mph (104 km/h)
Rate of climb at 8,120 ft (2,472 m) min	1,536 ft (472 m) min
Service ceiling	25,500 ft (7,770 m)
Service ceiling, one engine out	8,500 ft (2,590 m)
T.O to 50 ft (15 m):	
STOL	1,120 ft (341 m)
CAR Pt 3	1,700 ft (515 m)
Landing from 50 ft (15 m):	
STOL	1,026 ft (311 m)
CAR Pt 3	2,160 ft (658 m)
Range with max fuel, 30 min reserve	920 miles (1,480 km)

Source: Reference 4 Figure 4

References

1. Blakelock, John H. "Automatic Control of Aircraft and Missiles", John Wiley & Sons, Inc., New York, 1965.
2. Etkin, Bernard, "Dynamics of Flight", John Wiley & Sons, Inc., New York, 1967.
3. Perkins, C. E. and Hage, R. E., "Airplane Performance, Stability and Control", John Wiley & Sons, Inc., New York, 1963.
4. Jane's "All the World's Aircraft", 1967 Edition.
5. Innis, Robert C.; Holzhauser, Curt A.; and Quiqley, Hervey C.: Airworthiness Considerations for STOL Aircraft. NASA TN D-5594, 1970.

Appendix A: Derivation of Analytical Expressions for Selected Stability Derivatives

Analytical expressions for several stability derivatives are not included in available references or are not adequately developed. Consequently, these needed expressions are developed and presented in this appendix.

Derivation of $C_{y_{p_F}}$ and $C_{n_{p_F}}$

Rolling about the X_A axis produces change in angle of attack at the vertical tail. This angle change produces a side force at the tail and a yawing moment about the Z_A axis. The restoring rolling moment produced is negligible compared to the wing's contribution.

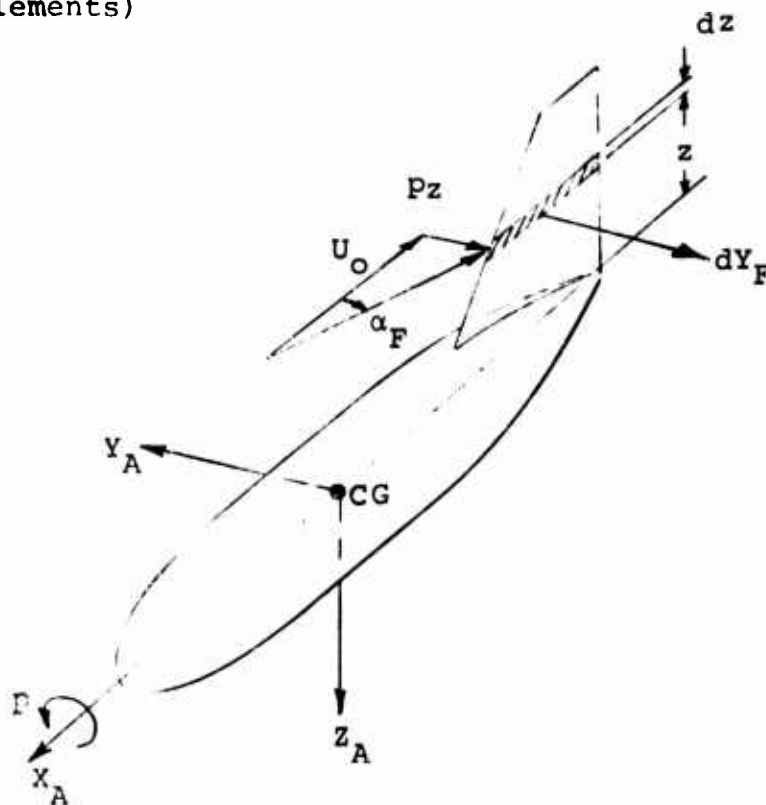
From the sketch, the local surface angle of attack is

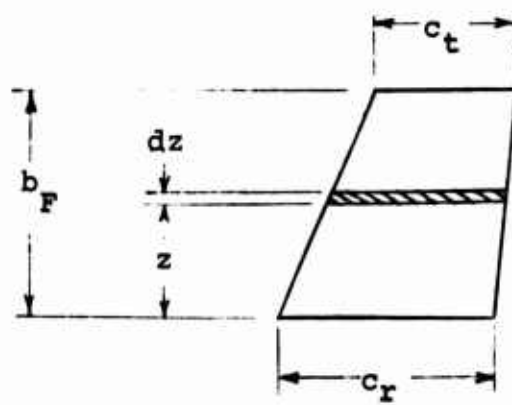
$$\alpha_F(z) = \frac{pz}{U_0}$$

Side force generated is then

$$dY_F = -\frac{1}{2} \rho U_0^2 a_F \cdot \frac{pz}{U_0} c_F(z) dz$$

(assuming constant lift curve slope a_F on fin elements)





Assume that

$$c_F(z) = c_r - \left(\frac{c_r - c_t}{b_F} \right) z$$

Then

$$\begin{aligned} Y_F &= \int dy_F = -\frac{1}{2} \rho U_0^2 a_F \frac{p}{U_0} \int_0^{b_F} \left[c_r z - \left(\frac{c_r - c_t}{b_F} \right) z^2 \right] dz \\ &= -\frac{1}{2} \rho U_0^2 a_F \frac{p}{U_0} \left[\frac{c_r b_F^2}{2} - \frac{(c_r - c_t) b_F^2}{3} \right] \\ &= -\frac{1}{2} \rho U_0^2 a_F \frac{p}{U_0} \frac{c_r b_F^2}{6} \left[1 + 2 \frac{c_t}{c_r} \right] \end{aligned}$$

Next, define

$$\lambda_F = c_t / c_r,$$

and approximate fin area as

$$S_F \approx b_F \left(\frac{c_r + c_t}{2} \right) = \frac{c_r b_F}{2} (1 + \lambda_F)$$

So

$$Y_F = -\frac{1}{2} \rho U_0^2 a_F \frac{p}{U_0} \frac{b_F}{3} S_F \left(\frac{1 + 2 \lambda_F}{1 + \lambda_F} \right)$$

and

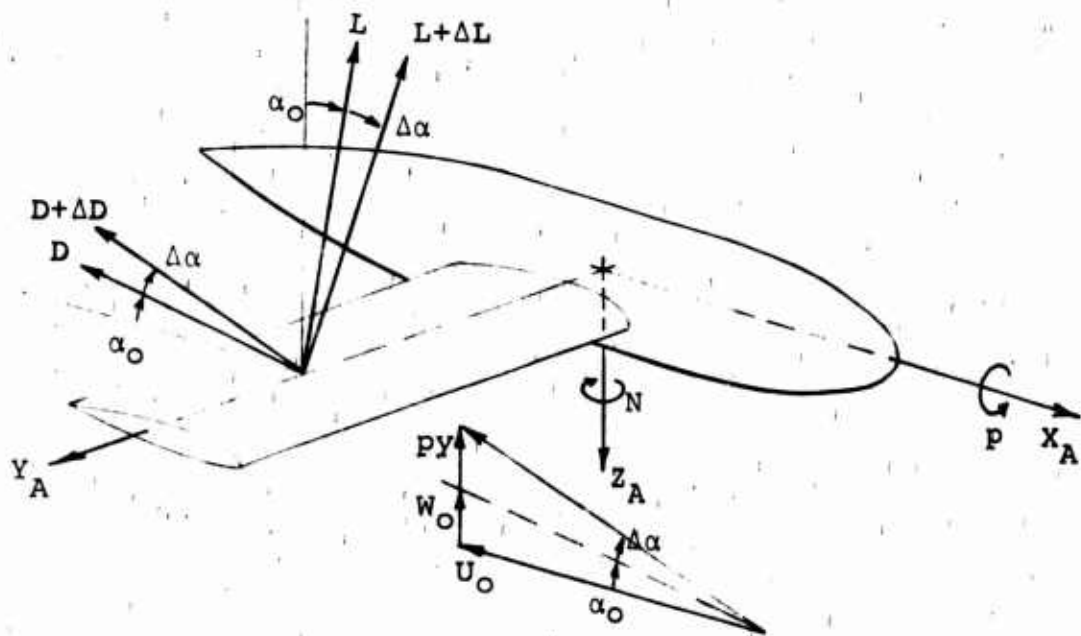
$$C_{Yp_F} \equiv \frac{Y_F / qS}{(pb/2U_0)} = -\frac{2}{3} a_F \frac{S_F}{S} \frac{b_F}{b} \left(\frac{1 + 2 \lambda_F}{1 + \lambda_F} \right)$$

Similarly,

$$C_{np_F} = -C_{Yp_F} \frac{l_F}{b} = \frac{2}{3} a_F \frac{b_F}{b} \frac{S_F}{S} \frac{l_F}{b} \left(\frac{1 + 2 \lambda_F}{1 + \lambda_F} \right)$$

Derivation of C_{n_p}

A roll rate (p) produces a differential change in angle of attack (α) on each wing. The change in α produces a differential inclination and a differential change in magnitude of the lift and drag vectors on each wing, with a resulting yawing moment.



The local angle of attack at a spanwise station y is

$$\alpha(y) = \alpha_0 + \frac{py}{U_0}$$

The lift and drag on a chordwise element of width dy are

$$dL(y) = \frac{1}{2} \rho U_0^2 c(y) a \alpha(y) dy$$

and

$$dD(y) = \frac{1}{2} \rho U_0^2 c(y) [C_{D_{f_w}} + k (a \alpha(y))^2] dy \quad k = \frac{1}{\pi AR}$$

The yawing moment on a chordwise element of width dy at spanwise station y is

$$dN(y) = -dL(y) \cdot \alpha(y) \cdot y + dD(y) \cdot y$$

or

$$dN(y) = q [-a(\alpha_0 + \frac{py}{U_0})^2 + C_{D_{f_w}} + ka^2 (\alpha_0 + \frac{py}{U_0})^2] c(y) y dy$$

where

$$q = \frac{1}{2} \rho U_0^2$$

Now calculate yawing moment:

$$N = \int_{-b/2}^{b/2} dN(y)$$

So

$$N = \int_{-b/2}^{b/2} q c(y) \left[-a \alpha_o^2 y - 2 a \alpha_o \frac{py^2}{U_o} - a \frac{p^2 y^3}{U_o^2} + C_{Df_w} y + k a^2 \alpha_o^2 y + 2ka^2 \alpha_o \frac{py^2}{U_o} + ka^2 \frac{p^2 y^3}{U_o^2} \right] dy$$

Terms marked \nearrow will, when integrated, equal zero by symmetry, so

$$N = \left[-2 a \alpha_o \frac{p}{U_o} q + 2 k a^2 \alpha_o \frac{p}{U_o} q \right] \int_{-b/2}^{b/2} y^2 c(y) dy$$

Next, evaluate integral assuming an elliptical wing planform and obtain, for the integral,

$$\frac{\pi}{4} \frac{c_r}{2} \left(\frac{b}{2}\right)^3 = \frac{1}{4} \left(\frac{b}{2}\right)^2 s$$

So

$$N = -\frac{1}{4} (a \alpha_o - k a^2 \alpha_o) \frac{pb}{2U_o} \cdot qSb$$

or, since $C_{L_o} = a \alpha_o$,

$$N = -\frac{C_{L_o}}{4} \left(1 - \frac{a}{\pi AR}\right) \frac{pb}{2U_o} \cdot qSb$$

Finally,

$$C_{n_{p_w}} = \frac{N/qSb}{(pb/2U_o)} = -\frac{C_{L_o}}{4} \left[1 - \frac{a}{\pi AR}\right]$$

Appendix B. Estimate of Moments and Products of Inertia

No moment and product of inertia data have been located for the "Twin Otter". Reference 5 gives data for the "Buffalo" but does not specify the axes used. Accordingly, estimates have been made as necessary. The basis of these estimates is presented in this Appendix.

In this report, the following values of the inertia parameters will be used:

	Buffalo	Twin Otter
$I_x, \text{sl-ft}^2$	273000	24300
$I_y, \text{sl-ft}^2$	215000	22000
$I_z, \text{sl-ft}^2$	447000	41000
$J_{xz}, \text{sl-ft}^2$	0	0

Notes:

- 1 These values will be assumed to apply to the A-frame axis system. It will be assumed that changes between flight conditions are negligible.
2. Although Reference 5 gives a value of J_{xz} , it does not specify the axis system used. This product of inertia term is very sensitive to small angular changes in the axis system orientation. It is considered advisable to assume $J_{xz} = 0$ rather than use a value whose basis is unknown.

MOMENTS OF INERTIA

1. DHC-5 "Buffalo" - Reference #5 gives moments of inertia for a gross weight of 38,000 lbs.

$$\begin{aligned}I_x &= 273,000 \text{ slug-ft}^2 \\I_y &= 215,000 \text{ slug-ft}^2 \\I_z &= 447,000 \text{ slug-ft}^2 \\J_{xz} &= +36,000 \text{ slug-ft}^2\end{aligned}$$

Note: Axis system unspecified in Reference 5. Waterline axes assumed.

2. DHC "Twin Otter" - Corresponding data was not available for this aircraft, and the moments of inertia were estimated.

$$\begin{aligned}I_x &= 24,300 \text{ slug-ft}^2 \\I_y &= 22,010 \text{ slug-ft}^2 \\I_z &= 41,020 \text{ slug-ft}^2\end{aligned}$$

The weight of each item in the aircraft was evaluated using information in Sechler & Dunn, Airplane Structural Analysis & Design, and Reference 4. The mass of each component was then calculated, and used in the appropriate formula to determine moment of inertia in a waterline axis system, as shown in the following.

DHC - "TWIN OTTER"
ESTIMATED WEIGHT BREAKDOWN

Item	Weight, W, lbs	Mass, m, slugs	Method of Estimation
fuselage	1000	31.0	8.3% x G.W.
wing	1500	48.0	12.5% x G.W.
ailerons & flaps	50		.85 lb/ft ² x 56 ft ² } wing = 1550#
elevators	35		1.0 lb/ft ² x 35 ft ² }
horizontal stab.	130	5.13	2.0 lb/ft ² x 65 ft ² } horizontal tail = 165#
rudder	45		1.3 lb/ft ² x 34 ft ² }
vertical fin	155	6.21	2.3 lb/ft ² x 66 ft ² } vertical tail = 200#
fuel tanks	150		.48 lb/gal x 315 imp. gal.
engines	600	24.8	289 lbs/engine ~ Jane's } engines = 800#
engine installation	200		1.7% x G.W.
props	350	10.9	3% x G.W.
main gear	250	7.76	2% x G.W.
nose gear	150	4.66	1.25% x G.W.
radio	100	3.1	-
instruments	100	3.1	-
furnishings	500	15.5	~ 25 lbs/pass.
miscellaneous	575	17.8	
pilots	340	10.55	2 x 170 lbs
oil	40	1.24	5 gal. x 8 lb/gal.
empty wt	6270	194.4	
passengers	3230	100.2	19 persons x 170 lb/person
fuel	2500	77.6	8 lb/gal x 315 imperial gal.
gross weight	12,000	372.2	method of weight estimation from: E. Sechler & G. Dunn. Airplane Structural Analysis & Design Dover Publications, New York, 1963

DHC TWIN OTTER

$$I_x$$

MOMENT OF INERTIA ABOUT THE LONGITUDINAL AXIS

ITEM	EQUATION	VALUES		INERTIA
wing	$m \left\{ \frac{b^2}{12} + z^2 \right\}$	b = 65.0'	z = -3.5'	1.745 x 10 ⁴
engines	$m \{y^2 + z^2\}$	y = 9.3'	z = -3.5'	.246 x 10 ⁴
props	$m \{y^2 + z^2\}$	y = 9.3'	z = -3.5'	.108 x 10 ⁴
fuselage	$m \cdot R^2$	R = 3.5'		.038 x 10 ⁴
furnishings	$m \cdot R^2$	R = 3.5'		.019 x 10 ⁴
vert. tail	$m \cdot z^2$	z = 5.4'		.018 x 10 ⁴
horiz. tail	$m \left\{ \frac{b^2}{12} + z^2 \right\}$	b = 21.2'	z = -4.5'	.030 x 10 ⁴
fuel & tanks	$m \cdot R^2$	R = 4.0'		.132 x 10 ⁴
passengers	$m \{y^2 + z^2\}$	y = 2.0'	z = -1.0'	.050 x 10 ⁴
main gear	$m \cdot R^2$	R = 7.0'		.038 x 10 ⁴
nose gear	$m \cdot z^2$	z = -4.5'		.0095 x 10 ⁴
				2.434 x 10 ⁴
				slug-ft ²
<p>Note: components not shown are assumed to contribute negligible I_x</p>				

DHC TWIN OTTER

I_y

MOMENT OF INERTIA ABOUT THE LATERAL AXIS

ITEM	EQUATION	VALUES	INERTIA
fuselage	$m\left\{\frac{R^2}{2} + \frac{\ell^2}{12} + x^2\right\}$	$R=3.5'$ $\ell=41'$ $x=-1.5'$	$.460 \times 10^4$
pilots passengers furnishings misc.	$m\left\{\frac{\ell^2}{12} + x^2\right\}$	$\ell = 16.5'$ $x = 3.35'$	$.480 \times 10^4$
fuel & tanks	$m\left\{\frac{\ell^2}{12} + x^2\right\}$	$\ell = 8.0'$ $x = 3.5'$	$.144 \times 10^4$
wing	$m\left\{\frac{\ell^2}{12} + \left(\frac{\bar{c}}{4}\right)^2\right\}$	$\ell = 6.5'$ $\bar{c} = 6.5'$	$.029 \times 10^4$
engines	$m \cdot R^2$	$R = 5.0'$	$.062 \times 10^4$
props	$m \cdot R^2$	$R = 7.0'$	$.053 \times 10^4$
main gear	$m \cdot R^2$	$R = 4.5'$	$.016 \times 10^4$
nose gear	$m \cdot R^2$	$R = 13.0'$	$.125 \times 10^4$
horiz. tail	$m \cdot R^2$	$R = 25.8'$	$.342 \times 10^4$
vert. tail	$m(x^2 + z^2)$	$x = -27.5'$ $z = -5.4'$	$.490 \times 10^4$
			<hr/> <hr/> 2.201×10^4 slug-ft ²
	Note: Components not shown are assumed to contribute negligible I_y		

DHC TWIN OTTER

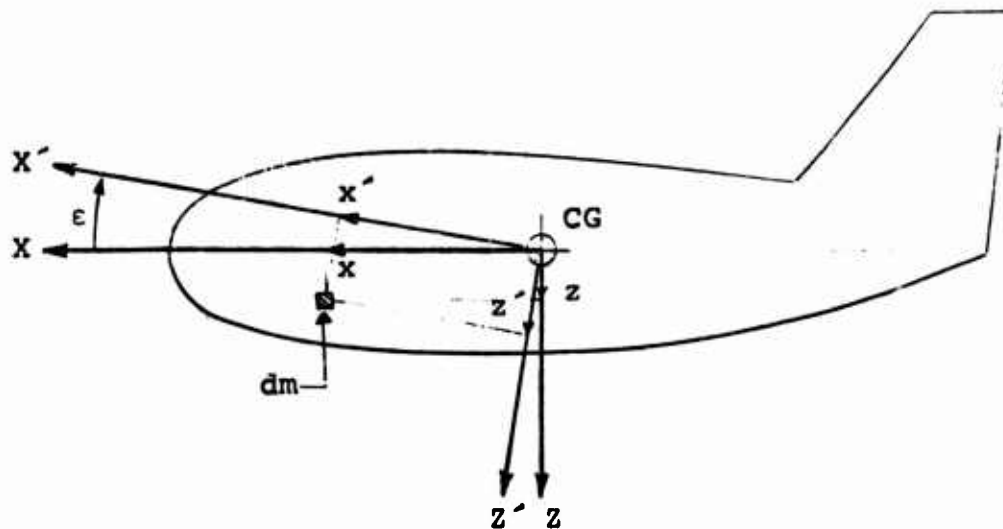
$$I_z$$

MOMENT OF INERTIA ABOUT THE VERTICAL AXIS

ITEM	EQUATION	VALUES	INERTIA
fuselage	$I_{z_{Fus}} \approx I_{y_{Fus}}$		$.460 \times 10^4$
pilots passengers furnishings misc.	$I_z \approx I_y$		$.480 \times 10^4$
fuel & tanks	$m \cdot \frac{l^2}{12}$	$l = 8.0$	$.044 \times 10^4$
wing	$m \left\{ \frac{\bar{c}^2 + b^2}{12} + \left(\frac{\bar{c}}{4} \right)^2 \right\}$	$\bar{c} = 6.5'$ $b = 65'$	1.720×10^4
engines	$m \{y^2 + x^2\}$	$y = 9.3'$ $x = 5.0'$	$.278 \times 10^4$
props	$m \{y^2 + x^2\}$	$y = 9.3'$ $x = 7.0'$	$.148 \times 10^4$
main gear	$m \cdot y^2$	$y = 6.5'$	$.033 \times 10^4$
nose gear	$m \cdot x^2$	$x = 13.0'$	$.125 \times 10^4$
horiz. tail	$m \cdot x^2$	$x = -25.8'$	$.342 \times 10^4$
vert. tail	$m \cdot x^2$	$x = -27.5'$	$.472 \times 10^4$
			<hr/> 4.102×10^4 slug-ft ²
	Note: components not shown are assumed to contribute negligible I_z		

Derivation of Expressions for Change in Inertias with Rotation of Axes

Inertia values are dependent on the set of axes chosen. In this part of Appendix B, equations are derived which show the effect on inertia values produced by rotating the reference axes through an angle ϵ about the Y_A axis. (The Y_A axis is universally chosen to be normal to the aircraft's plane of symmetry, so reorientations of the X_A and Z_A axes only need be considered.)



From the sketch, the moments and product of inertia in the X Y Z axis system are:

$$\begin{aligned} I_x &= \int (y^2 + z^2) \, dm \\ I_y &= \int (x^2 + z^2) \, dm \\ I_z &= \int (x^2 + y^2) \, dm \\ J_{xz} &= + \int x z \, dm \end{aligned} \tag{B1}$$

and, in the $X' Y' Z'$ axis system, they are:

$$\begin{aligned} I_{x'} &= \int (y'^2 + z'^2) dm \\ I_{y'} &= \int (x'^2 + z'^2) dm \\ I_{z'} &= \int (x'^2 + y'^2) dm \\ J_{xz'} &= \int x' z' dm \end{aligned} \tag{B2}$$

Also from the sketch, the following relations can be obtained:

$$\begin{aligned} x' &= x \cos \epsilon - z \sin \epsilon \\ y' &= y \\ z' &= z \cos \epsilon + x \sin \epsilon \end{aligned} \tag{B3}$$

The desired relations are obtained by substituting equations (B3) into equations (B2) and by making use of the trigonometric identity

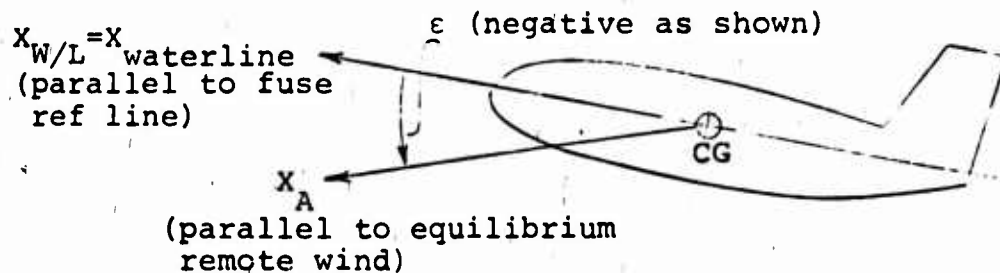
$$\sin^2 \epsilon + \cos^2 \epsilon = 1$$

These relations are

$$\begin{aligned} I_{x'} &= I_x \cos^2 \epsilon + I_z \sin^2 \epsilon + 2 J_{xz} \cos \epsilon \sin \epsilon \\ I_{y'} &= I_y \\ I_{z'} &= I_z \cos^2 \epsilon + I_x \sin^2 \epsilon - 2 J_{xz} \cos \epsilon \sin \epsilon \\ J_{xz'} &= J_{xz} \cos 2\epsilon + (I_z - I_x) \cos \epsilon \sin \epsilon \end{aligned} \tag{B4}$$

Estimation of Angle ϵ Between $X_{\text{waterline}}$ and X_A Axes

In this part of Appendix B, an estimate is made of the magnitude of the angle ϵ that is associated with the use of stability axes for the three flight conditions being considered.



Assume that wing incidence has been chosen by the manufacturer to produce a level fuselage attitude when the aircraft is in flight at "Economy Cruise Speed" at 10,000 ft and at an arbitrarily-chosen average gross weight,

For Buffalo:

$$\begin{aligned} W_{\text{average}} &= W_{T.O \text{ max}} - \frac{\text{max payload}}{2} \\ &= 41000 - 13843/2 \quad (\text{Reference 4 or Figure 3, this report}) \\ &= 34078 \text{ lbs} \end{aligned}$$

$$V_{\text{Econ cr}} = 208 \text{ mph} = 306 \text{ fps @ 10,000 ft (same)}$$

$$q_{\text{Ec}} = \frac{1}{2} \rho U_o^2 = \frac{.001754}{2} (306)^2 = 82.0 \text{ lbs/ft}^2$$

$$C_{L_{\text{Ec}}} = W/qS = 34078/(82)(945) = .44$$

For Twin Otter:

$$W_{\text{average}} = 11,579 - \frac{4430}{2} \quad (\text{Reference 4 or Figure 4, this report})$$

$$= 9364 \text{ lbs}$$

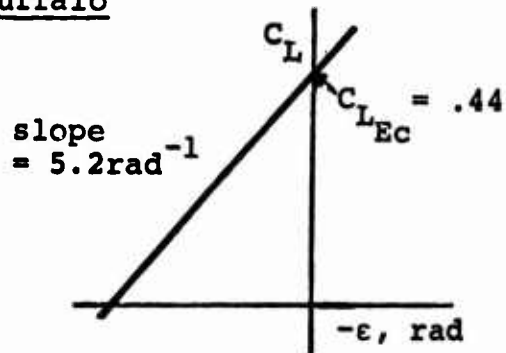
$$V_{\text{Econ cr}} = 156 \text{ mph} = 230 \text{ fps @ 10,000 ft (same)}$$

$$q_{\text{Ec}} = \frac{.001754}{2} (230)^2 = 46.5 \text{ lbs/ft}^2$$

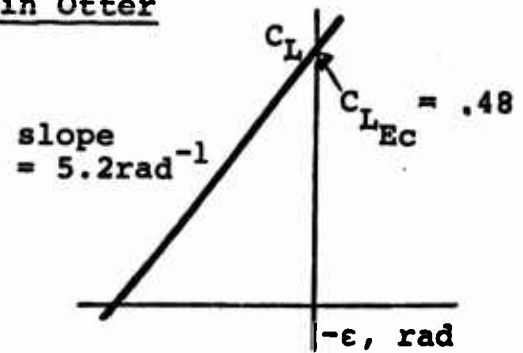
$$C_{L_{\text{Ec}}} = 9364 / (46.5)(420) = .48$$

Next, assuming slope of lift curve is as calculated in Section VII (= 5.2/rad for both aircraft), one can sketch lift curves:

Buffalo



Twin Otter



From these sketches, one can infer ϵ (angle between X_A axis and $X_{W/L}$ axis) at a given C_L :

$$\epsilon = \frac{C_L - C_{L_{\text{Ec}}}}{5.2} \quad (\text{rad})$$

Now, calculate this angle for each flight condition considered in this report:

Aircraft	Flight Cond.	C_{L_0} (Section VII)	$C_{L_{Ec}}$	$-\epsilon$	
				rad	deg
Buffalo	Cruise	.30	.44	-.0270	-1.55
	Slow Flt	.77	↓	.0635	3.64
	Lndg Appr	1.49	↓	.202	11.6
Twin Otter	Cruise	.42	.48	-.0115	-.66
	Slow Flt	.78	↓	.0577	3.30
	Lndg Appr	1.65	↓	.225	12.9

Note: Calculation has not accounted for flap effects. Use of flaps (as in Landing Approach Flight Condition) will reduce ϵ substantially.

The above table shows that $|e|$ is largest for the Landing Approach flight condition. Accordingly, the change in inertia magnitude due to axis system rotation will be investigated at this flight condition.

Equations (B4) and the waterline-referenced inertias of page B1 are used to prepare the following table (assuming $J_{xz} = 0$):

	Buffalo ($\epsilon = -11.6^\circ$)	Twin Otter ($\epsilon = -12.9^\circ$)
$I_x = I_{x_{W/L}}, \text{ sl-ft}^2$	273000	24300
$I_x' = I_{x_A}, \text{ sl-ft}^2$	280000	25040
% change	2.5%	3%
$I_z = I_{z_{W/L}}, \text{ sl-ft}^2$	447000	41000
$I_z' = I_{z_A}, \text{ sl-ft}^2$	440500	40135
% change	-1.5%	2%

This table shows that inertia values are only slightly affected by small axis rotations. It is concluded on the basis of this table that variations in inertias due to small axis rotations can be reasonably neglected.

Appendix C Calculation of Stability Derivatives

This appendix shows the step-by-step calculations carried out to obtain the derivatives presented in Section VII.

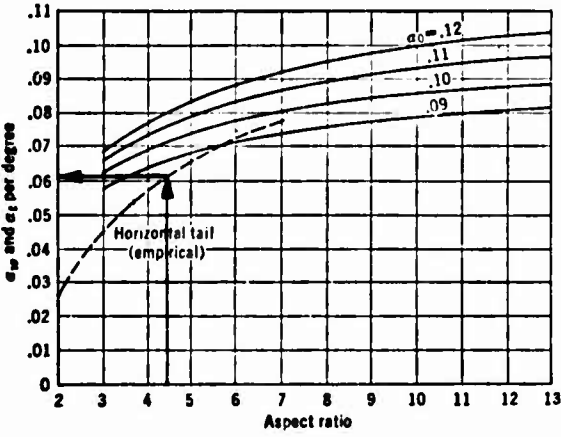
In this appendix, the parameters needed to evaluate the non-dimensional stability derivatives are developed (Items 1 - 72). The source of each parameter is shown. Then, the non-dimensional stability derivatives are calculated (Items 73 - 99) using the expressions presented in Section VI, Table I. Finally, in Items 100 - 111, certain dynamic constants (e. g., $c/2U_0$) needed to calculate the dimensional derivatives are tabulated. Also presented is a summary of moments and products of inertia developed in Appendix B.

Some of the parameters appearing in this appendix are used only here, and are not included in the list of symbols appearing in the front of this report. However, these parameters are fully defined where they are introduced in Appendix C.

Appendix C

Calculation of Derivatives

NO.	PARAMETER	SOURCE	VALUE	
			BUFFALO	TWIN OTTER
1	S, gross wing area, ft ²	Fig. 3, 4	945	420
2	b, wing span, ft	Fig. 3, 4	96	65
3	c, mean aerodynamic chord, ft $= \frac{2}{S} \int_0^{b/2} c_{geom}^2 dy$	Ref. 2	10.1	6.5
4	c _{geom} , geometric wing chord, ft	Fig. 3, 4	$\begin{cases} 11.77 & (0 < y < 16.4') \\ 14.92 - .186y & (16.4 < y < 48') \end{cases}$	6.5
5	C _{Lα} , lift curve slope of aircraft = lift curve slope of wing, rad ⁻¹ $= \frac{a_{\infty}}{1 + \frac{a_{\infty}}{\pi AR}}$	Ref. 3	5.2	5.2
6	a _∞ , two dimensional lift curve slope of wing section	(Est)	2π	2π
7	AR, aspect ratio of wing $= b^2/S$	(def.)	9.75	10
8	e, airplane efficiency factor	(Est)	.75	.75
9	S _T , horizontal tail area (including elevator), ft ²	Fig. 3,4	233	100
10	l _T , distance, wing quarter chord to horizontal tail quarter chord, ft	Fig. 3,4	46	25

NO.	PARAMETER	SOURCE	VALUE	
			BUFFALO	TWIN OTTER
11	a_T , lift curve slope of horizontal tail, rad^{-1}  <p>The graph shows the lift curve slope a_T (in rad^{-1}) on the y-axis (ranging from 0 to 0.11) versus the aspect ratio on the x-axis (ranging from 2 to 13). Five curves are plotted for different angles of attack α_0: 0.09, 0.10, 0.11, and 0.12. A dashed line labeled 'Horizontal tail (empirical)' is also shown, starting at approximately (2, 0.06) and increasing to (4.4, 0.065). The curves for $\alpha_0 = 0.09$ and 0.10 are the highest, while the curve for $\alpha_0 = 0.12$ is the lowest.</p>	Figure \wedge p221, Ref 3	.061/o =3.5/rad	.061/o =3.5/rad
12	AR_T , aspect ratio of horizontal tail = b_T^2/S_T	(def.)	4.4	4.4
13	b_T , horizontal tail span, ft	Fig. 3,4	32	21
14	η_T , horizontal tail efficiency factor In absence of any experimental data, assume η_T of Buffalo high T - tail is 1.00. Assume fuselage interference on Twin Otter tail is compensated by prop slip stream and therefore $\eta_T = 1.00$	(Est)	1.00	1.00
15	$r = l_T/b_T$	-	.96	.77

NO.	PARAMETER	SOURCE	VALUE	
			BUFFALO	TWIN OTTER
16	z_T , vertical distance, horizontal tail a.c. to zero lift line, ft	Fig. 3,4	18.5	3.0
17	$m = z_T / \frac{b}{2}$	-	.38	.1
18	TR, wing taper ratio = c_r / c_t	Item 4	2	1

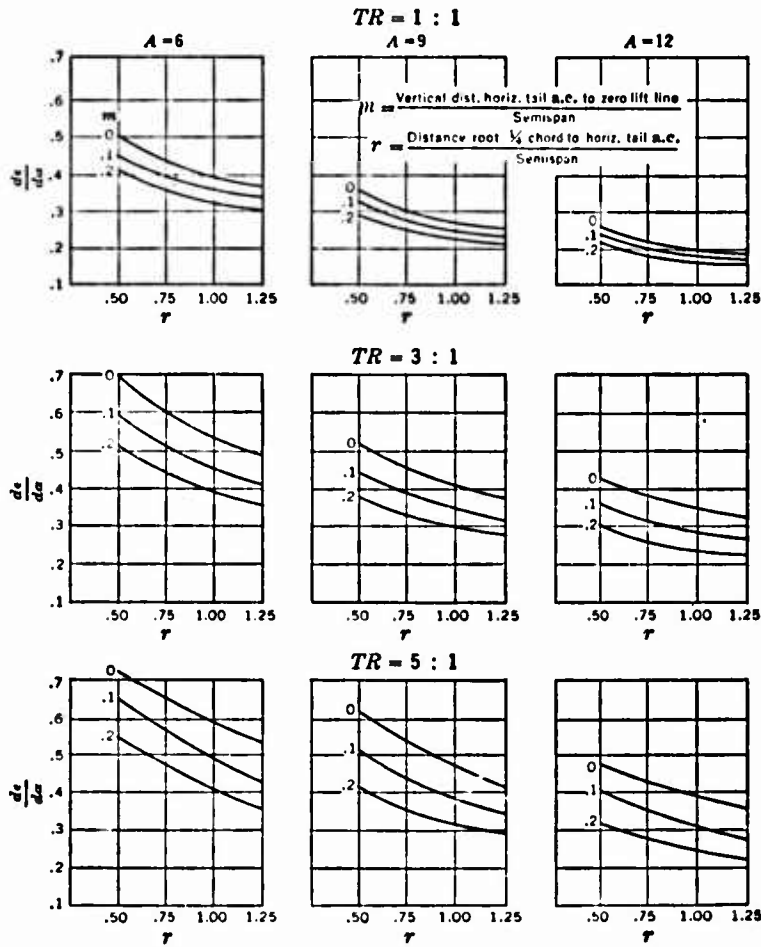
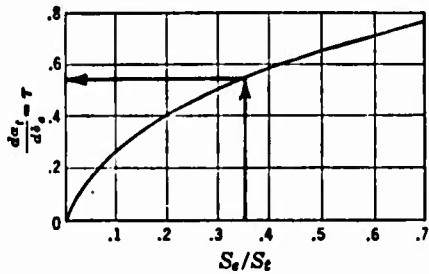


FIGURE 5-10. Downwash charts.

Ref. 3, p 224

NO.	PARAMETER	SOURCE	VALUE	
			BUFFALO	TWIN OTTER
19	$d\epsilon/d\alpha$, rate of change of downwash angle at tail with change in angle of attack, rad/rad	above charts	.17	.25
20	S_e , elevator area, ft ²	Fig. 3,4	81.5	35
21	S_e/S_T	20/9 ▲ Ref. 3, p 250	.35	.35
	 <p>FIGURE 5-33. Elevator effectiveness.</p>			
22	$d\alpha_T/d\delta_e$, elevator effectiveness	above chart	.54	.54
23	S_{wet} , wetted area of aircraft, ft ² $= S_{wet_w} + S_{wet_{fuse}} + S_{wet_T}$ $+ S_{wet_F} + S_{wet_{nac}}$		5590	2248
24	$S_{wet_w} \approx 2S$	-	1890	840
25	$S_{wet_{fuse}} \approx l_{fuse} \cdot c_{fuse}$	-	2300	900

NO.	PARAMETER	SOURCE	VALUE	
			BUFFALO	TWIN OTTER
26	$S_{wet_T} \approx 2 S_T$	-	466	200
27	$S_{wet_F} \approx 2 S_F$	-	304	164
28	$S_{wet_{nac}} \approx 2 [l_{nac} \cdot \bar{c}_{nac}]$	-	630	144
29	l_{fuse} , fuselage length, ft	Fig. 3,4	77	47.5
30	\bar{c}_{fuse} , average fuselage circumference, ft	"	30	19
31	l_{nac} , nacelle length, ft	"	21	12
32	\bar{c}_{nac} , average nacelle circumference, ft	"	15	6
33	f , equivalent flat plate area of aircraft, ft^2	chart below	30	16.5

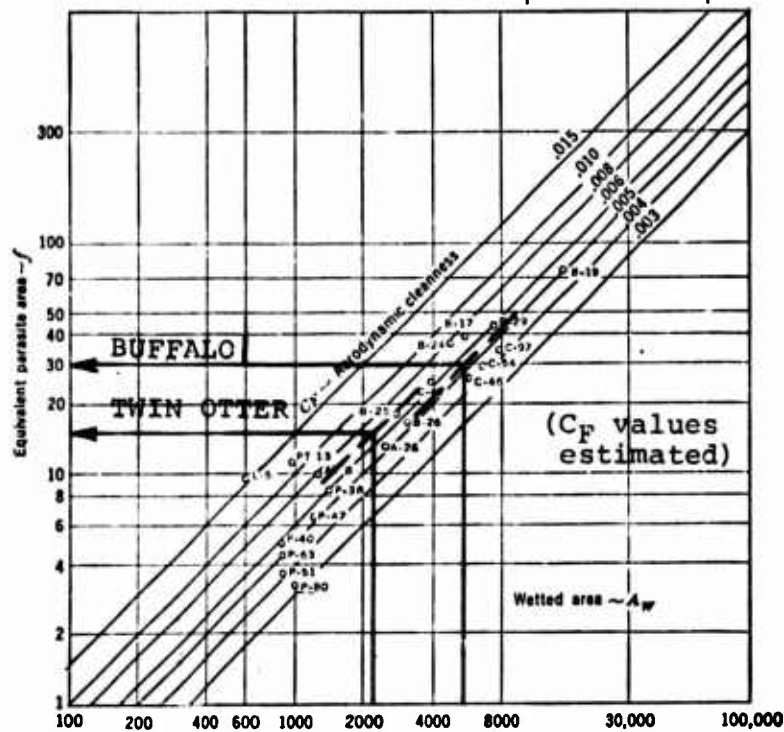


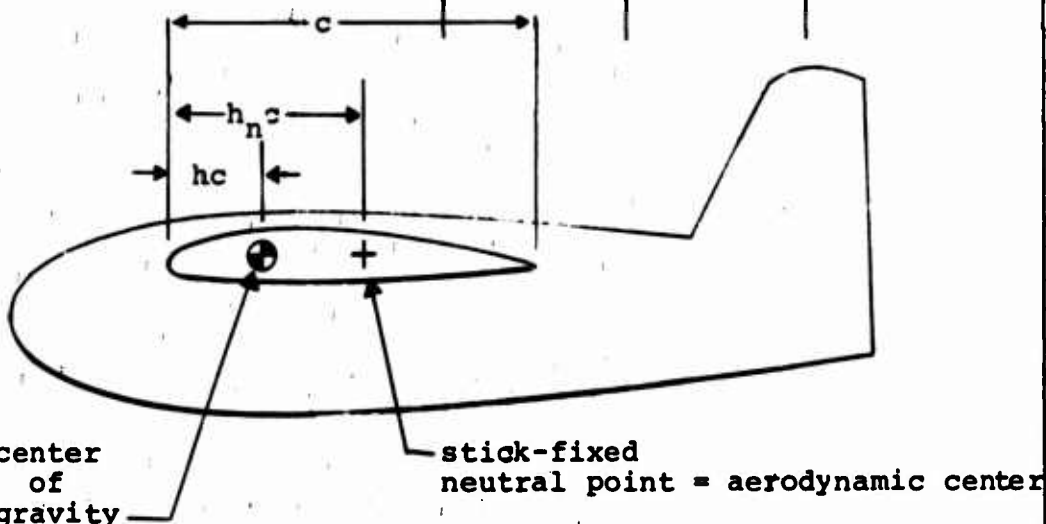
FIGURE 2-70. Wetted area chart.

Ref. 3, p 98

NO.	PARAMETER	SOURCE	VALUE	
			BUFFALO	TWIN OTTER
34	C_{Df} , parasite drage coefficient of aircraft = f/S Note: These values of C_{Df} were used to calculate max. forward speeds and rates D_f of climb to compare with figures published in Reference 4. The agreement was good. Analytical estimates of C_{Df} (or f) should only be considered to be rough D_f estimates. The values shown here are reasonable ones, adequate for this study's purpose.	(def.)	.032	.039
35	ρ , atmospheric air density, slugs/ft ³ Cruise Slow Flt Lndg Appr	Table II, Std Atmos Tables	 .001756 .002378 .002378	 .001756 .002378 .002378
36	U_o , aircraft forward speed at equilibrium flight condition, fps Cruise Slow Flt Lndg Appr	Table II	 400 215 154	 278 176 120
37	q , dynamic pressure, lbs/ft ² $\approx \frac{1}{2} \rho U_o^2$ Cruise Slow Flt Lndg Appr	-	 140.5 55.0 28.4	 68.0 36.9 17.3
38	C_{L_o} , aircraft lift coefficient at equilibrium flight condition = W/qS Cruise Slow Flt Lndg Appr	-	 .30 .77 1.49	 .42 .78 1.65

NO.	PARAMETER	SOURCE	VALUE	
			BUFFALO	TWIN OTTER
39	C_{D_0} , aircraft drag coef. at equilibrium flight condition $= C_{D_f} + C_{L_0}^2 / \pi e A R$ Cruise Slow Flt Lndg Appr	-		
			.036	.047
			.057	.065
			.127	.155
40	θ_0 , angle of rotation, at equilibrium flight condition, of X_A axis from horizontal plane, rad or deg Cruise Slow Flt Lndg Appr	Fig. 2, this rpt.	0	0
			0	0
			-7.5°	-7.5°
			-.131 rad	-.131 rad
Note: Item 39: Landing Approach Condition involves use of flaps. However, insufficient information is available on flap geometry to make a valid estimate of $\Delta C_{D_{flaps}}$. Therefore, the "noflap" data is applied pending receipt of the required flap data.				

NO.	PARAMETER	SOURCE	VALUE	
			BUFFALO	TWIN OTTER
41	$-(h-h_n)$, stick-fixed static margin, fraction of c Note: It will be assumed in this report that aircraft parameters are such that the static margin is limited to values between .25 (most fwd C.G.) and .05 (most aft C.G.) Therefore: $(h-h_n)$ (most fwd C.G.) (normal C.G.) (most aft C.G.) In this report, the <u>normal C.G.</u> value will be used.	Ref. 2, Ref. 3 - - -	 -.25 -.15 -.05	 -.25 -.15 -.05
42	(not used)			
43				
44				
45				



NO.	PARAMETER	SOURCE	VALUE	
			BUFFALO	TWIN OTTER
46	S_F , vertical tail area (including rudder), ft^2	Fig. 3,4	152	82
47	b_F , vertical tail span, ft	Fig. 3,4	14.0	11.0
48	$c_{F_{geom}}$, vertical tail chord, ft	Fig. 3,4	13.3 (root) 8.5 (tip)	9.2 (root) 5.7 (tip)
49	AR_F , aspect ratio of vertical fin $fin = b_F^2 / S_F$	(def.)	1.29	1.48
50	AR_{Fe} , effective aspect ratio of vertical fin (to account for stabilizer end-plate effect) = $1.55 AR_F$	Ref. 3, p 325	2.00	2.30

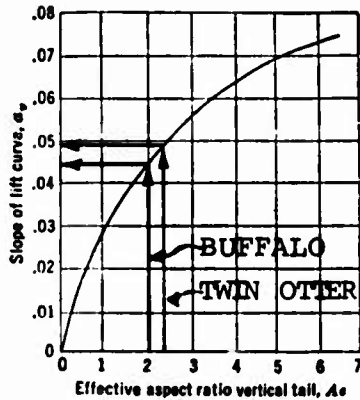
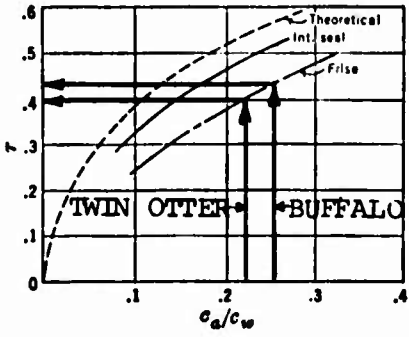


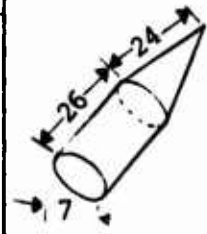
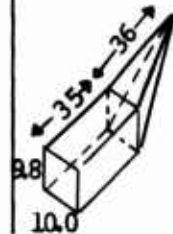
FIGURE 8-8. Slope of lift curve, vertical tail. From NACA TN 775, "Analysis of Wind-tunnel Data on Directional Stability and Control," by H. R. Pass.

▲
↑
Ref. 3, p 324
↓
▼

NO.	PARAMETER	SOURCE	VALUE	
			BUFFALO	TWIN OTTER
51	a_F , lift curve slope of vertical tail, deg^{-1} or rad^{-1}	above figure	$\left\{ \begin{array}{l} .044/\text{deg} \\ 2.5/\text{rad} \end{array} \right.$	$\left\{ \begin{array}{l} .049/\text{deg} \\ 2.8/\text{rad} \end{array} \right.$
52	λ_F , taper ratio of vertical tail $= c_{F \text{ tip}} / c_{F \text{ root}}$	Item (48)		.64
53	l_F , distance, wing quarter chord to vertical tail quarter chord, ft	Fig. 3,4	44	25.5
54	Z_F , vertical distance, aircraft CG to mean chord of vertical tail, ft	Fig. 3,4	10	5
55	$d\alpha/d\beta$, rate of change of side-wash angle at vertical tail with change in side-slip angle, rad/rad . Estimate requires wind tunnel data. Will arbitrarily use value of .1 here.	(Est)	.1	.1
56	S_r , area of rudder, ft^2	Fig. 3,4	60	34
57	S_r/S_F	(56)/46	.4	.4
58	$d\alpha_F/d\delta_r$, rudder effectiveness	chart @ Item 22	.58	.58
59	Z_w , vertical distance of root quarter chord below fuselage center line, ft	Fig. 3,4	-3.5	-3.0
60	h , fuselage height at wing root, ft	Fig. 3,4	9.8	7.0
61	w , fuselage width at wing root, ft	Fig. 3,4	10.0	6.0

NO.	PARAMETER	SOURCE	VALUE	
			BUFFALO	TWIN OTTER
62	c_a/c , ratio, aileron chord to local wing chord  <p>FIGURE 9-15. Aileron effectiveness.</p>	Fig. 3,4	.25	.22
63	τ , aileron effectiveness	above figure	.43	.40
64	y_1 , distance, aircraft centerline to inboard end of aileron, ft	Fig. 3,4	33.0	14.0
65	y_2 , distance, aircraft centerline to outboard end of aileron, ft	Fig. 3,4	47.0	31.0
66	Volume of fuselage, ft ³	Fig. 3,4	4600	1300

Source: Ref. 3, p358



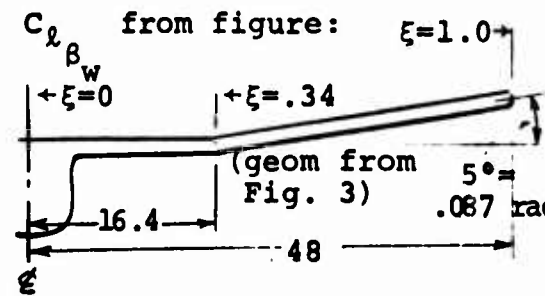
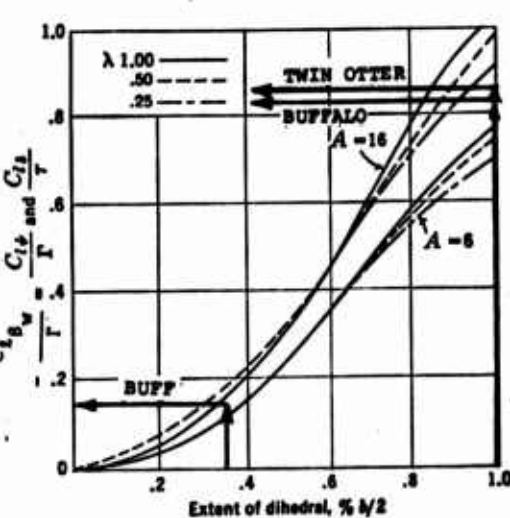
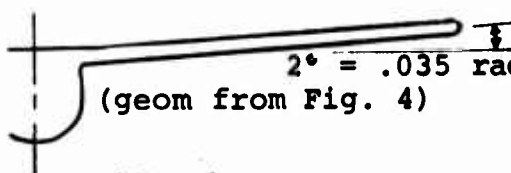
NO.	PARAMETER	SOURCE	VALUE	
			BUFFALO	TWIN OTTER
67	$C_{D_{f_w}}$, wing profile drag coefficient *	Ref. C1 (below)	.006	.006
			(representative values from data plots of ref.)	
68	C_{D_W} , wing drag coefficient* $= C_{D_{f_w}} + C_{L_o}^2 / \pi A$	Ref. 3, p 73		
	Cruise		.009	.012
	Slow Flt		.025	.025
	Lndg Appr		.077	.093
	Reference C1: "Theory of Wing Sections Including a Summary of Airfoil Data", Abbott & Von Doenhoff, Dover Publications, Inc., N.Y., 1959.			
	* See note at Item (39)			
69	} (not used)			
70				
71				
72				

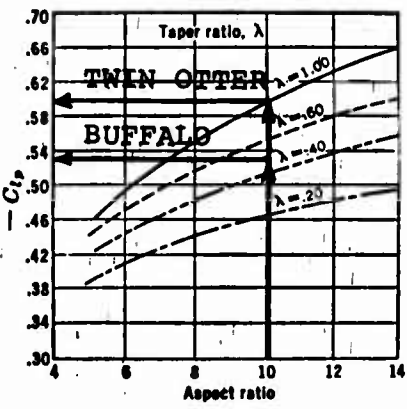
NO.	BUFFALO	TWIN OTTER
73	$C_{x_u} = -3C_{D_o} - C_{L_o} \tan \theta_o$ <p>Cruise $= -3(.036) - 0 = -.108$</p> <p>Slow Flt $= -3(.057) - 0 = -.171$</p> <p>Lndg Appr $= -3(.127) - (1.49)(-.131)$ $= -.186$</p>	<p>Cruise $= -3(.047) - 0 = -.141$</p> <p>Slow Flt $= -3(.065) - 0 = -.195$</p> <p>Lndg Appr $= -3(.151) - (1.65)(-.131)$ $= -.237$</p>
74	$C_{x_\alpha} = C_{L_o} \left[1 - \frac{2 C_{L_\alpha}}{\pi e AR} \right]$ $= C_{L_o} \left[1 - \frac{2(5.2)}{\pi(.75)(9.75)} \right]$ $= .547 C_{L_o}$ <p>Cruise $= .547 (.30) = .164$</p> <p>Slow Flt $= .547 (.77) = .441$</p> <p>Lndg Appr $= .547 (1.49) = .815$</p>	$= C_{L_o} \left[1 - \frac{2(5.2)}{\pi(.75)(10)} \right]$ $= .558 C_{L_o}$ <p>Cruise $= (.558)(.42) = .234$</p> <p>Slow Flt $= (.558)(.78) = .435$</p> <p>Lndg Appr $= (.558)(1.65) = .920$</p>

NO.	BUFFALO	TWIN OTTER
75	$C_{z_u} = -2 C_{L_o}^{38}$ <p>Cruise $= -2 (.30) = - .60$</p> <p>Slow Flt $= -2 (.77) = - 1.54$</p> <p>Lndg Appr $= -2 (1.49) = - 2.98$</p>	<p>Cruise $= -2 (.42) = - .84$</p> <p>Slow Flt $= -2 (.78) = - 1.56$</p> <p>Lndg Appr $= -2 (1.65) = - 3.30$</p>
76	<p>Define V_T, horizontal tail volume:</p> $V_T = \eta_T \frac{l_T}{c} \frac{S_T}{S}$ <p style="text-align: center;"> 10 9 3 1 </p> <p>$= (1.0) \frac{(46)}{(10.1)} \frac{(233)}{(945)} = 1.12$</p>	<p>$= (1.0) \frac{(25)}{(6.5)} \frac{(100)}{(420)} = .915$</p>
77	$C_{z_\delta} = -2 a_T \frac{V_T}{76} \frac{d\epsilon}{d\alpha}^{19}$ <p>$= -2 (3.5) (1.12) (.17) = - 1.33$</p>	<p>$= -2 (3.5) (.915) (.25) = - 1.60$</p>

NO.	BUFFALO	TWIN OTTER
78	$C_{z_{\alpha}} = - (C_{L_{\alpha}} + C_{D_o})$ <p style="text-align: center;">(5) (39)</p> <p>Cruise = - (5.2 + .036) = - 5.24</p> <p>Slow Flt = - (5.2 + .057) = - 5.26</p> <p>Lndg Appr = - (5.2 + .127) = - 5.33</p>	<p>Cruise = - (5.2 + .047) = - 5.25</p> <p>Slow Flt = - (5.2 + .065) = - 5.27</p> <p>Lndg Appr = - (5.2 + .155) = - 5.36</p>
79	$C_{z_q} = - 2 a_T V_T$ <p style="text-align: center;">(11) (76)</p> <p>= - 2 (3.5) (1.12) = - 7.83</p>	<p>= - 2 (3.5) (.915) = - 6.40</p>
80	$C_{z_{\delta_e}} = a_T \frac{d\alpha_T}{d\delta_e} \frac{s_T}{s} \eta_T$ <p style="text-align: center;">(11) (9) (22) (1) (14)</p> <p>= (3.5) (.54) $\left(\frac{233}{945}\right)$ (1.0) = .465</p>	<p>= (3.5) (.54) $\left(\frac{100}{420}\right)$ (1.0) = .450</p>
81	$C_{m_{\alpha}} = C_{L_{\alpha}} \left(h - \frac{h_n}{n} \right)$ <p style="text-align: center;">(5) (41)</p> <p>= (5.2) (-.15) = - .78</p> <p>(for normal CG)</p>	<p>= (5.2) (-.15) = - .78</p> <p>(for normal CG)</p>

NO.	BUFFALO	TWIN OTTER
86	$C_{Y\beta} = - a_F \frac{s_F}{S} (1 - \frac{d\sigma}{d\beta})$ $= - (2.5) \left(\frac{152}{945}\right) (1 - .1)$ $= - .362$	$= - (2.8) \frac{82}{420} (1 - .1)$ $= - .492$
87	$C_{Yp} = - \frac{2}{3} a_F \frac{b_F}{b} \frac{s_F}{S} \frac{1 + 2\lambda_F}{1 + \lambda_F}$ $= - \frac{2}{3} (2.5) \left(\frac{14}{96}\right) \left(\frac{152}{945}\right) \left(\frac{1+2(.64)}{1+.64}\right)$ $= - .055$	$= - \frac{2}{3} (2.8) \left(\frac{11}{65}\right) \left(\frac{82}{420}\right) \left(\frac{1+2(.62)}{1+.62}\right)$ $= - .085$
88	$C_{Yr} = 2 a_F \frac{l_F}{b} \frac{s_F}{S}$ $= 2 (2.5) \left(\frac{44}{96}\right) \left(\frac{152}{945}\right) = .368$	$= 2 (2.8) \left(\frac{25.5}{65}\right) \left(\frac{82}{420}\right) = .429$
89	$C_{Y\delta_r} = - a_F \frac{s_F}{S} \frac{d\alpha_F}{d\delta_r}$ $= - (2.5) \left(\frac{152}{945}\right) (.58) = - .233$	$= - (2.8) \left(\frac{82}{420}\right) (.58) = - .317$

NO.	BUFFALO	TWIN OTTER
90	<p> $C_{l\beta} = C_{l\beta_w} + C_{l\beta_{fuselage}} + C_{l\beta_F}$ </p> <p> from figure: $\xi=1.0$ $\leftarrow \xi=0$ $\rightarrow \xi=.34$ </p>  <p>(geom from Fig. 3) $5^\circ = .087 \text{ rad}$</p> <p> $C_{l\beta_w} = \left[\left(\frac{C_{l\beta_w}}{\Gamma} \right)_{\xi=1.0} - \left(\frac{C_{l\beta_w}}{\Gamma} \right)_{\xi=.34} \right] \Gamma$ </p> <p> $AR = 9.75, \lambda = .5$ </p> <p> $= [(-.84) - (-.14)] \cdot .087 = -.061$ </p> <p> $C_{l\beta_{fuselage}} = 1.2 \sqrt{AR} \frac{z_w}{b} \cdot \frac{h+w}{b}$ </p> <p> $= 1.2 \sqrt{9.75} \left(\frac{-3.5}{96} \right) \left(\frac{9.8+10}{96} \right) = -.028$ </p> <p> $C_{l\beta_F} = C_{y\beta} \frac{z_F}{b}$ </p> <p> $= (-.362) \left(\frac{10}{96} \right) = -.036$ </p> <p> $C_{l\beta} = -.061 - .028 - .036 = -.125$ </p>	 <p> $AR = 10, \lambda = 1.0$ </p>  <p> $2^\circ = .035 \text{ rad}$ (geom from Fig. 4) </p> <p> $C_{l\beta_w} = \left(\frac{C_{l\beta_w}}{\Gamma} \right) \Gamma = (-.86) (.035) = -.030$ </p> <p> $= 1.2 \sqrt{10} \left(\frac{-3.0}{65} \right) \left(\frac{7+6}{65} \right) = -.035$ </p> <p> $= (-.492) \left(\frac{5}{65} \right) = -.038$ </p> <p> $= -.030 - .035 - .038 = -.103$ </p> <p>Source: Ref. 3, p 344</p>

NO.	BUFFALO	TWIN OTTER
91	<p>C_{l_p} from figure →</p> <p>for AR = 9.75, $\lambda = .5$:</p> <p>$C_{l_p} = - .53$</p>	 <p>for AR = 10, $\lambda = 1.0$:</p> <p>$C_{l_p} = - .60$</p>
92	$C_{l_r} = C_{l_{r_w}} + C_{l_{r_f}}$ $= \frac{C_{L_0}}{4} + C_{Y_r} \frac{z_F}{b}$ <p>Cruise</p> $= \frac{.30}{4} + (.368) \left(\frac{10}{96} \right) = .075 + .038$ <p>Slow Flt</p> $= \frac{.77}{4} + .038 = .231$ <p>Lndg Appr</p> $= \frac{1.49}{4} + .038 = .410$	<p>Cruise</p> $= \frac{.42}{4} + (.429) \left(\frac{5}{65} \right) = .105 + .033$ <p>Slow Flt</p> $= \frac{.78}{4} + .033 = .233$ <p>Lndg Appr</p> $= \frac{1.65}{4} + .033 = .451$

Source: Ref. 3, p 357

NO.	BUFFALO	TWIN OTTER
93	$C_{l\delta r} = C_{y\delta r} \frac{z_F}{b}$ <p style="text-align: center;"> (89) (2) (54) </p> $= (-.233) \left(\frac{10}{96} \right) = -.024$	$= (-.317) \left(\frac{5}{65} \right) = -.024$
94	$C_{l\delta a} = \frac{2 a \tau}{Sb} \int_{y_1}^2 c_y dy$ <p style="text-align: center;"> (5) (63) (65) </p> <p style="text-align: center;"> (1) (2) (64) (4) </p> $= \frac{2(5.2)(.43)}{(945)(96)} \int_{33}^{47} (14.82 - .186y) y dy$ $= .0000493 [7.41(47^2 - 33^3) - .062(47^3 - 33^3)] = .20$	$= \frac{2(5.2)(.40)}{(420)(65)} \int_{14}^{31} 6.5 y dy$ $= .00099 \left(\frac{31^2 - 14^2}{2} \right) = .38$
95	$C_{n\beta} = C_{n\beta F} + C_{n\beta \text{ fuselage}}$ $C_{n\beta F} = - C_{y\beta F} \frac{l_F}{b}$ <p style="text-align: center;"> (86) (53) </p> <p style="text-align: center;"> (2) </p> $= - (-.362) \left(\frac{44}{96} \right) = .166$ <p style="text-align: center;"> (66) (60) </p> <p style="text-align: center;"> (vol fuse) </p> $C_{n\beta \text{ fuse}} = - 1.3 \frac{h}{Sb w}$ <p style="text-align: center;"> (1) (2) (61) </p> $= - 1.3 \frac{(4600)}{(945)(96)} \left(\frac{9.8}{10} \right) = -.065$ $C_{n\beta} = .166 - .065 = .101$	$= - (-.492) \left(\frac{25.5}{65} \right) = .193$ $= - 1.3 \frac{(1300)}{(420)(65)} \left(\frac{7}{6} \right) = -.072$ $C_{n\beta} = .193 - .072 = .121$

NO.	BUFFALO	TWIN OTTER
96	$C_{n_p} = C_{n_{p_w}} + C_{n_{p_f}}$ $C_{n_{p_w}} = -\frac{C_{L_0}}{4} \left[1 - \frac{C_{L_0}}{\pi AR} \right]$ $= -\frac{C_{L_0}}{4} \left[1 - \frac{5.2}{9.75\pi} \right]$ $= -.207 C_{L_0}$ $C_{n_{p_f}} = -C_{y_{p_f}} \frac{l_F}{b}$ $= -(-.055) \left(\frac{44}{96} \right) = .025$ <p>Cruise</p> $C_{n_p} = -.207(.30) + .025$ $= -.037$ <p>Slow Flt</p> $= -.207(.77) + .025 = -.134$ <p>Lndg Appr</p> $= -.207(1.49) + .025 = -.283$	$= -\frac{C_{L_0}}{4} \left[1 - \frac{5.2}{10\pi} \right]$ $= -.208 C_{L_0}$ $= -(-.085) \left(\frac{25.5}{65} \right) = .033$ <p>Cruise</p> $= -.208(.42) + .033 = -.054$ <p>Slow Flt</p> $= -.208(.78) + .033 = -.129$ <p>Lndg Appr</p> $= -.208(1.65) + .033 = -.310$

NO.	BUFFALO	TWIN OTTER
97	$C_{n_r} = C_{n_{r_F}} + C_{n_{r_w}}$ $C_{n_{r_F}} = - \frac{\ell_F}{b} C_{y_{r_F}}$ $= - \left(\frac{44}{96}\right) (.368) = - .169$ $C_{n_{r_w}} = - C_{D_w/4}$ <p>Cruise</p> $C_{n_r} = \frac{-.009}{4} - .169 = - .171$ <p>Slow Flt</p> $= - \frac{.025}{4} - .169 = - .175$ <p>Lndg Appr</p> $= - \frac{.077}{4} - .169 = - .188$	$= - \left(\frac{25.5}{65}\right) (.429) = - .168$ <p>Cruise</p> $C_{n_r} = - \frac{.012}{4} - .168 = - .171$ <p>Slow Flt</p> $= - \frac{.025}{4} - .168 = - .174$ <p>Lndg Appr</p> $= - \frac{.093}{4} - .168 = - .191$
98	$C_{n_{\delta_r}} = - C_{y_{\delta_r}} \frac{\ell_F}{b}$ $= - (- .233) \left(\frac{44}{96}\right) = .107$	$= - (- .317) \left(\frac{25.5}{65}\right) = .124$
99	$C_{n_{\delta_a}} = 0$	

NO.	PARAMETER	BUFFALO			TWIN OTTER		
		CRUISE	SLOW FLIGHT	LANDING APPROACH	CRUISE	SLOW FLIGHT	LANDING APPROACH
100	q S	132,500	52,000	26,850	28,750	15,500	7,260
101	q S/U _o	331	242	174	103	88	61
102	q Sc	1.34x10 ⁶	.5252x10 ⁶	.2715x10 ⁶	185,500	100,800	47,100
103	q Sc/U _o	3350	2440	1760	667	572	392
104	q Sb	12.75x10 ⁶	5.0x10 ⁶	2.58x10 ⁶	1.855x10 ⁶	1.008x10 ⁶	.471x10 ⁶
105	q Sb/U _o	31,850	23,200	16,700	6,670	5,720	3,920
106	c/2U _o	.0126	.0235	.0328	.0117	.0185	.027
107	b/2U _o	.120	.223	.312	.1170	.185	.270
108	m	1240	1240	1240	372	372	372
109	I _x	273,000	273,000	273,000	24,300	24,300	24,300
110	I _y	215,000	215,000	215,000	22,000	22,000	22,000
111	I _z	447,000	447,000	447,000	41,000	41,000	41,000

Appendix D. Transient Responses to Control Inputs

In this appendix, transient responses (or time histories) of aircraft motions in response to step control inputs are presented. Equations 48-53 of Section V and the numerical values developed elsewhere in this report are used.

Figure D1 shows the response in pitch rate $\dot{\theta}$, pitch angle $\Delta\theta$, angle of attack α , altitude Δh , and forward speed $(\Delta U/U_0)$ resulting from a step elevator input $\Delta\delta_e$ for the "Buffalo" aircraft in the cruise flight condition.

Figure D2 shows the response (again for the Buffalo in cruise flight) in the same parameters resulting from a step change in thrust ΔT .

Figures D3 and D4 present Buffalo $\Delta\delta_e$ and ΔT responses respectively with the aircraft at the slow flight condition.

Figures D5 and D6 present the same responses for the landing approach condition. In Figures D5-D6 (and in Figures D17-D18), altitude (Δh) is plotted as the change from the nominal altitude resulting from a steady descent at -7.5° flight path angle.

Figures D7-D12 present lateral responses for the Buffalo. Figure D7 shows the response in sideslip angle β , roll rate $\dot{\phi}$, roll angle ϕ , yaw rate $\dot{\psi}$, and yaw angle ψ resulting from a 1° step aileron input δ_a at the cruise flight condition.

Figure D8 shows the lateral response in cruise flight due to a 1° step rudder input δ_r .

Figures D9 and D10 present δ_a and δ_r responses respectively for the Buffalo at the slow flight condition.

Figures D11 and D12 present the same information for the landing approach configuration.

Finally, Figures D13-D24 present the same information for the Twin Otter aircraft as is given in Figures D1-D12 for the Buffalo.

Time constants, natural frequencies and damping ratios associated with the transient responses shown in figures D1-D24 are presented in Table D1. These were generated as part of the transient response computer program.

TABLE D1

Summary of Characteristic Response Parameters
For "Buffalo" and "Twin Otter" Aircraft

		BUFFALO			TWIN OTTER			
		CRUISE	SLOW FLIGHT	APPROACH	CRUISE	SLOW FLIGHT	APPROACH	
Longitudinal	SHORT PERIOD OSCILLATION							
	$\omega_n - \frac{\text{RAD}}{\text{SEC}}$	2.93	1.98	1.42	3.14	2.46	1.69	
	ζ	.794	.855	.856	.710	.780	.783	
	$1/\zeta\omega_n - \text{SEC}$.43	.59	.82	.45	.52	.76	
	LONG PERIOD OSCILLATION							
	$\omega_n - \frac{\text{RAD}}{\text{SEC}}$.084	.147	.205	.132	.198	.289	
	ζ	.166	.108	.082	.140	.101	.069	
	$1/\zeta\omega_n - \text{SEC}$	72	63	59.8	54	50.3	50	
	Lateral	LATERAL OSCILLATION						
		$\omega_n - \frac{\text{RAD}}{\text{SEC}}$	1.78	1.26	1.09	2.46	1.95	1.66
ζ		.162	.169	.193	.202	.254	.360	
$1/\zeta\omega_n - \text{SEC}$		3.48	4.69	4.77	2.02	2.02	1.67	
SPIRAL MODE (MINUS SIGN INDICATES DIVERGENCE)								
$\tau_s - \text{SEC}$		75.7	-379	-78.5	788	-48.5	-21.8	
ROLL SUBSIDENCE								
$\tau_R - \text{SEC}$.328	.446	.650	.185	.221	.376	

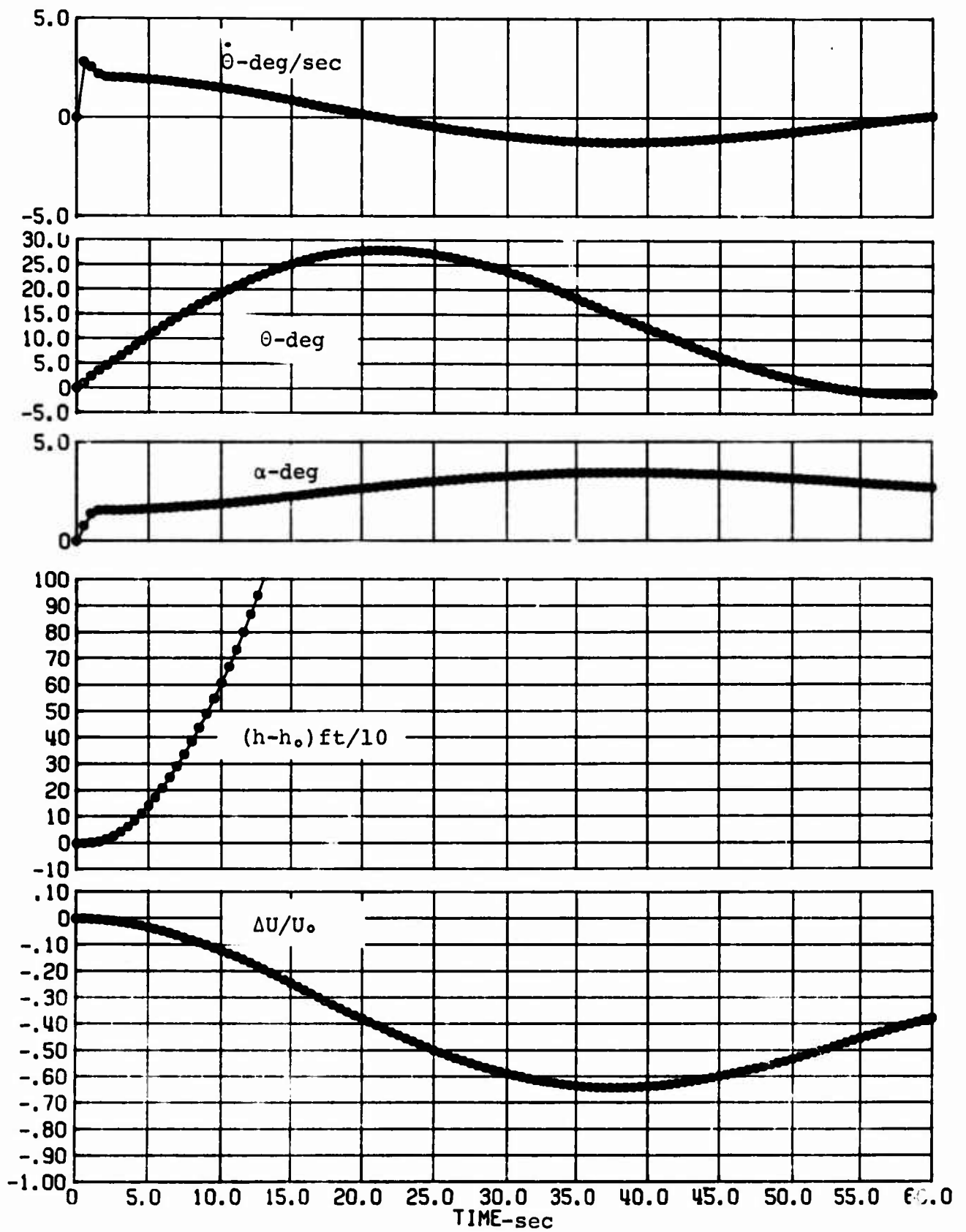


FIG.D-1 Response To 1° Step Elevator Input (Buffalo, Cruise)

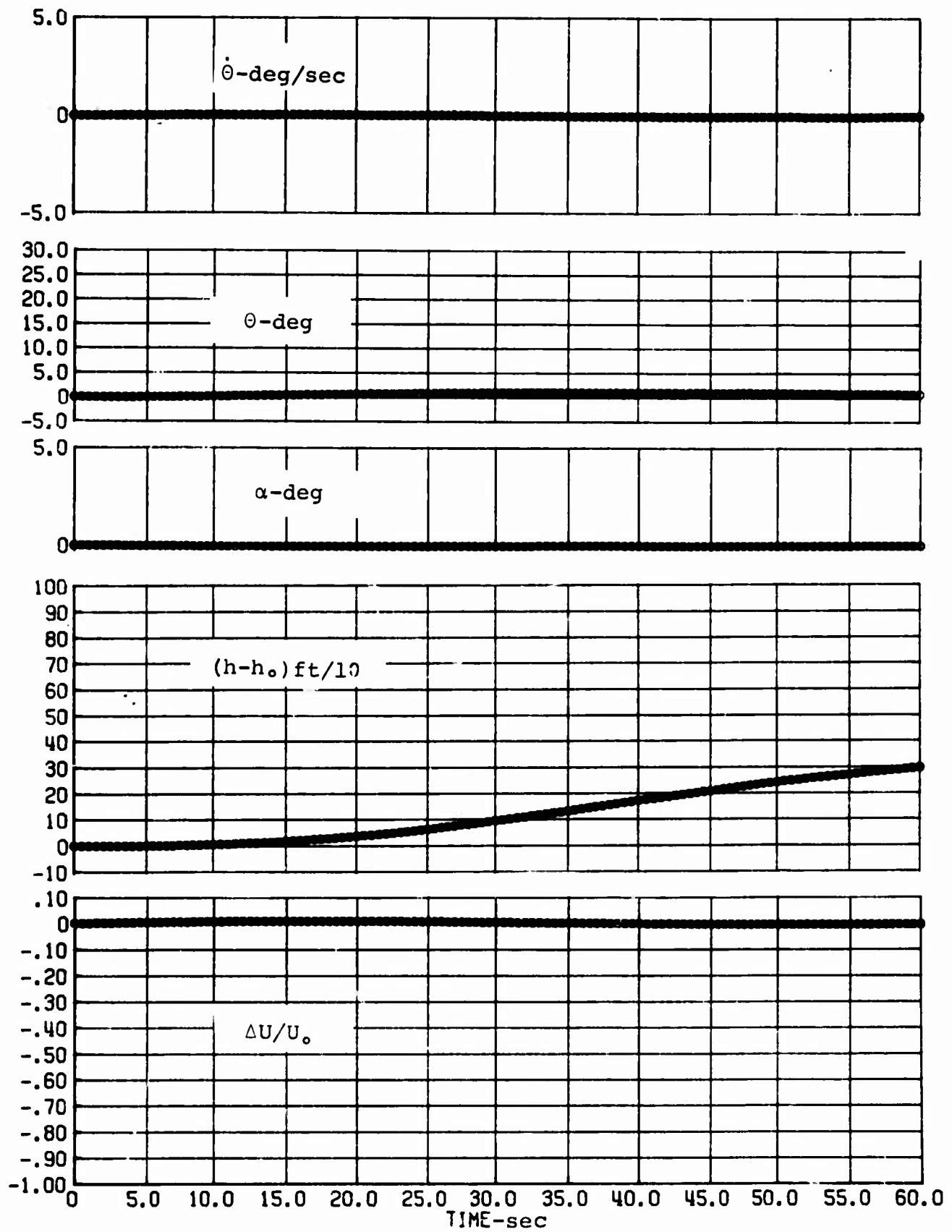


FIG.D-2 Response To 10% Thrust Input (Buffalo, Cruise)

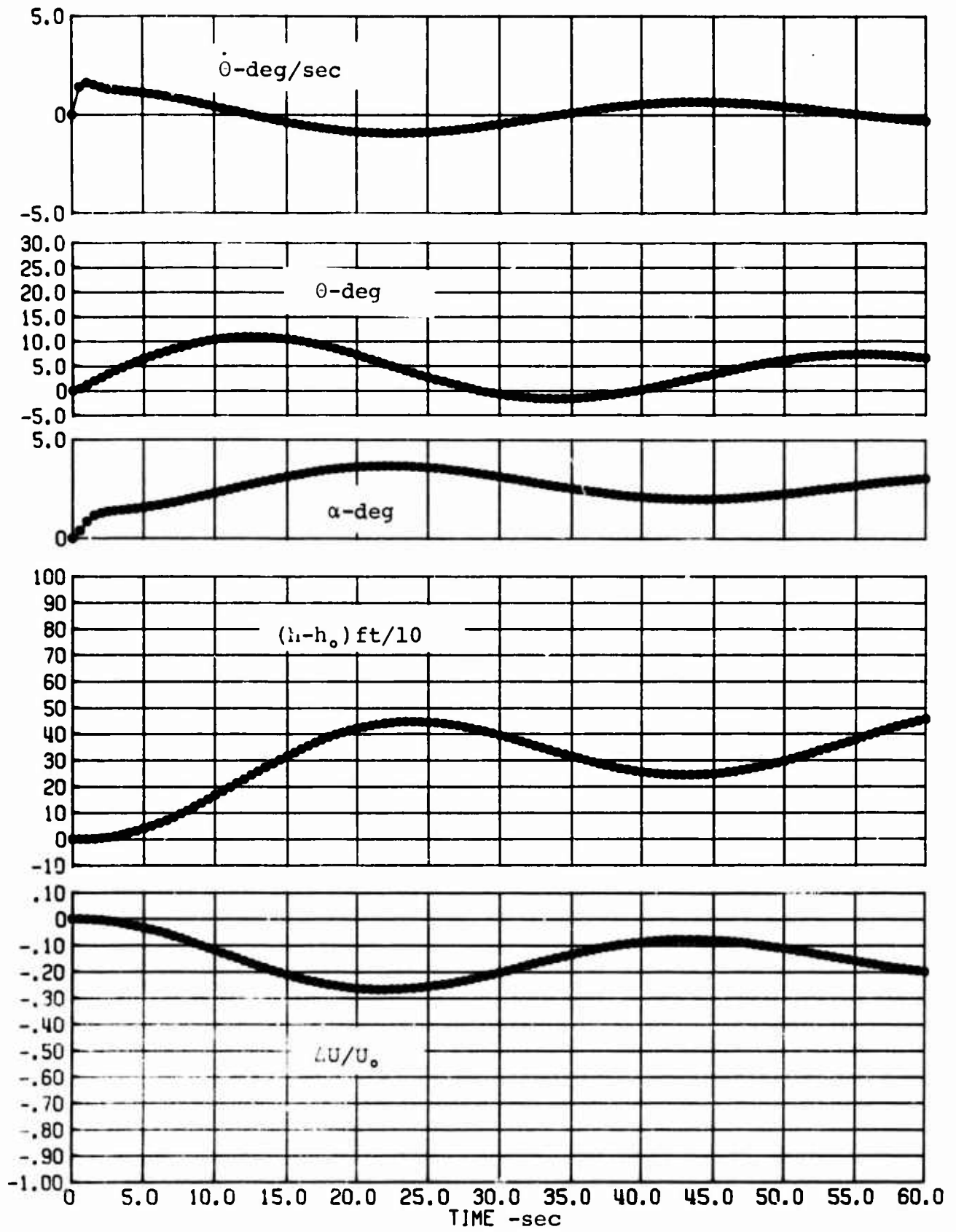


FIG. D-3 Response To 1° Step Elevator Input (Buffalo, Slow Flight)

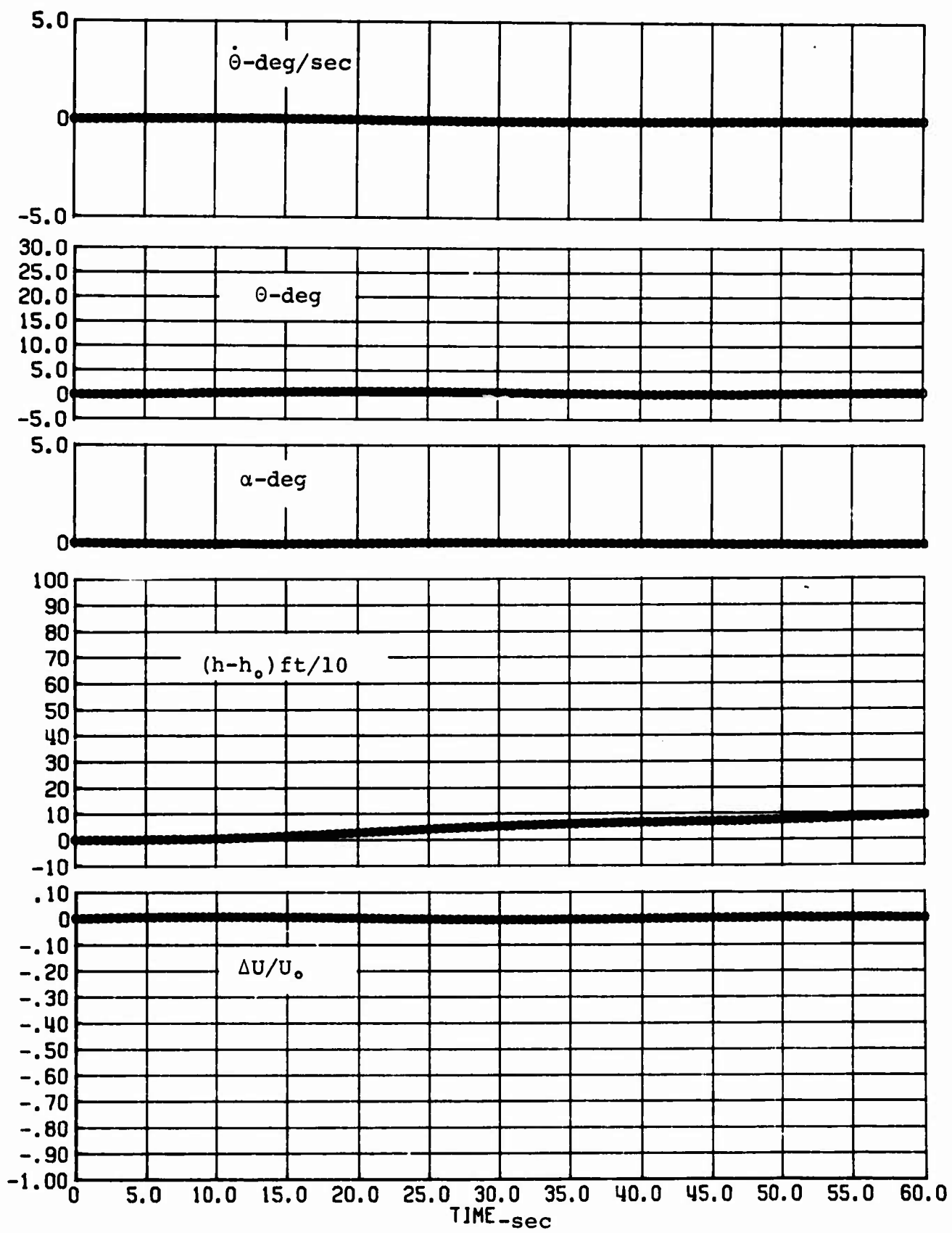


FIG. D-4 Response To 10% Thrust Input (Buffalo, Slow Flight)

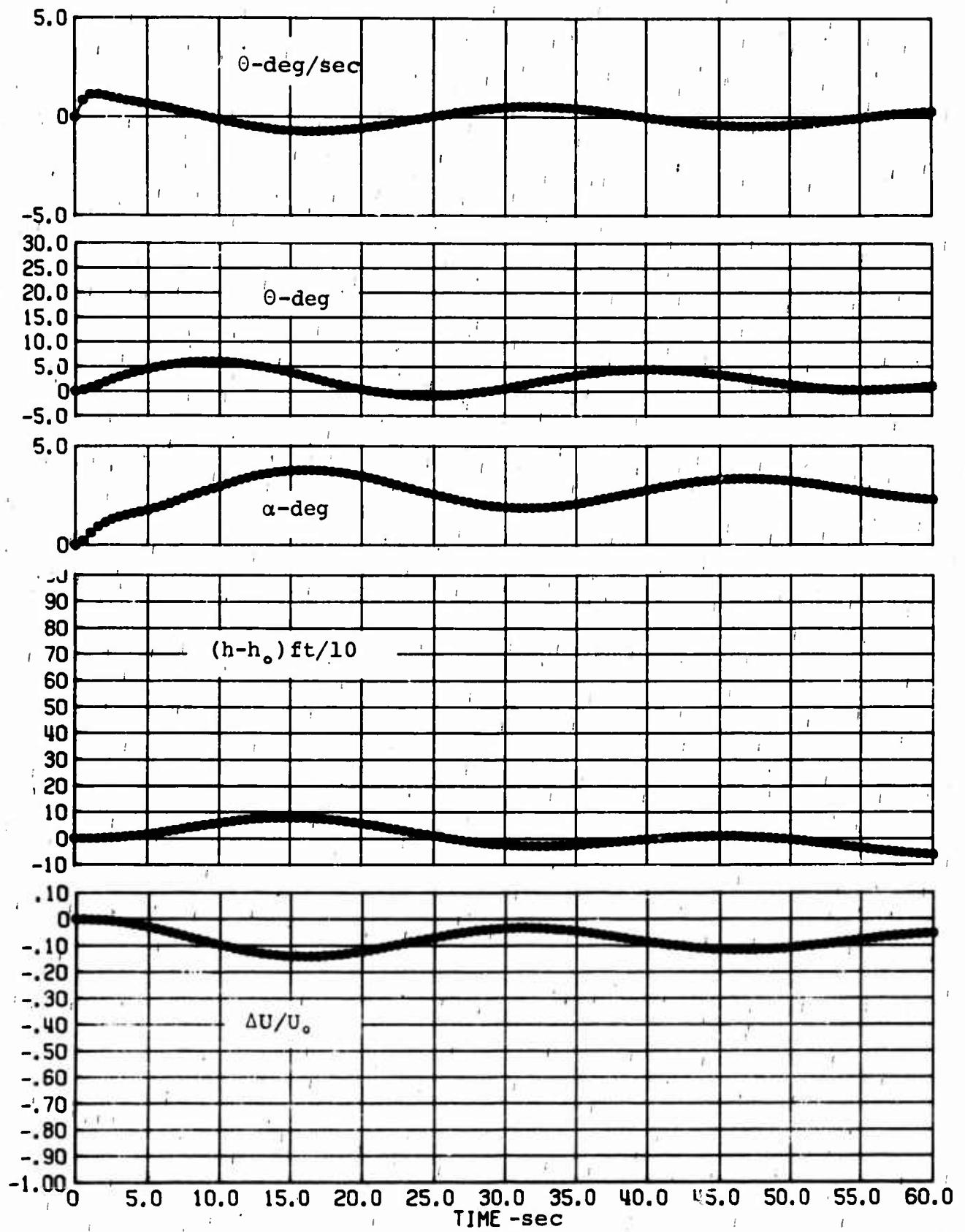


FIG.D-5 Response To 1° Step Elevator Input (Buffalo, Approach)

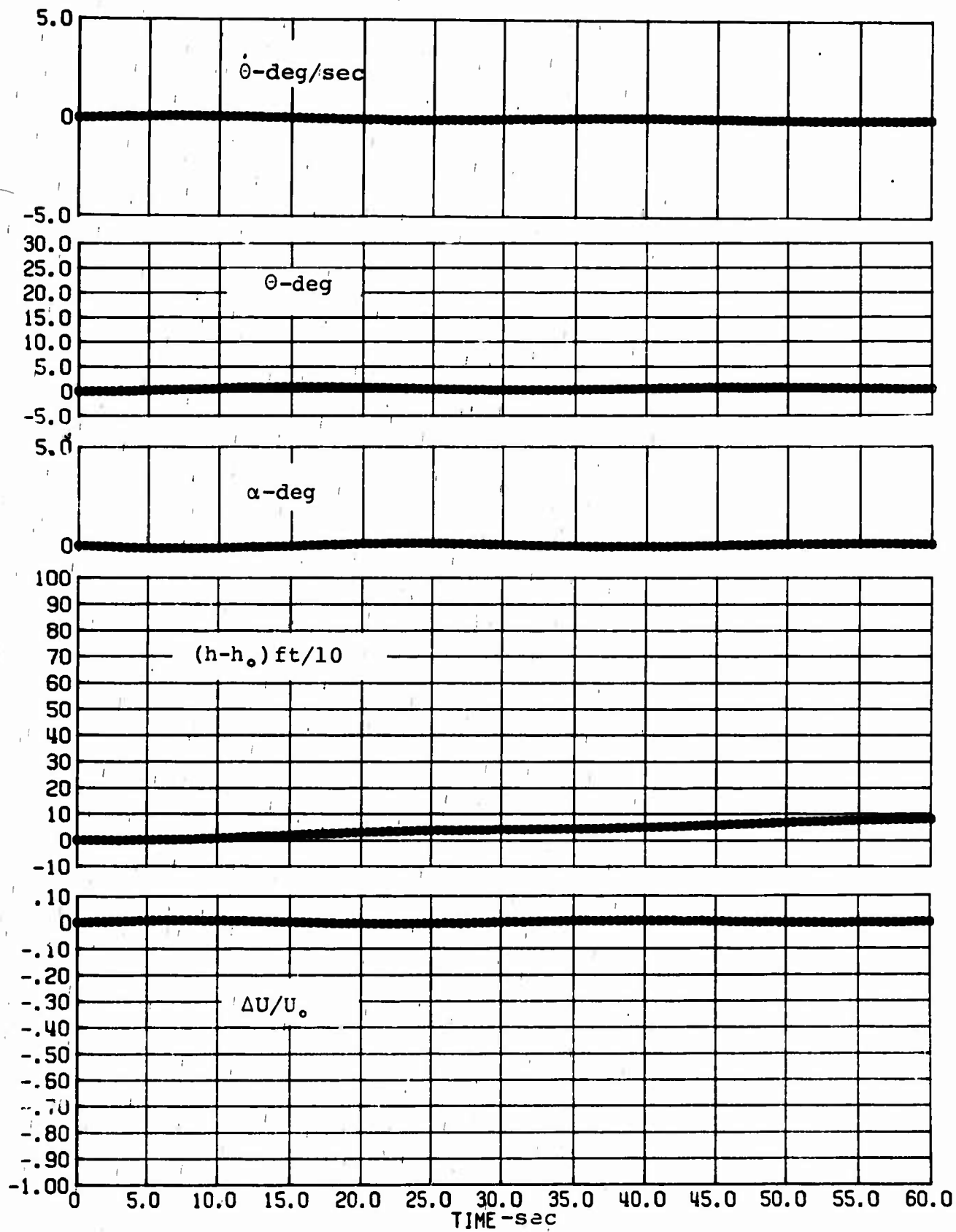


FIG.D-6 Response To 10% Thrust Input (Buffalo, Approach)

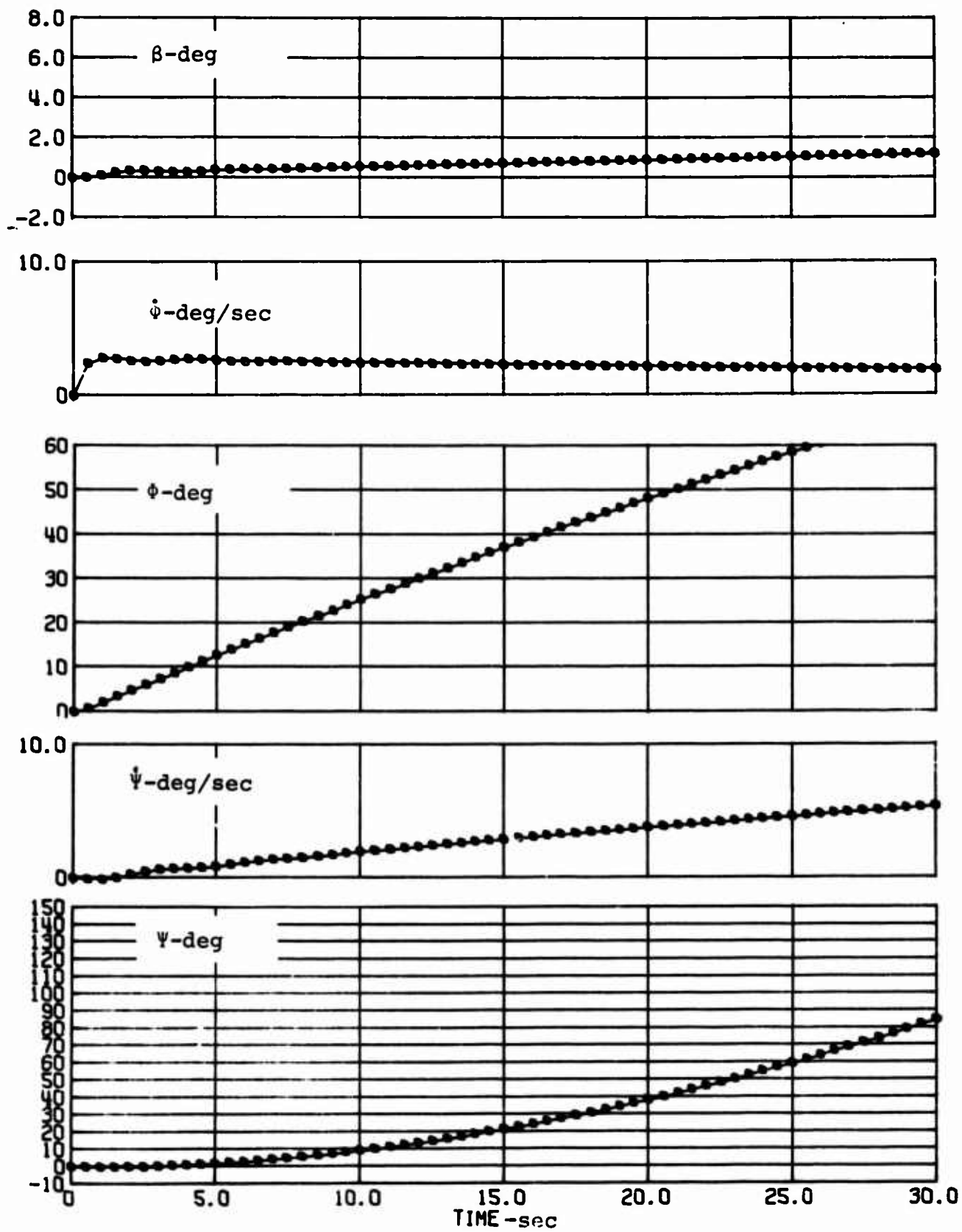


FIG.D-7 Response To 1° Step Aileron Input (Buffalo,Cruise)

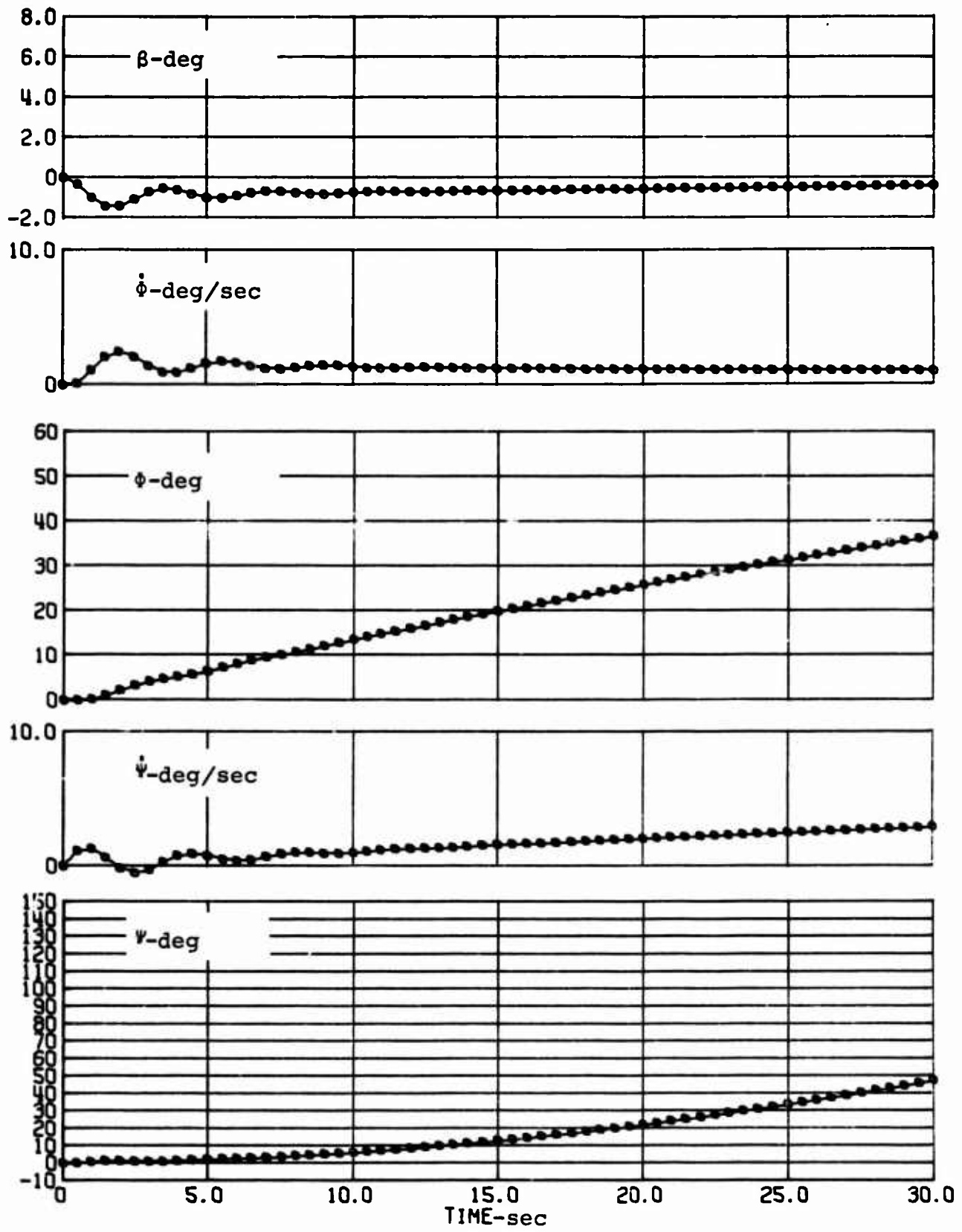


FIG.D- 8 Response To 1° Step Rudder Input (Buffalo,Cruise)

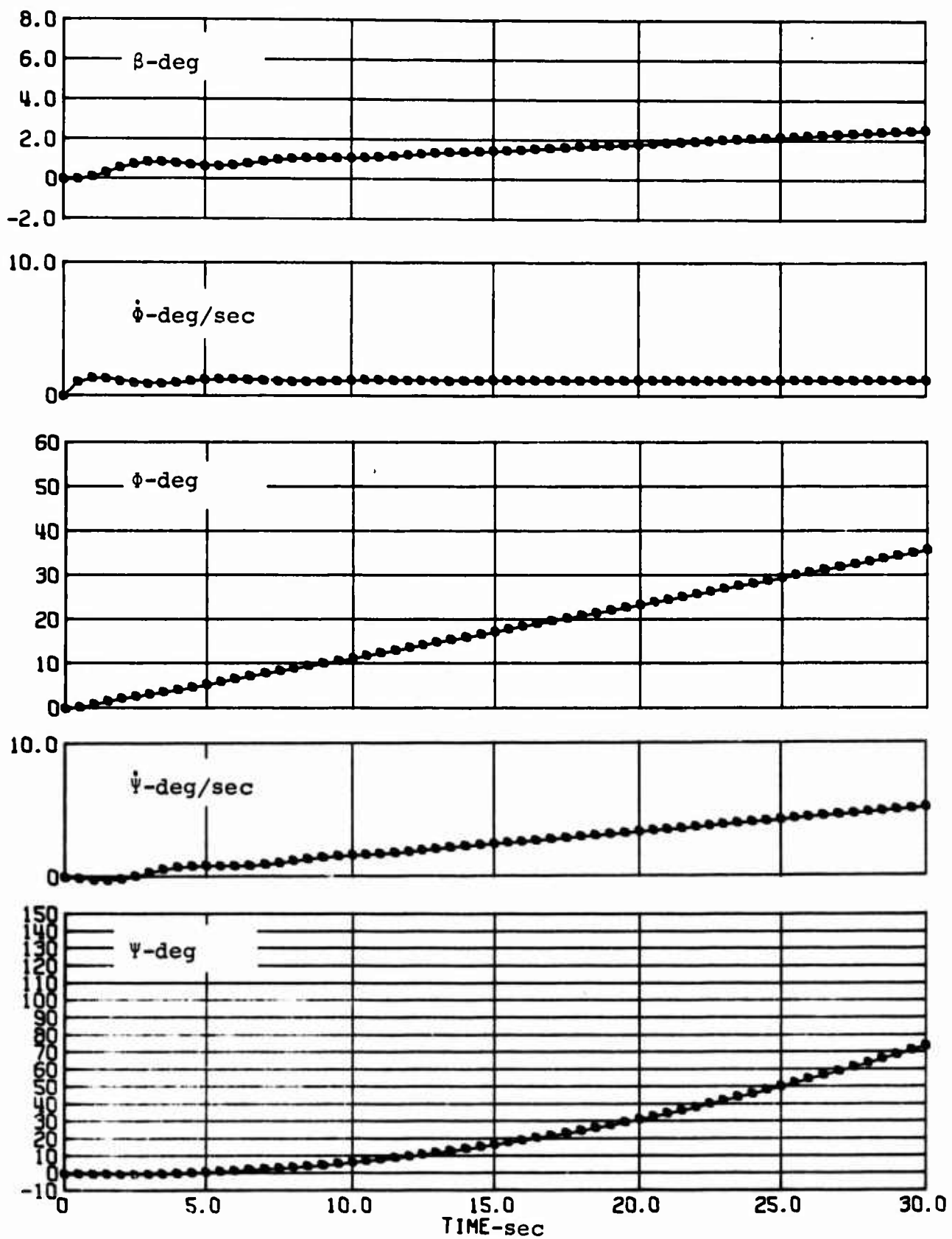


FIG.D-9 Response To 1° Step Aileron Input (Buffalo, Slow Flight)

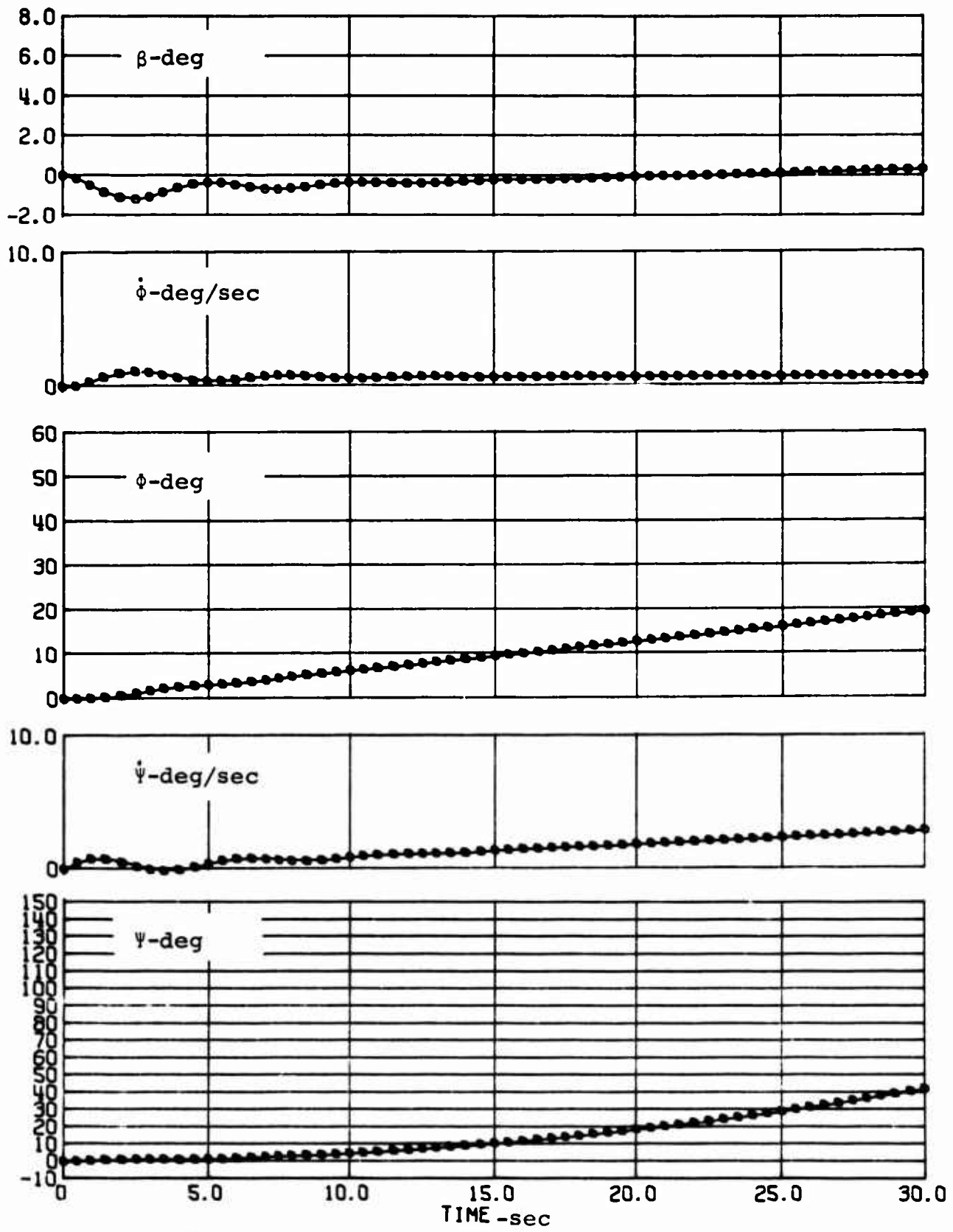


FIG.D-10 Response To 1° Step Rudder Input (Buffalo, Slow Flight)

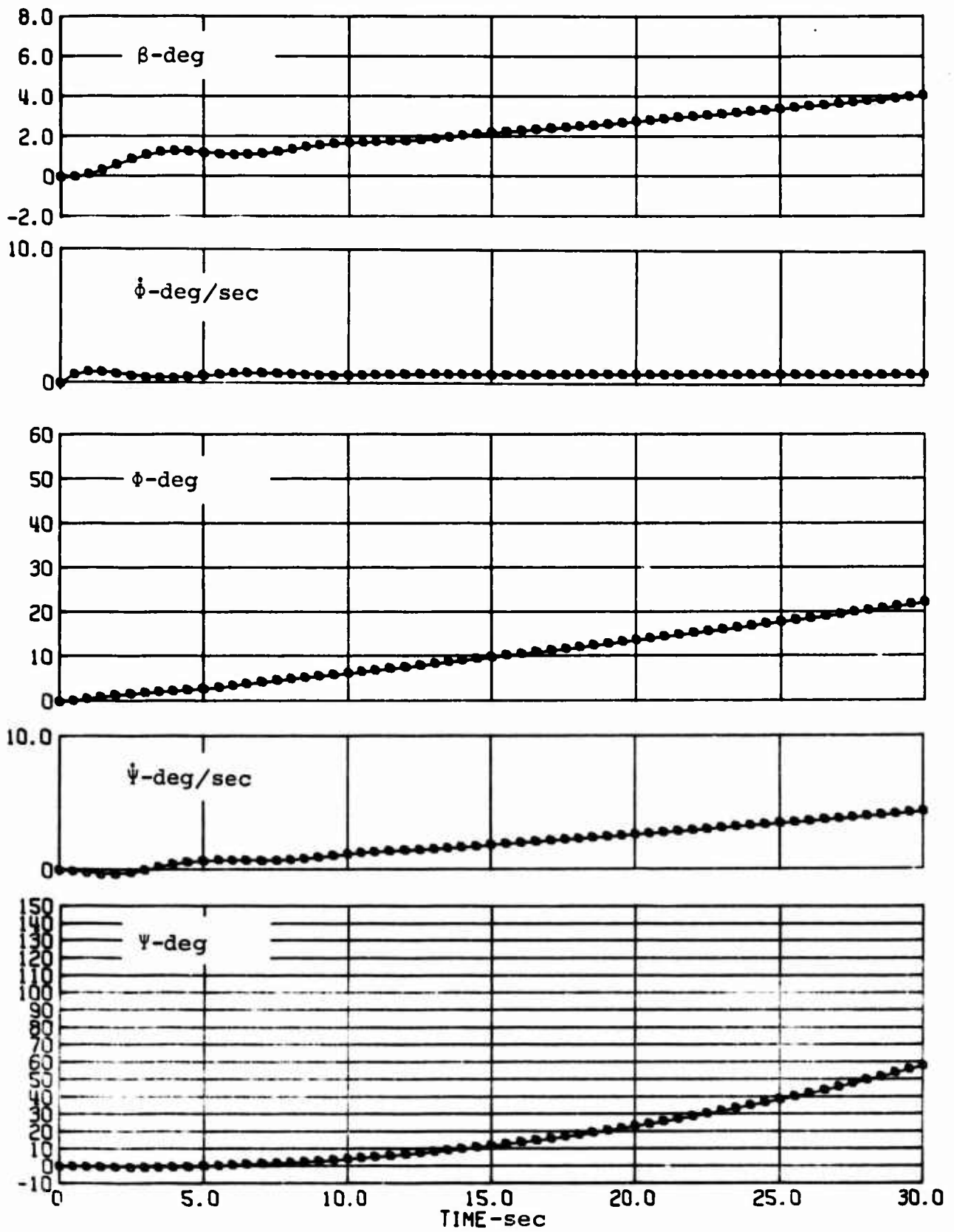


FIG.D-11 Response To 1° Step Aileron Input (Buffalo, Approach)

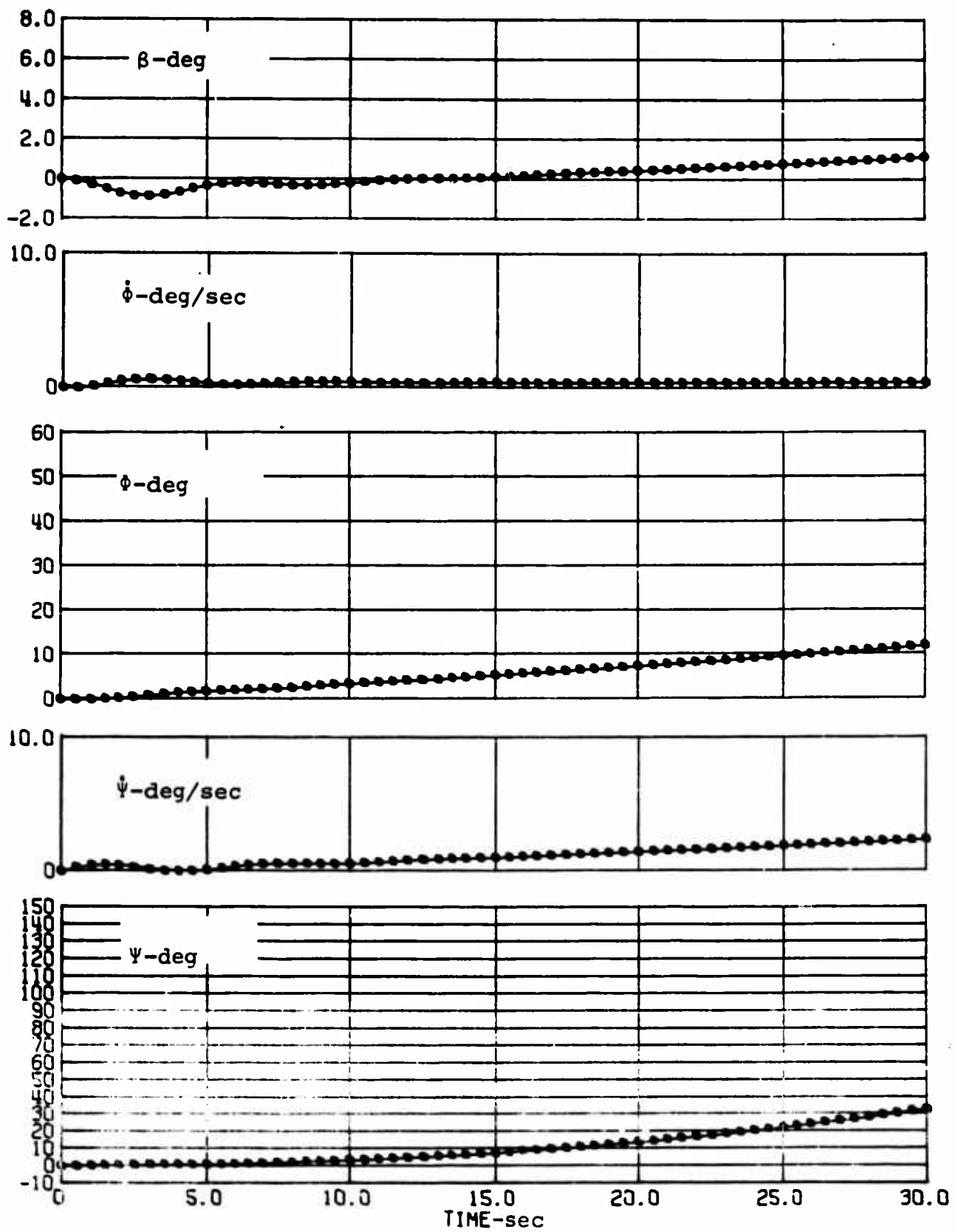


FIG.D-12 Response To 1° Step Rudder Input (Buffalo, Approach)

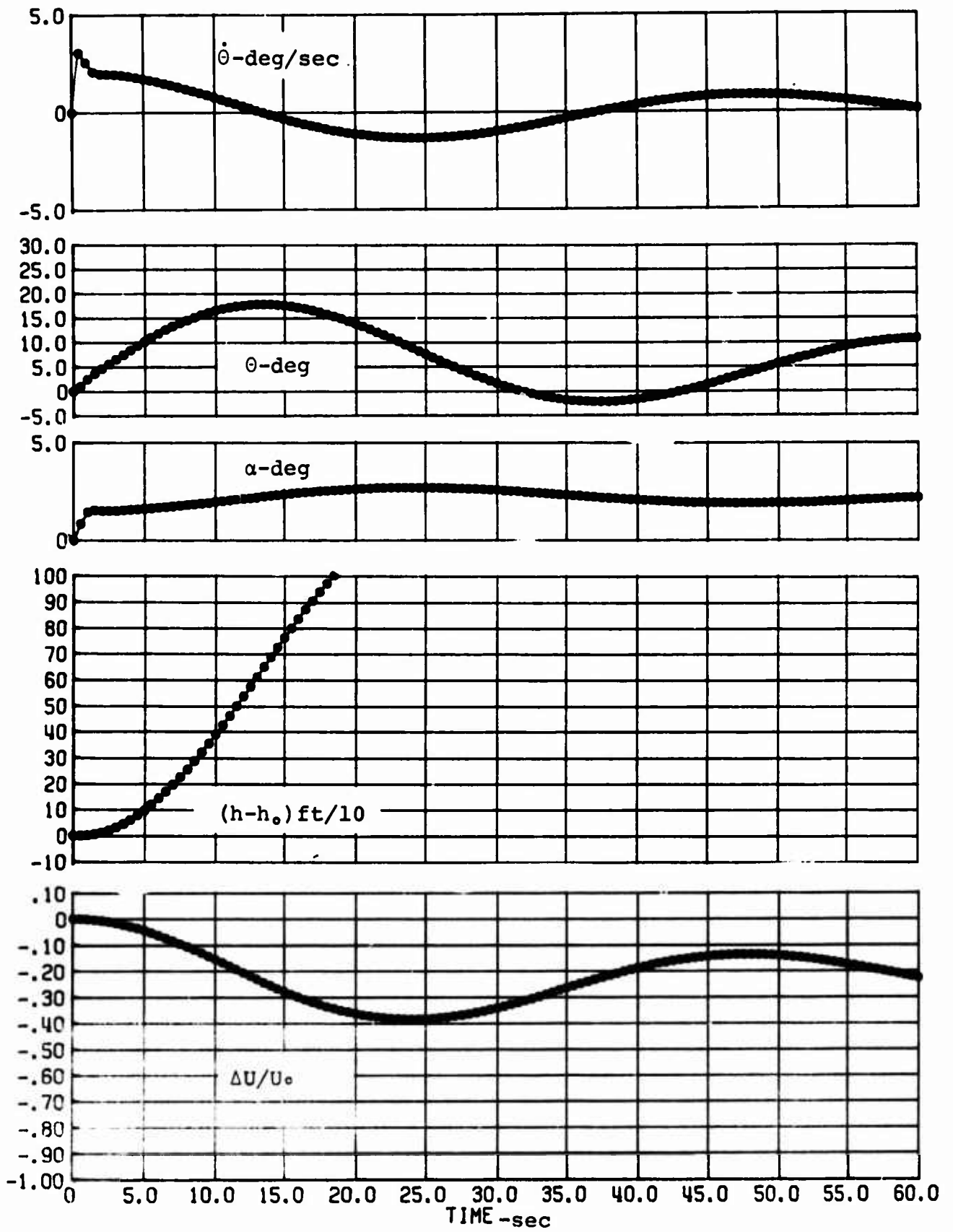


FIG.D-13 Response To 1° Step Elevator Input (Twin Otter, Cruise)

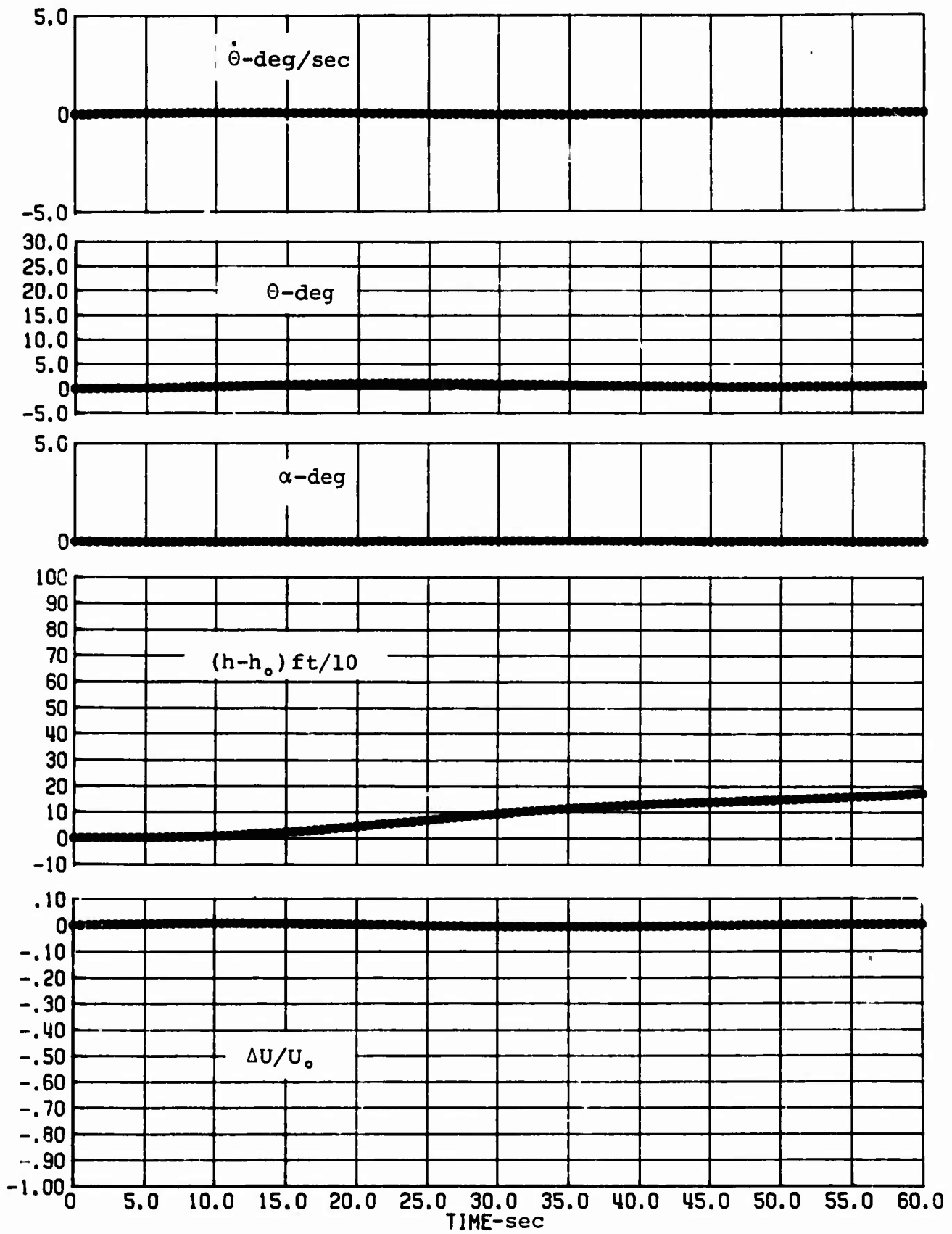


FIG.D-14 Response To 10% Thrust Input (Twin Otter, Cruise)

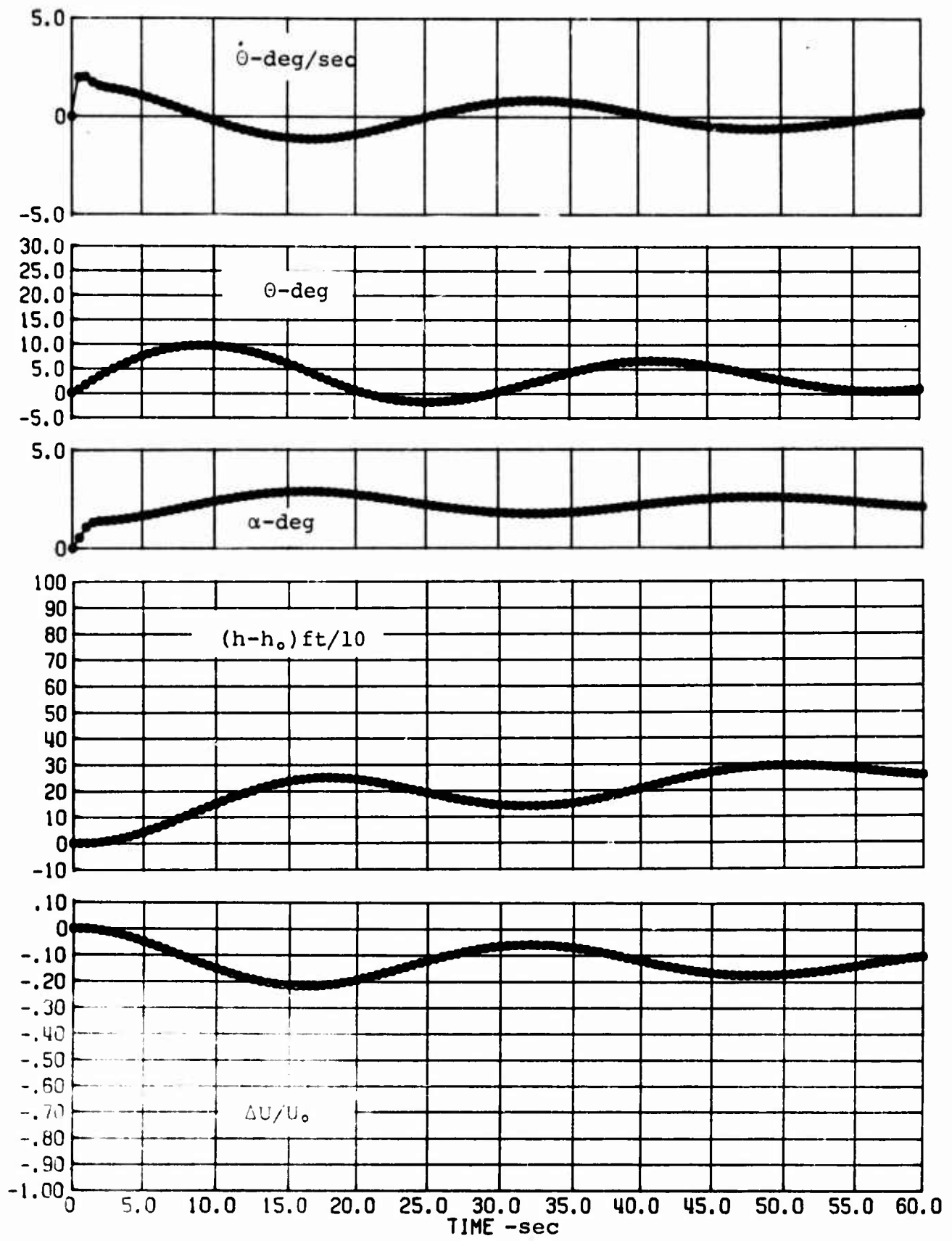


FIG.D-15 Response To 1° Step Elevator Input (Twin Otter, Slow Flight)

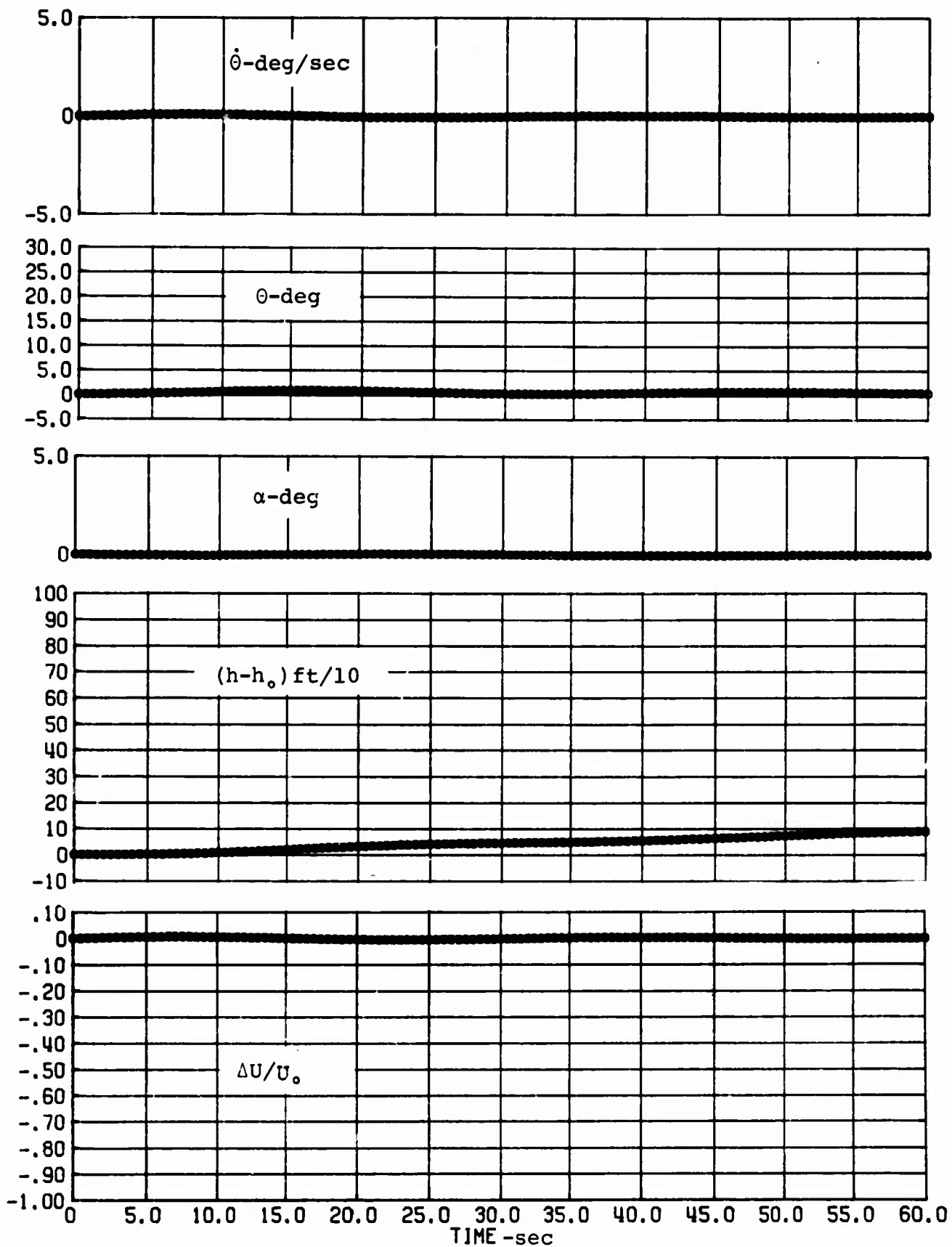


FIG.D-16 Response To 10% Thrust Input (Twin Otter, Slow Flight)

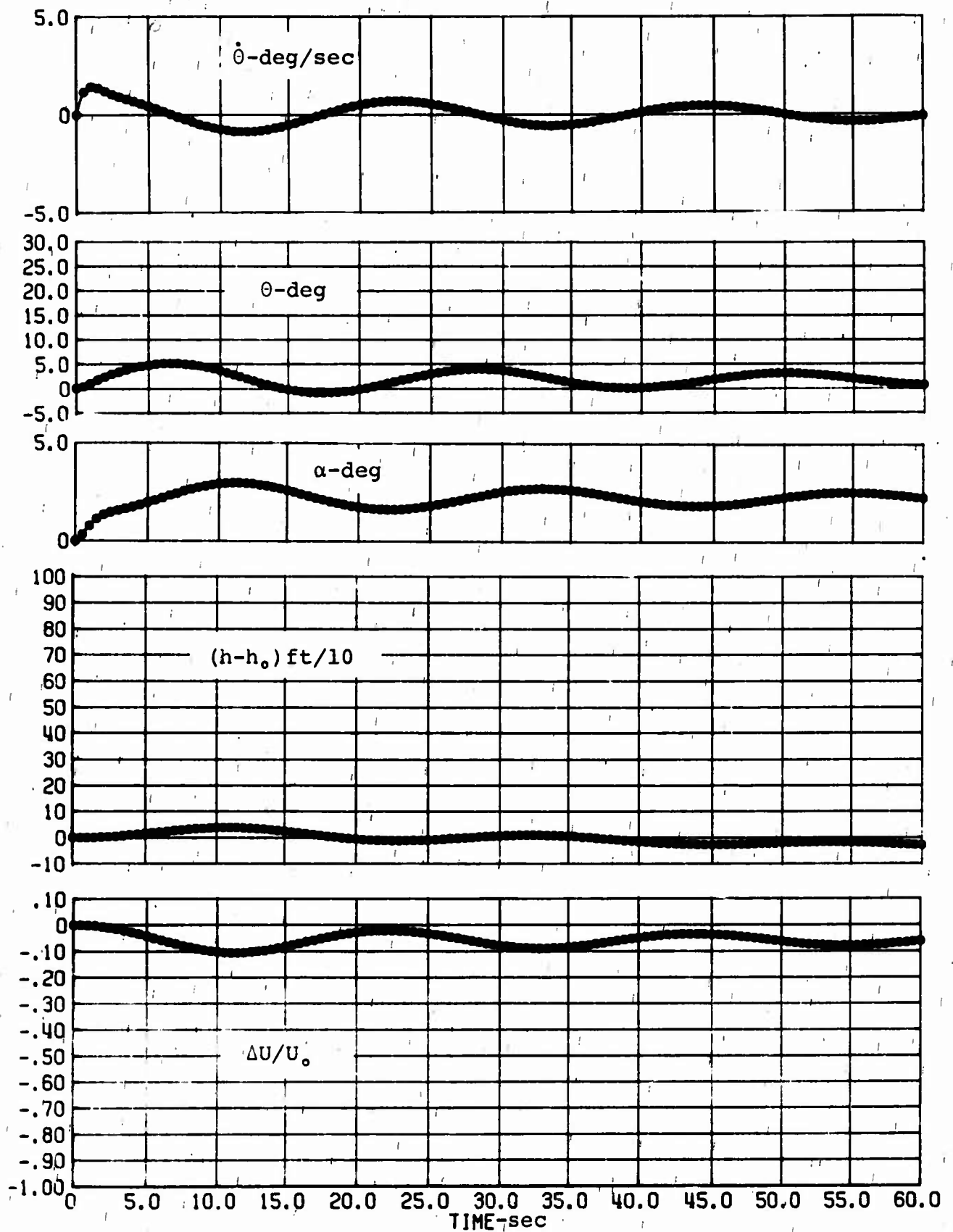


FIG.D-17 Response To 1° Step Elevator Input (Twin Otter, Approach)

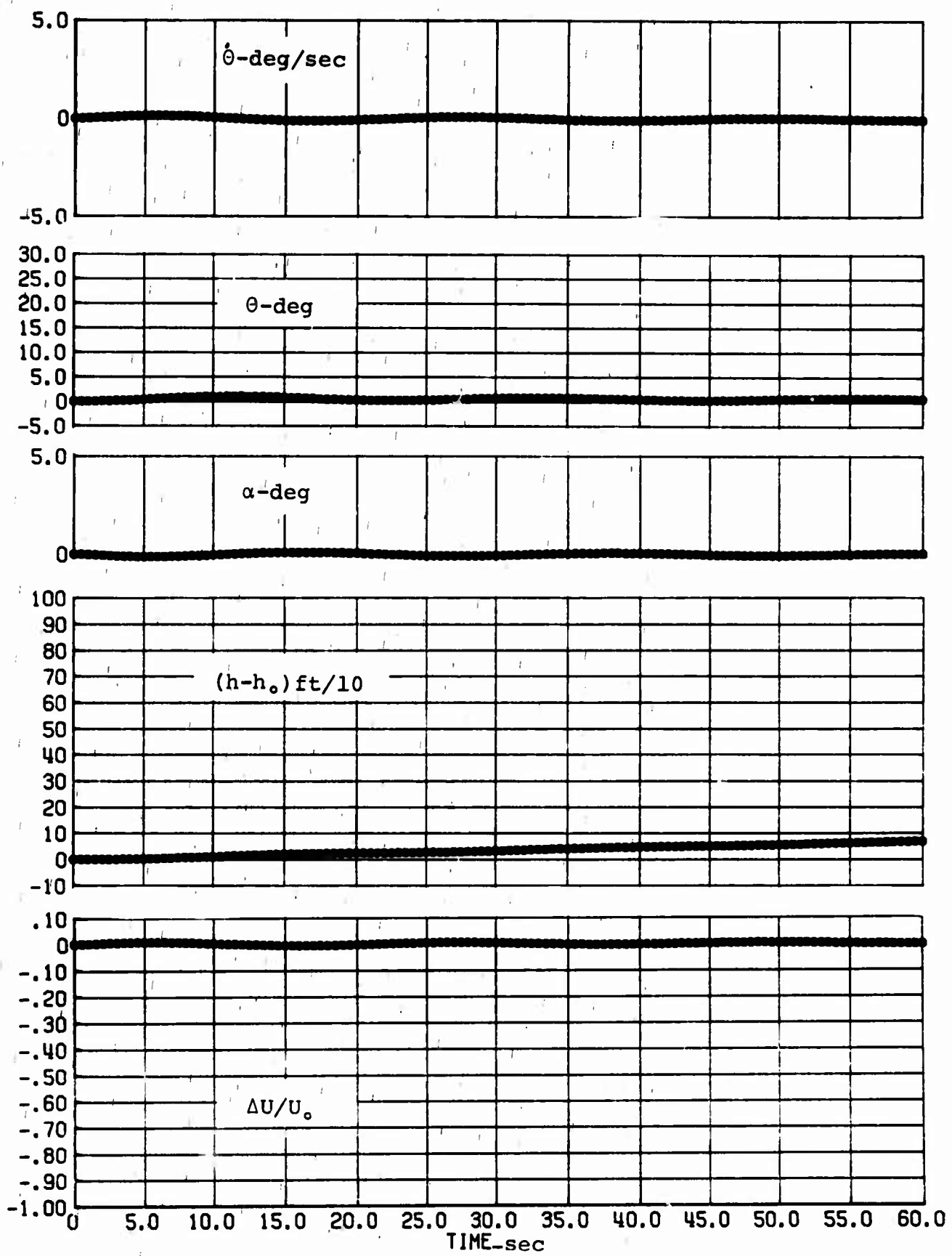


FIG.D-18 Response To 10% Thrust Input (Twin Otter, Approach)

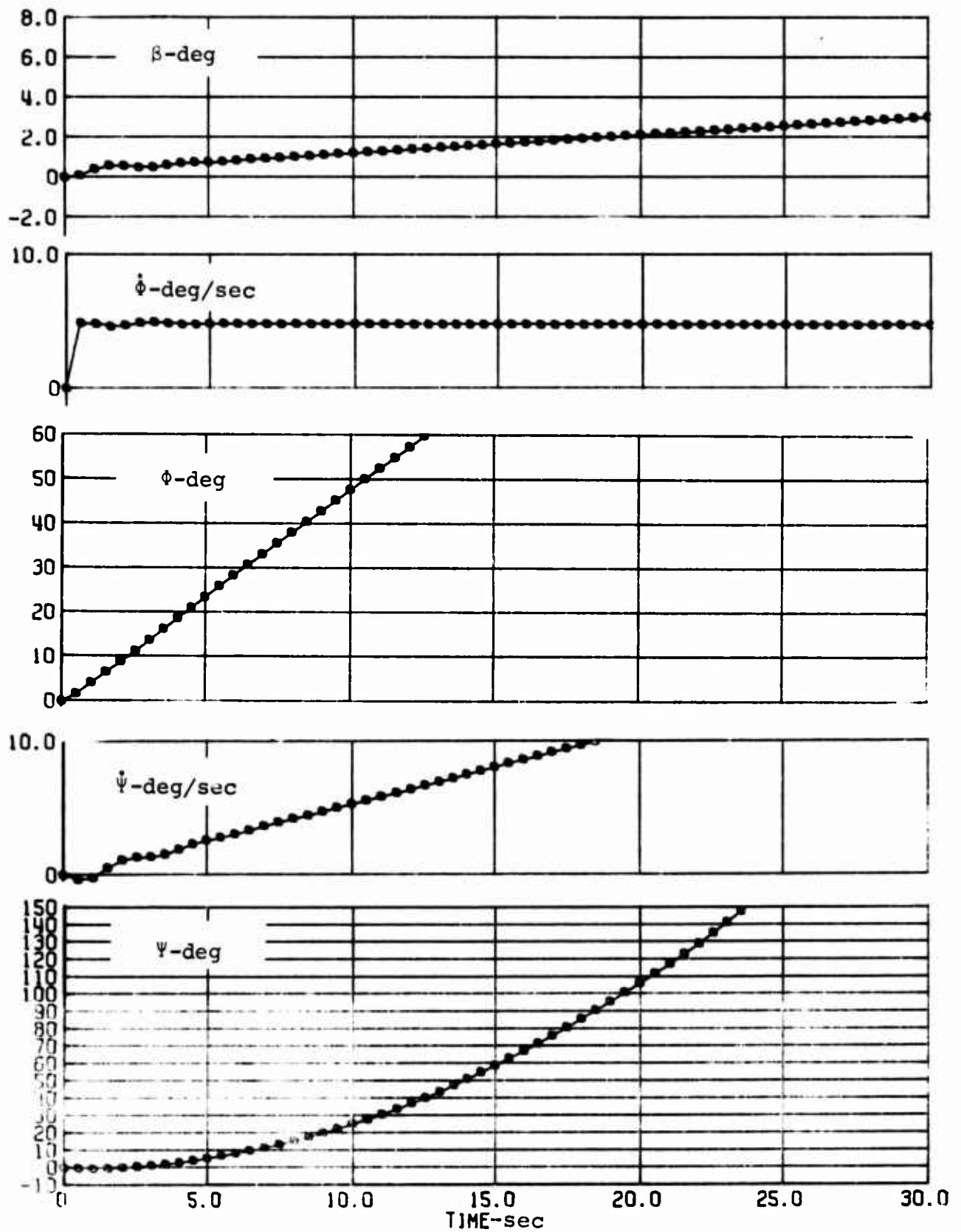


FIG.D-19 Response To 1° Step Aileron Input (Twin Otter,Cruise)

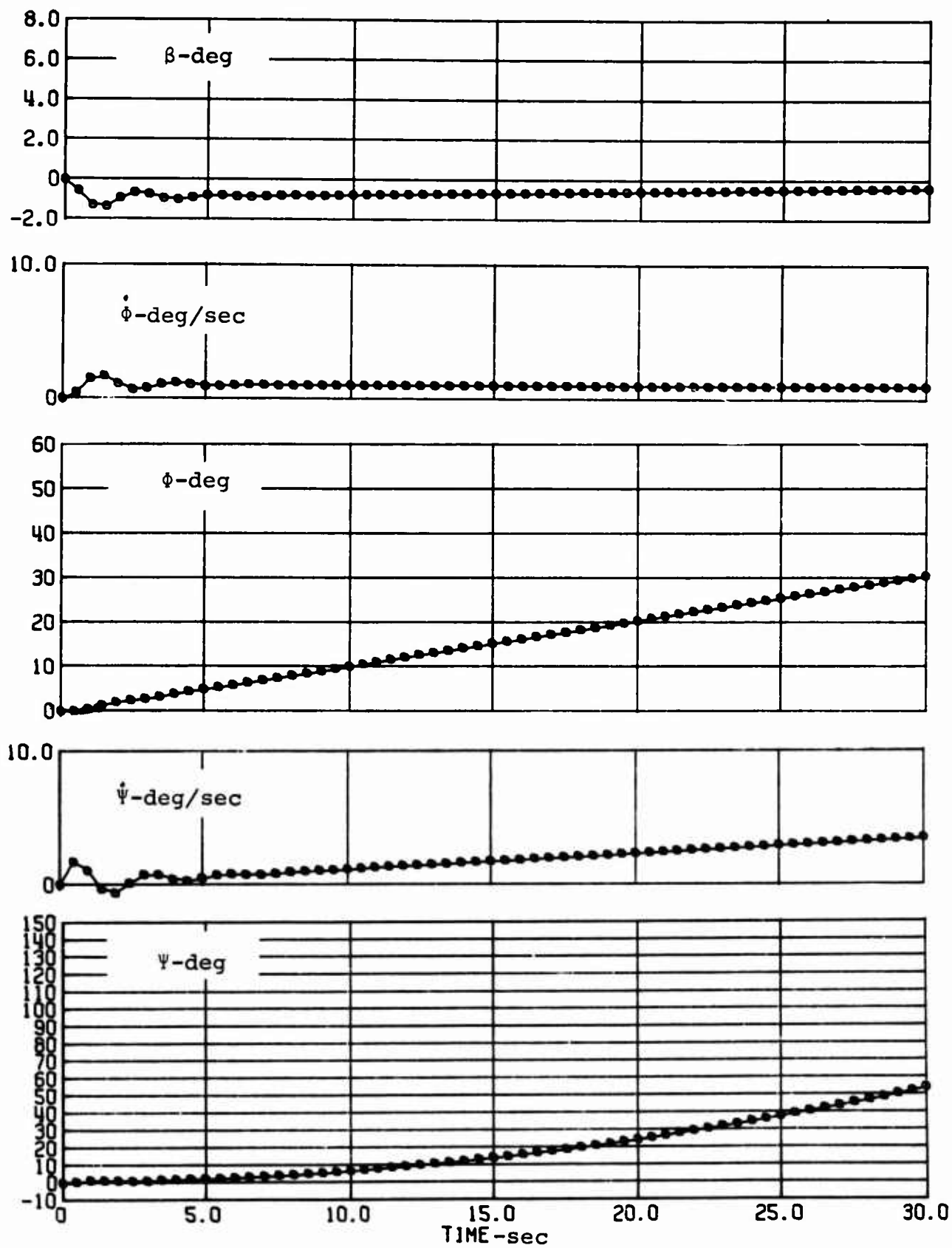


FIG.D-20 Response To 1° Step Rudder Input (Twin Otter, Cruise)

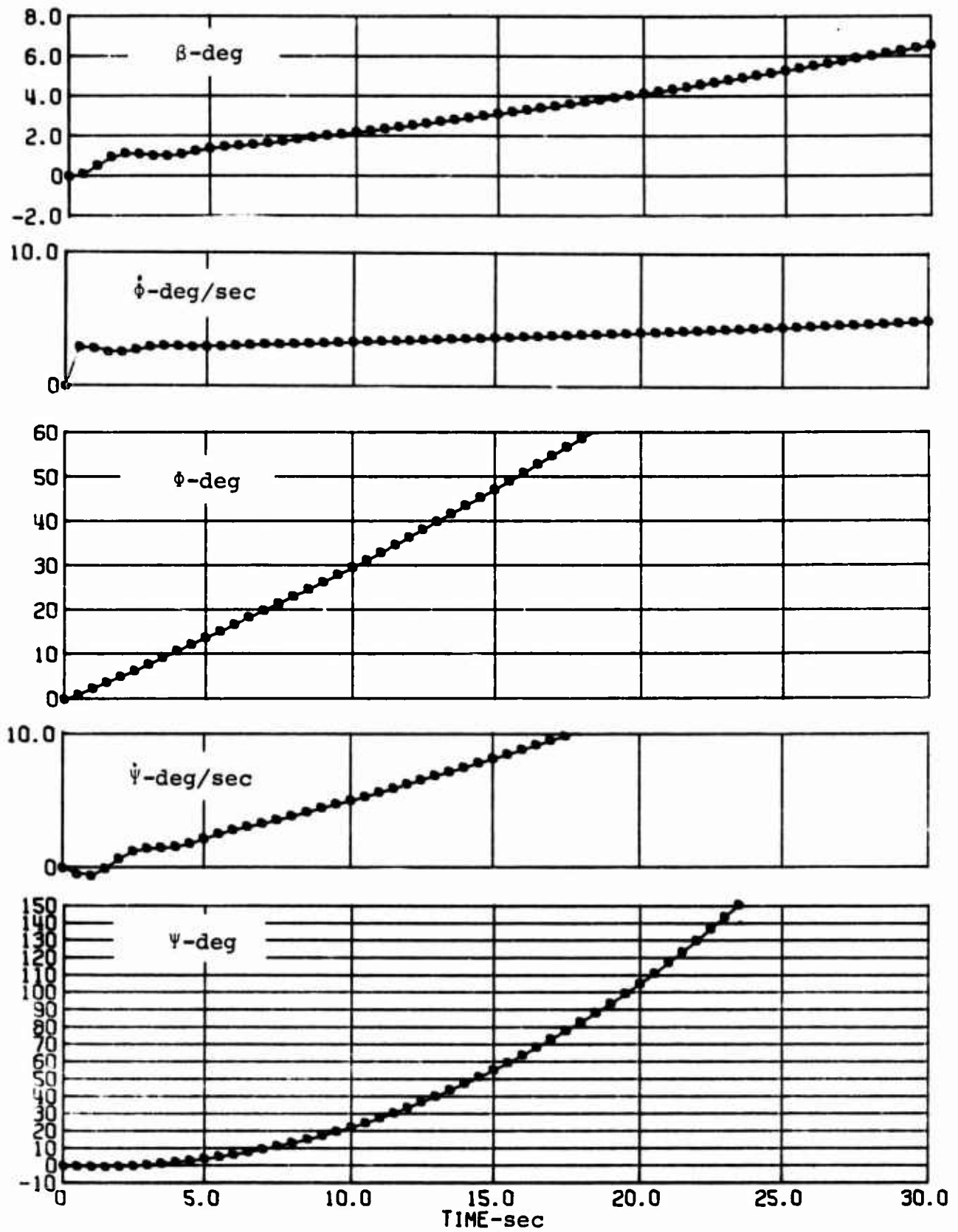


FIG.D-21 Response To 1° Step Aileron Input (Twin Otter, Slow Flight)

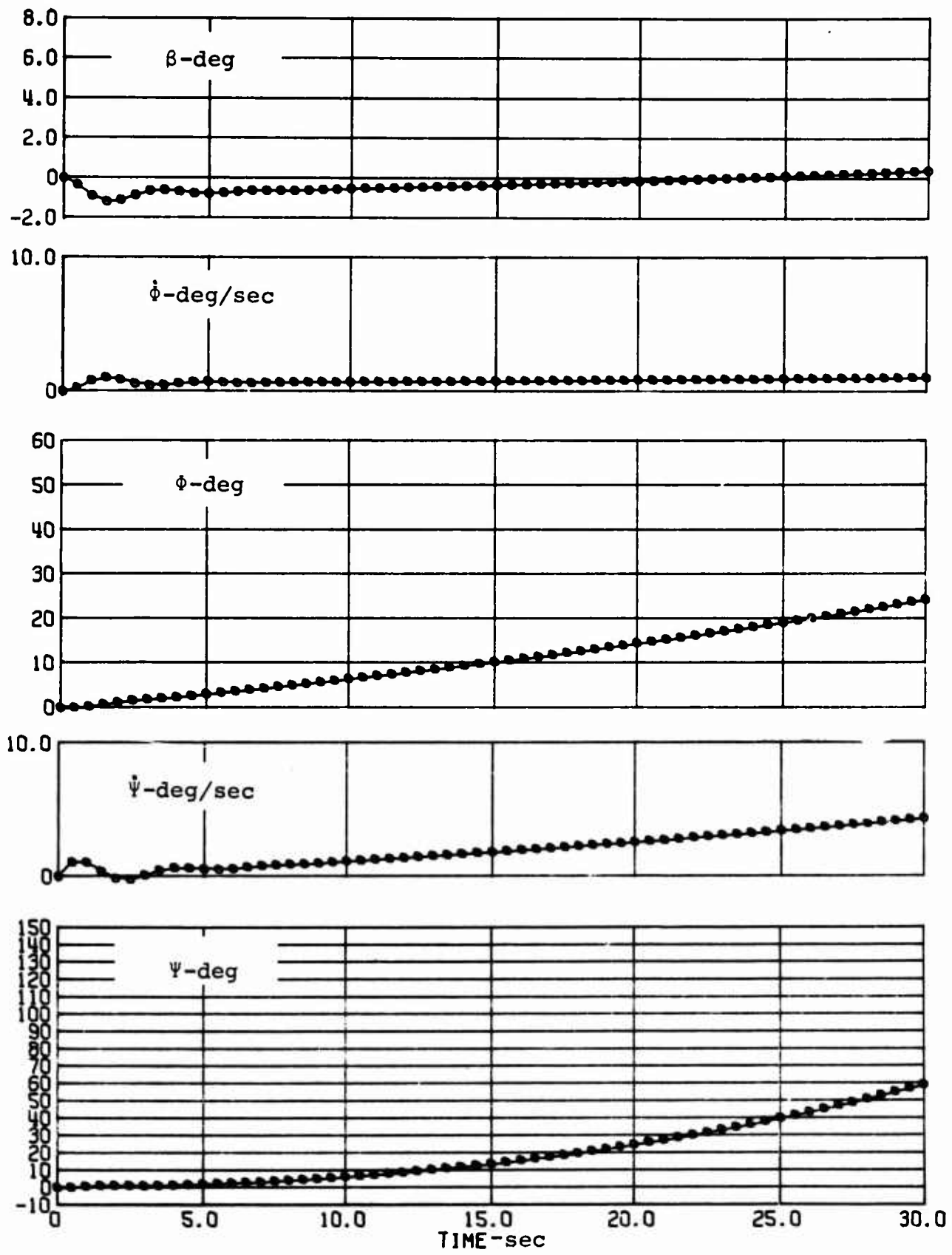


FIG.D-22 Response To 1° Step Rudder Input (Twin Otter, Slow Flight)

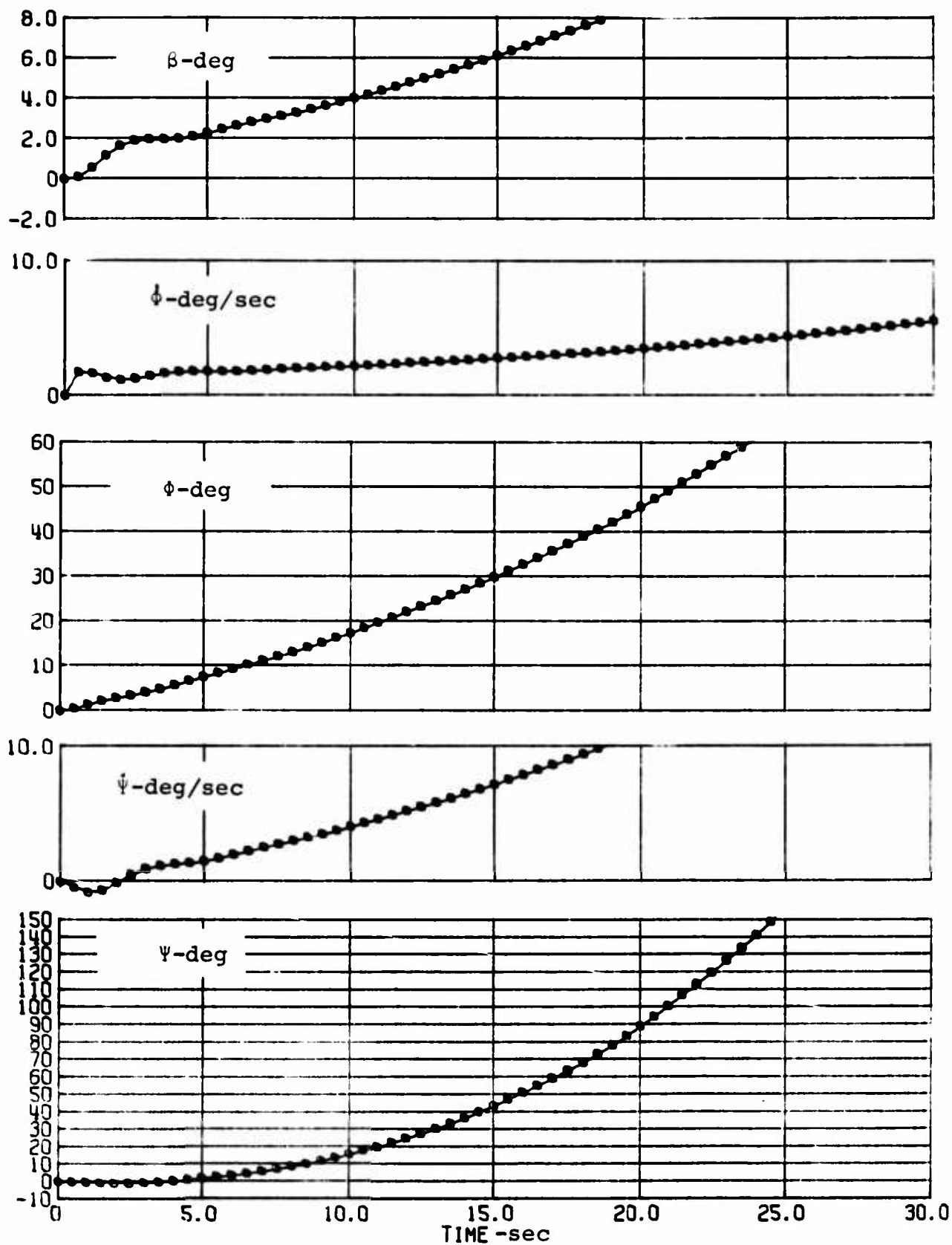


FIG.D-23 Response To 1° Step Aileron Input (Twin Otter, Approach)

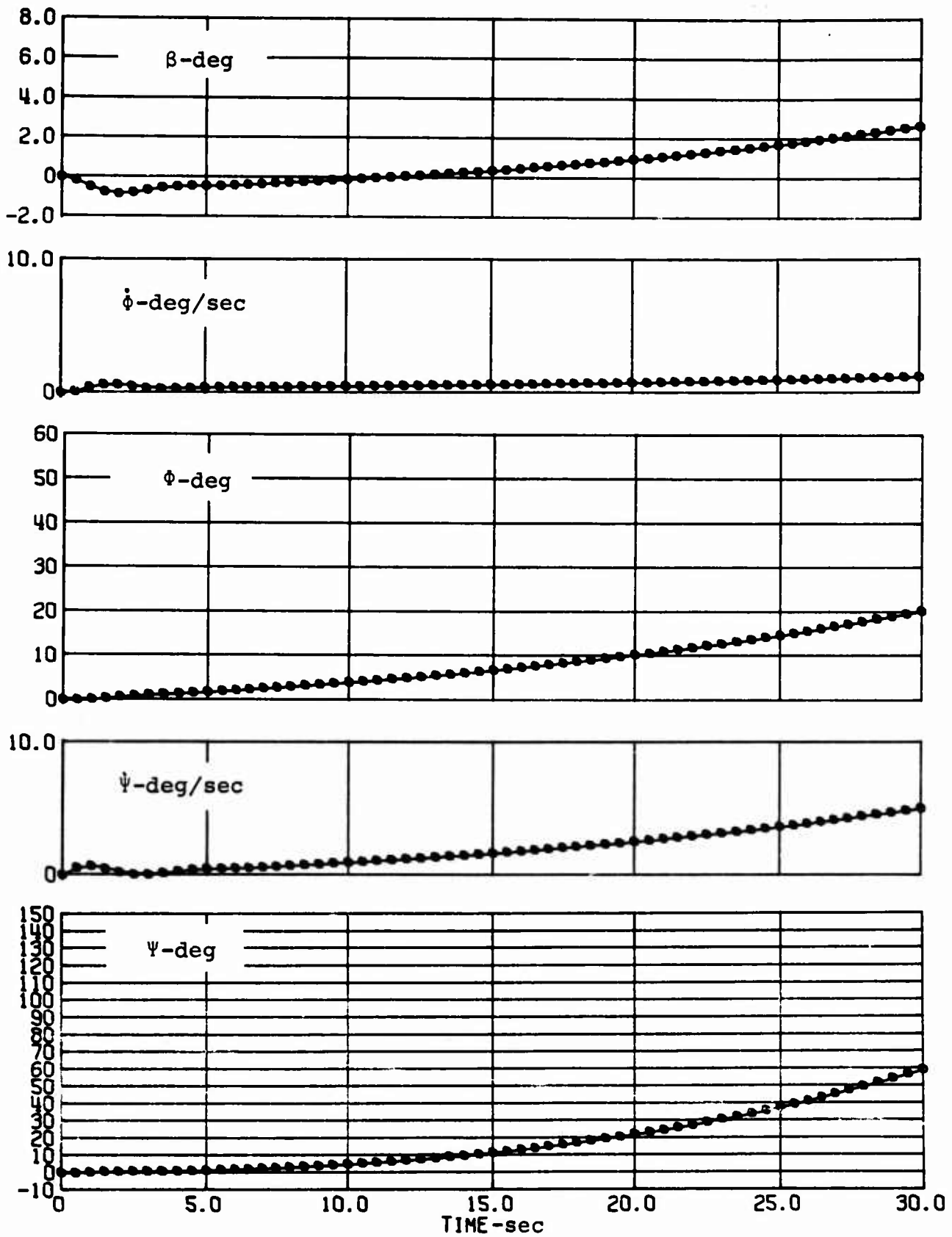


FIG.D-24 Response To 1° Step Rudder Input (Twin Otter, Approach)